

M.Sc. Thesis

A Compact, High Precision Position Sensing Embedded System for Fast Steering Mirror

Muhammad Wasif

4321928

Abstract

A fast steering tip-tilt mirror is widely used as a pointing and tracking device in aerospace engineering, in laser beam stabilizers and in many other applications. A fast steering mirror has the capability to project light in two-dimensional space. The correct positioning of the mirror is crucial for the device overall operation. In this project a complete feedback control system is deployed to ensure the correct positioning of the tip-tilt mirror. A novice approach is used in the implementation of feedback position sensor, ensuring high performance and low cost. A robust phase sensitive detection technique is used for signal processing. A compact design of embedded system is implemented, facilitating fast analog to digital conversion (ADC), good processing power (32 bit processor at 64 MHz) and fast (2 Msps) two channels digital to analog conversion (DAC). Finally, a PID algorithm is used to perform feedback control calculations ensuring correct positioning of the tip-tilt mirror.

A COMPACT, HIGH PRECISION POSITION SENSING EMBEDDED SYSTEM FOR FAST STEERING MIRROR

THESIS

SUBMITTED IN PARTIAL FULFILLMENT OF THE
REQUIREMENTS FOR THE DEGREE OF

MASTER OF SCIENCE

in

EMBEDDED SYSTEMS

by

Muhammad Wasif

born in Lahore, Pakistan

Student number : 4321928

This work was performed at:

Flexible Optical B.V
Polakweg 10-11
2288 GG Rijswijk ZH
The Netherlands

**Delft University OF Technology Department of Computer
Engineering**

The undersigned hereby certify that they have read and recommend to the Faculty of Electrical Engineering, Mathematics and Computer Science for acceptance a thesis entitled A Compact, High Precision Position Sensing Embedded System for Fast Steering Mirror by Muhammad Wasif as a partial fulfillment of the requirements for the degree of Master of Science.

Committee Members :

Advisor: Arjan Van Genderen, CE, TU Delft

Advisor: Gleb Vdovin, 3mE, TU Delft / Flexible Optical B.V

Chairperson: Stephan Wong, CE, TU Delft

ECT: 40

Abstract

A fast steering tip-tilt mirror is widely used as a pointing and tracking device in aerospace engineering, in laser beam stabilizers and in many other applications. A fast steering mirror has the capability to project light in two-dimensional space. The correct positioning of the mirror is crucial for the device overall operation. In this project a complete feedback control system is deployed to ensure the correct positioning of the tip-tilt mirror. A novice approach is used in the implementation of feedback position sensor, ensuring high performance and low cost. A robust phase sensitive detection technique is used for signal processing. A compact design of embedded system is implemented, facilitating fast analog to digital conversion (ADC), good processing power (32 bit processor at 64 MHz) and fast (2 Msps) two channels digital to analog conversion (DAC). Finally, a PID algorithm is used to perform feedback control calculations ensuring correct positioning of the tip-tilt mirror.

Contents

Report Title	ii
Contents	1
Contents	5
Contents	9
1 Introduction	10
1.1 Optics and alignment	10
1.2 Mechanical actuator	12
1.3 Feedback system	13
1.4 Sensing mechanism	14
1.5 Signal processing	14
1.6 Problem Description	14
1.6.1 Goals and challenges	15
2 Literature study	17
2.1 Sensors	17
2.1.1 Optical Sensors	17
2.1.1.1 Lateral effect PSD	17
2.1.1.2 Quadrant PSD	18
2.1.1.3 Reflective sensor	19
2.1.1.4 CCD camera	19

2.1.2	Mechanical sensors	20
2.1.3	Inductive and capacitive sensors	21
2.2	Signal detection and noise filtration	21
2.2.1	Phase sensitive detection (PSD)	22
2.2.2	PSD Analysis	22
2.2.3	Spectrum Analysis	24
2.2.4	Low pass filter	25
2.3	Feedback control system	26
2.4	Embedded Controller and Interfacing	28
2.4.1	Development board and supported tools	30
2.4.2	Electronics Interface	31
2.4.3	Communication Interface	32
3	Proposed Approach and Design	34
3.1	Sensing technique	34
3.1.1	Modulated signal	37
3.1.2	Moving average filter	39
3.2	Analog electronics	39
3.2.1	Photodetector	39
3.2.1.1	Photovoltaic mode	40
3.2.1.2	Photoconductive mode	40
3.2.1.3	OPT101 Photodiode	41
3.2.2	LED interface	41
3.2.3	DAC interface	42
3.2.4	ADC interface	45
4	Implementation	47
4.1	Modulated square waves	47
4.1.1	Timers/Counter peripheral	48
4.1.1.1	Input Clock	48

4.1.1.2	Trigger and clock control	49
4.1.1.3	Timer modes	49
4.1.1.4	Waveform mode configuration	51
4.1.1.5	Compare register values	53
4.1.1.6	Timer interrupt	53
4.2	Analog to Digital Converter (ADC)	55
4.3	Digital to Analog converter (DAC)	58
4.4	Universal asynchronous receiver transmitter (UART)	60
4.5	PID Controller	62
4.5.1	Fixed point implementation	63
4.6	Modifications	64
4.6.1	Photodetector	64
4.6.1.1	Transimpedance amplifier and VBP104S photodiode	66
4.6.2	Enhancing the optical gain	66
4.6.3	Slowing down the frequency	68
5	Results	69
5.1	Modulated waves	69
5.2	DAC output	69
5.3	Photo detector response	70
5.4	Moving average filter	71
5.5	User Interface	72
5.6	Tip-tilt mirror and the displacement sensor	73
5.6.1	Interference Calibration	75
5.6.2	Output response with an active feedback	77
5.6.3	Sensor resolution	78
5.6.4	Sensor response time	78
5.7	Shape formation	80
6	Conclusions and Future work	82

6.1	Conclusions	82
6.2	Future work	83

List of Figures

1.1	Tip tilt mirror in precision eye pupil tracking.	11
1.2	Different types of tip-tilt mechanical actuators. (a) Voice coil levitation actuator. (b) A spring supported actuator. (c) Piezoelectric actuator.	12
1.3	Overall basic diagram of the required feedback system.	15
2.1	The quadrant position detector)	18
2.2	The Reflective sensor. (a) Reflective surface at short distance, having detector receiving more light. (b) Reflective surface at longer distance, having detector receiving less light.	19
2.3	CCD chip with an array of photo sensitive sensors.	20
2.4	(a) A noise free modulated signal. (b) Modulated signal buried in noise.	23
2.5	Fourier spectrum of the modulated noisy signal. The horizontal scale represents the frequency and the vertical scale represents the amplitude (signal strength). (a) Spectrum during time interval t to $(t + \tau)$. (b) Spectrum during time interval $(t + \tau)$ to $(t + 2\tau)$. (c) The resulted spectrum after adding (a) and (b).	25
2.6	The effect of the low pass on the signal and noise. The strength (amplitude) of the signal increases linearly with time while the strength of the noise increases only by the square root of the time.	26
2.7	Basic structure of the system with feedback control.	27
2.8	PID control block.	28
2.9	Typical response of PID control.	29
2.10	Olimex SAM3-P256 development board [16].	31
2.11	Different types of electronics interface, DAC, UART, ADC and I/O required at different stages of the embedded system.	32

3.1	(a) Four red SMD LEDs mounted on sheet holder along with the photo detector. (b) Photo detector attached with the mechanical actuator placed in front of the mounted LEDs. (c) The mechanical actuator is displaced to the left. (d) Side view of the assembly.	35
3.2	The driving signal for the four LEDs and the resulting signal of photo detector (PD). The high state in the signal is considered to turn ON the LED and the low state to turn OFF the LED, the resulting photo current profile is shown in the PD Output waveform.	36
3.3	Signal extraction from individual LED sources. (a) Extraction of displacement information from LED1 by the multiplication of the PD output with the LED1 modulated signal. (b) The modulated signal having wrong phase, leading to wrong extraction of LED1 information.	37
3.4	Fourier spectrum of a square wave of frequency ω_o	38
3.5	(a) Photodiode configuration in photovoltaic mode. (b) Photodiode configuration in photoconductive mode.	40
3.6	Texas instruments OPT101, photodiode integrated with transimpedance amplifier [30].	41
3.7	OPT101 recommended external component values according to gain and bandwidth characteristic in photovoltaic mode [30].	42
3.8	(a) Responsivity of the OPT101 photodetector to the incident light[30]. (b) Reflective intensity of emitted light by the LED [31].	43
3.9	Electronics interface for the LEDs, here, $R_1 = 4.7 \text{ k}\Omega$ and $R_2 = 10 \text{ k}\Omega$	43
3.10	Electronics interface for the DAC.	45
3.11	Reduction of quantization error due to increase in resolution from 12 bits to 14 bits by the oversampling technique[40].	46
4.1	Timer/counter peripheral block of the SAM3S4B MCU[20].	48
4.2	Clock selection for each timer channel.	49
4.3	Timer/counter trigger and clock control block.	50
4.4	Timer/counter functional diagram in waveform mode [20].	51
4.5	Timer operation in WAVSEL = 00. (a) Without initiation of any trigger. (b) With the initiation of SYNC trigger.	52
4.6	The wave generation at the output pins, according to the timers configuration.	54
4.7	The block diagram of the MCU's ADC unit [20].	55

4.8	The ADC operation and samples handling.	57
4.9	The ADC and wave pins connections.	58
4.10	The SAM3S4B DAC module.	59
4.11	(a)UART block of the MCU. (b) Baud rate selection from the master clock(MCK)[20].	61
4.12	Structure of the communication packet.	61
4.13	FTDI US232R, USB to serial converter .[45].	62
4.14	Fixed point implementation with 8 bits precision by using 16 bits integer.	63
4.15	The photodetector OPT101 response for different values of feedback resistor and capacitor. (a)R_ext = 13 kΩ and C_ext = 390 pF (b) R_ext = 13 kΩ with no capacitor. (c) R_ext = 14.33 kΩ and C_ext = 390 pF (d) R_ext = 14.33 kΩ and C_ext = 1 nF (e) R_ext = 3 kΩ and C_ext = 1 nF (f) R_ext = 3 kΩ and C_ext = 390 pF	65
4.16	(a) OPA381 transimpedance amplifier. (b) VBP104S photodiode.	66
4.17	Modified LED driver circuit.	67
5.1	Modulated waves to drive the four LEDs. (a) The top wave at pin TIOA0 of the MCU. The bottom wave at the pin TIOB0. (b) The top wave at the pin TIOA0 and the bottom wave at the pin TIOA1. (c) The top wave at the pin TIOA0 and the bottom wave at the pin TIOB1.	70
5.2	DAC output profile for the digital input range of 0 to 4000. (a) DAC output voltage without electronics interface. (b) DAC output voltage after the electronics interface. (c) Combined outputs, before the electronics interface (the top) and after the electronics interface (the bottom).	71
5.3	Photo detectors response from the modulated LED. (a) VBP104S response after the OPA381 amplifier. (b)VBP104S response after the OPA381 amplifier with higher optical gain. (c) OPT101 response. (d) OPT101 response with lower feedback capacitor and higher optical gain.	72
5.4	Moving average filter output for 16,32 and 64 points.	73
5.5	Keyboard interface for user control	74
5.6	(a) Fast steering mirror. (b) Sensor output from the four LEDs. (c) A close up of the actuator lever and inductive coil. (d) The photo detector and the four LEDs	75

5.7	The position sensor response. (a) and (d) A displacement in the horizontal X direction by the rotation of the micrometer. (b) and (d) Corresponding effect of the displacement on the sensor output.	76
5.8	(a) and (d) A displacement in the vertical Y direction by the rotation of the micrometer. (b) and (d) Corresponding effect of the displacement on the sensor output.	76
5.9	Interference in horizontal sensor data due to vertical displacement.	77
5.10	Output response with an active feedback.	78
5.11	Sensor outputs at a mean position and after a 10 um horizontal displacement.	79
5.12	Tip-tilt mirror projecting formation of different shapes. (a) A laterally inverted L shape. (b) A half square. (c) A full square with fast nonlinear input, without feedback correction. (d) A full square with fast nonlinear input, with feedback correction.	80
5.13	Input data to drive the tip-tilt mirror.	81

List of Tables

2.1	SAM3S4B important features[20].	31
3.1	Electrical characteristic of output voltage for the MCU's DAC [20]	44
4.1	Possible actions on the state of PIOA and PIOB	52
4.2	Configuration values for the generation of four modulated waves. . .	53
4.3	Implemented compare registers values	53
4.4	Configuration value with its defined functionality.	62
5.1	Moving averaging filter analysis.	73

Chapter 1

Introduction

After the invention of the laser and optical fiber, a new field called photonics was introduced in the technical studies of science. As optical fibers and lasers were mainly used in telecommunication applications, the photonics incorporated all technical aspects of electrical engineering including signal processing, sensing and detection of light, modulation, electronics amplifier and embedded systems. Now photonics have grown widely in many fields including medicine, robotics, astronomy and military technology [2]. In all these fields, photonics plays a major part in all kind of equipment, in agriculture the milking robots use laser detection mechanisms to locate the exact positioning of the cow teats such that milking pump can be inserted, all astronomical equipment make use of integrated photonics to capture and decode the light coming from very long distance objects, in medicine, laser surgery is very useful for eyesight correction, in computers the DVD/Blue-ray devices intensely use photonics parts to accurately read and write the digital data on the optical disk [1], in military the guided artillery is accompanied by laser guidance system that heavily rely on the principles of photonics. In all these applications the photonics is always accompanied by an embedded systems which plays a fundamental part in making the system work. The optics and sensors used in photonics devices forms a physical interaction with a system but all information generated by sensors and user commands are handled by an embedded system. The embedded system is also responsible for all kind of signal processing, calculations and feedback control implementation. All modern optical systems heavily rely on the performance of the embedded system and could lead to limited performance due to poor embedded system design hence making the correct design choices for the embedded systems is very crucial.

1.1 Optics and alignment

One important property of laser is that it can be aligned to travel in a straight path over a long distance and any deviation from the straight path can be easily tracked and detected. This property is very useful in mechanical systems where there is need of accurate alignment of the moving mechanical parts. In such systems,

optics is deployed as a tool to guide the mechanical system for accurate alignment and positioning. The optics mainly includes light source, fast steering mirrors and light sensitive detectors [4]. A light source could be a small laser diode or a simple light emitting diode, depending on the application and the total distance between the light source and the detector. Fast steering mirror refers to a device with a mirror that can change its geometry to guide the reflected light in a specific direction. One such popular device is a tip-tilt mirror, that has a reflected mirror with the capability of deformity in two dimensions. The mirror can rotate around its axis in two dimensional plane, hence it can deflect any incident light in two dimensional space. In a common tip-tilt assembly, the reflecting mirror is attached to a mechanical actuator that tends to rotate the mirror at a specific angle.

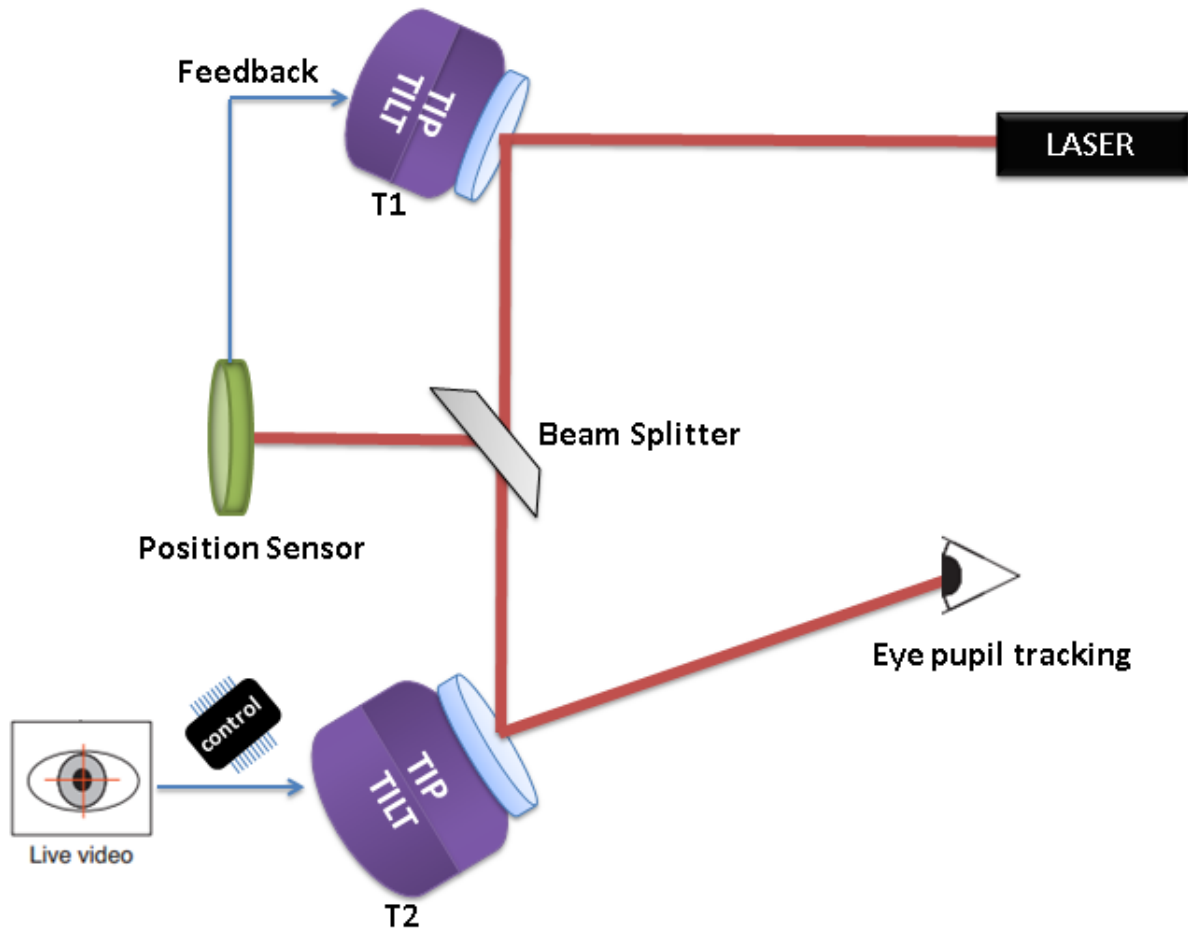


Figure 1.1: Tip tilt mirror in precision eye pupil tracking.

Figure 1.1 shows an example application of tip-tilt mirror in a eye pupil tracking [3]. Two two tip-tilt mirrors are used, T1 and T2. The laser beam is first projected on T1 that corrects miss alignments caused by any internal drift of the laser source. The position sensor detects that drift and feed it to T1 for correction. The mirror T2 generates the tracking position of the eye pupil based on the input from the live video of the human eye.

1.2 Mechanical actuator

The mechanical actuator normally contains a piezoelectric solid strip, a voice coil or a mechanical spring like assembly controlled by the electrical signal.

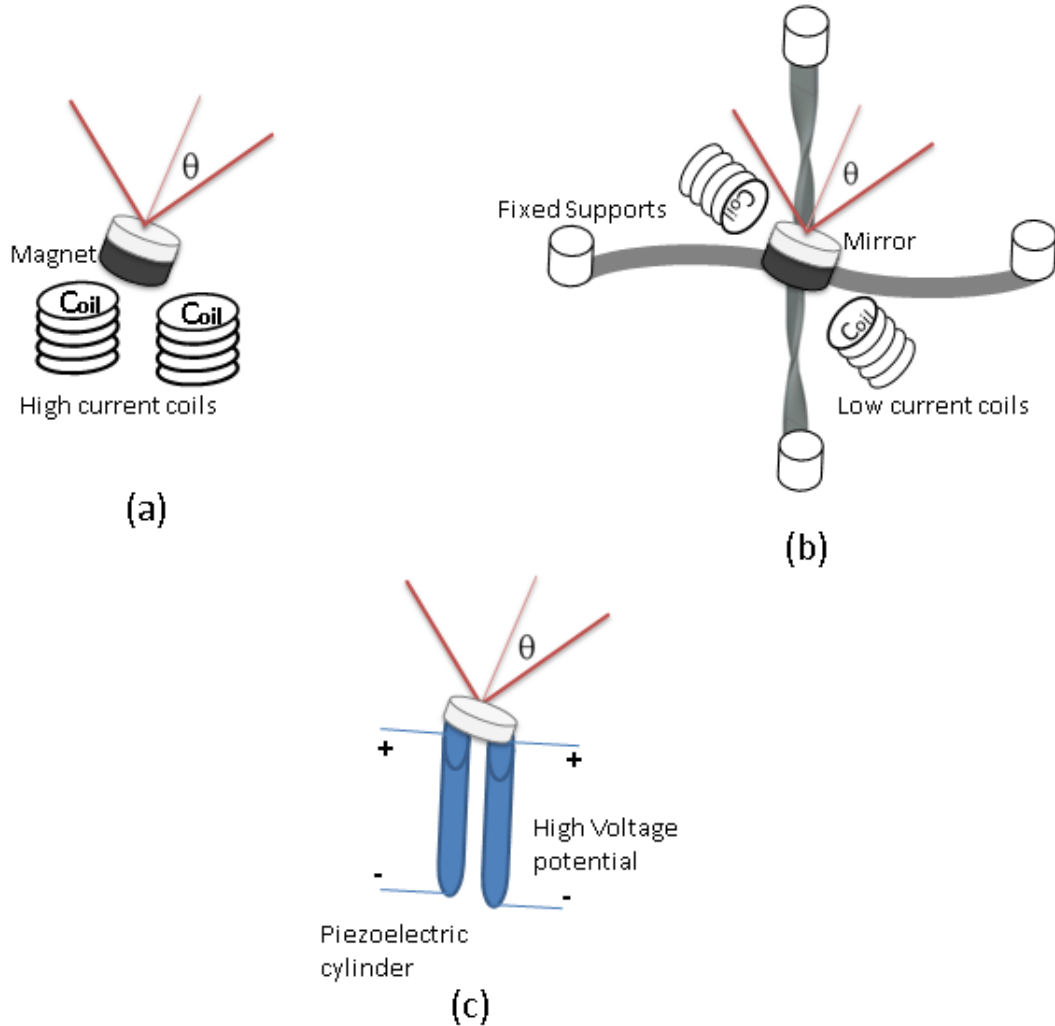


Figure 1.2: Different types of tip-tilt mechanical actuators. (a) Voice coil levitation actuator. (b) A spring supported actuator. (c) Piezoelectric actuator.

Figure 1.2 shows some common assemblies of the mechanical actuator. The voice coil actuator includes high current induction coils and magnets. The induction coils are simple electrical inductors that produce magnetic field when an electric current is passed through them. The magnets are attached at one side of the reflecting mirror and the mirror is levitated on the current carrying coils that have magnetic field around them. The high current coils are needed to generate strong magnetic field that can levitate the magnetic and mirror assembly, supporting their weight in the air. The motion of the levitated mirror can be controlled by placing multiple coils at different locations and controlling their magnetic field strength. One major issue is that the coils could heat up due to excessive current required

for sustainable levitation. To compensate for the coil heating an extra heat sink or cooling support will be required. This kind of actuator also requires a complicated assembly that could facilitate levitation of the mirror. On the positive side, it does not require any extra high voltage amplifier like in piezoelectric actuators.

The mechanical spring actuator is a modified form of the voice coil actuator. In this actuator the levitation in free air is not supported by the magnetic field, instead a supporting spring is used to support the levitation of the mirror. This eliminates the need for strong magnetic field. The mirror is suspended in an assembly with the help of the springs. The springs provide two degrees of movement when subjected to external force. The use of springs provide the support to hold the weight of the magnet and mirror. Making the system to be operated without having high current coil, which is required to support levitation in the case of voice coil actuators. This completely omits the need of heat sink and high magnetic field demands. However, this kind of actuator, compared to piezoelectric actuator, has low resonance frequency which limits the overall dynamic range of the system.

The piezoelectric material has the property of deforming its shape when subjected to external voltage. Cylindrical shape electrodes could be made out of piezoelectric material that can be directly attached to an external mirror. The piezoelectric assembly normally contains cylindrical or stripped like piezoelectric electrodes. The electrodes are directly attached to the mirror. This deformity is translated into changing the mirror position. The external voltage applied to the strip would induce deformity in the strips and this deformity is translated into the attached mirror. The deformity is directly controlled by the amplitude of the applied voltage. This type of actuator requires very high voltage, in the order of 400 volts, for its operation. That adds a need of expensive high voltage amplifier.

1.3 Feedback system

All actuators can be controlled through a given input voltage that directly controls the rotating angle of the mirror. The motion of the mechanical actuator is itself subjected to accurate positioning and requires some feedback sensing mechanism that can provide the right information about the correct positioning of the actuator. The time drift i.e, with time a system develops some drift in its alignment, causing non linearity, must be compensated with the help of a robust feedback system. The feedback system is responsible for keeping the mirror at the accurate position defined by the user input regardless of any external interference or drift. These fast steering mirrors must be able to provide very fine resolution in the rotation angle, normally in the order of 2 micro radians. The feedback system should facilitate this high resolution and the sensing mechanism must be sensitive enough to accurately sense the correct positioning of the actuator.

1.4 Sensing mechanism

To track the correct positioning of the mechanical actuator, a position sensing device is required. There are many different types of position sensors available, including optical, magnetic and capacitive position detectors. They can be used to accurately detect the position of the actuator. The magnetic sensors exploit the properties of electromagnetism and are useful in devices that doesn't have electromagnetic interference and contain only non magnetic components [6]. The capacitive sensors utilize the principle of a parallel plate capacitor and provides very good sensitivity but have smaller range and are quite expensive to use [5]. Optical sensors make use of the properties of light and could have many different mechanisms with their benefits and drawbacks. All these sensing mechanisms strictly depends on the application that can have specific requirements for sensitivity and dynamic range. For example the capacitive sensors provides a very good sensitivity in the position detection, in the order of few nanometers however it doesn't provide a wide range of position detection and is limited to only few millimeters of full scale reading. The magnetic sensors cannot be used in a system that has magnetic components which can induce strong electromagnetic interference but can provide good displacement range. Hence, it is important to opt for the correct sensing mechanism.

1.5 Signal processing

The signal generated by the sensors is often accompanied by a noise and in some situations the noise level might be higher than the signal itself. The sensor signal needs to be processed for noise elimination, in order to extract meaningful information. The processing could include digitizing the sensor signal and then using a DSP(digital signal processing) unit to apply standard signal processing techniques. How intensive the signal processing is performed, mainly depends on the sensor's performance and its noise level.

1.6 Problem Description

In the current problem, there is an available tip-tilt device based on mechanical spring assembly. This device has no support of an embedded system. The device is operated based on simple feed forward analog voltages. There is no feedback control and sensing mechanism. In this project, a complete embedded system is to be designed and deployed. To control and operate the mechanical actuator, a robust embedded system is required that can provide the facility for the implementation of feedback control system, sensing control, signal processing, noise elimination and handling user inputs. The design and implementation of the embedded system decides the limitations and abilities for the overall operation of the device, making the embedded system being the most important part of the system. There are some solutions possible for the embedded system design that can provide most of

the mentioned facilities to control the tip-tilt mechanical actuator. However, the size and the cost of the embedded system brings out the challenge to find a unique solution to the design. In the current scenario, the mechanical actuator assembly has a dimension of about 5 x 5 x 4 cm and the embedded system needs to fit inside that assembly covering as less of space as possible. In fact the only choice available for the embedded system is to fit in a printed circuit board (PCB) of size no larger than 4 x 4 cm. The second important constraint is to make the embedded system highly cost effective, according to the current requirement, the cost should not exceed 10 EUR. These two major constraints of small size and extremely low cost puts a major challenge towards the design of an embedded system that is robust and sensitive enough to facilitate all the functionality of the sensor control, signal processing, user interfacing and feedback control of the actuator.

The major objective of this thesis is to design and implement an embedded system like shown in Figure 1.3 for the tip-tilt mirror device. The system should be sensitive enough to correctly control the rotating motion of the mechanical actuator within the resolution of 2 micro radians. The design should fulfill all the size and cost constraints.

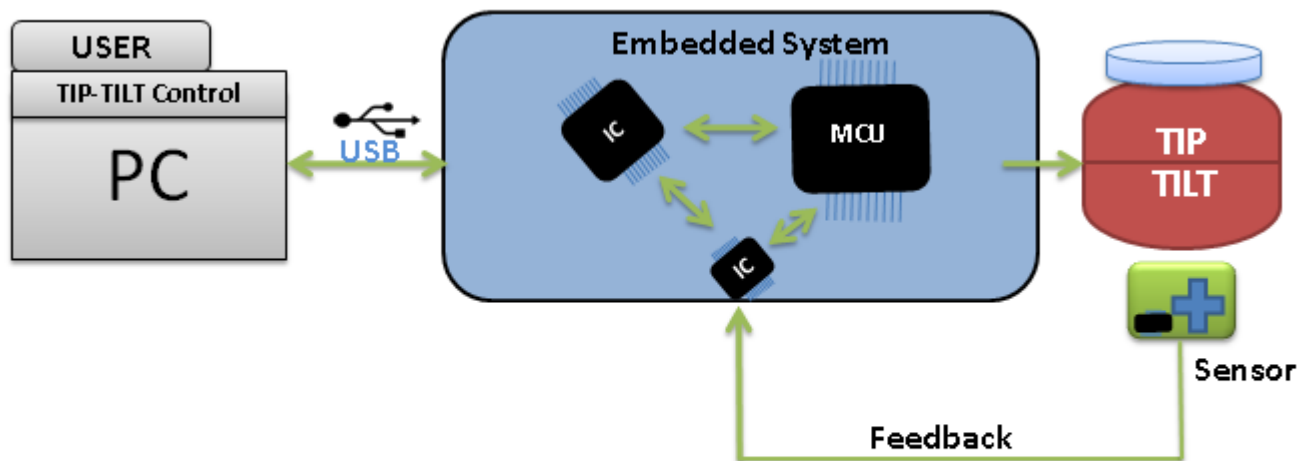


Figure 1.3: Overall basic diagram of the required feedback system.

1.6.1 Goals and challenges

The sensors that can provide very good resolution with a small assembly are mostly very expensive. Furthermore, some of the fast steering mirrors used here make use of magnetic coils which completely eliminates the use of magnetic sensors. One major goal and challenge would be to design and develop a sensing mechanism,

basically a custom made sensor that would be of low cost and must be able to provide the needed sensing resolution. The low cost sensors mostly have lots of noise and require robust signal processing techniques to extract the signal buried in excessive noise. The further challenge would be to understand and implement the signal processing technique that is robust enough to eliminate noise and recover the required signal. The high signal processing requires high speed analog to digital converter (the sampler) and a fast processing speed of the embedded controller, which demands the use of an expensive embedded controller which adds another challenge to the design. To keep the size and cost of the embedded system low, an embedded controller with an integrated analog to digital converter (ADC) would be used but these ADC provide low digital resolution of only 10 to 12 bits maximum. This isn't sufficient to reach the required resolution of 2 micro radiants due to the quantization error. One challenge is to come around a solution to provide the needed resolution while utilizing the cost effective built in ADC of the embedded controller. The overall challenge of this thesis project is to come up with the innovative solutions that would lead to an embedded systems implementation fulfilling the requirements of robustness, sensitivity, small size and extremely low cost. The following points summarizes the important project tasks and goals

- A design and implementation of a robust, low cost and high sensitivity position sensor.
- A choice of a low cost, small packaged embedded controller with integrated fast ADC and DAC units.
- An implementation of very good signal processing technique to enhance signal quality from the sensor.
- A suitable computer interface with the device.
- A deployment of a good feedback algorithm.
- A deployment of any additional analog electronics and circuits to facilitate proper functionality of the embedded system.
- Extra measures and techniques to increase the signal sensitivity by increasing the ADC resolution.
- Exploring possible alternatives to make better and suitable design choices.
- Keeping the overall cost and size of the embedded system as small as possible.

Chapter 2

Literature study

The embedded system is to be deployed on an available tip-tilt system that has a spring based mechanical actuator. The literature study includes the technical understanding of the requirements and the needs of the system where the embedded system is to be deployed. This will include the study for the available solutions and related literature for the sensors, signal processing, feedback control system, user software interface, analog electronics interface and the embedded controller.

2.1 Sensors

There are variety of position sensitive sensors available. Depending on their working principles they can be categorized as follows.

2.1.1 Optical Sensors

If some light source is attached to a mechanical actuator and the light beam from this source is directed on some sensor whose surface is sensitive to the beam position, then the resulted construction results in the detection of the position of the actuator by optical means. The most important part in this construction is the sensor whose surface is sensitive to the position of the incident beam. Most common optical position sensitive sensors include Lateral Effect PSD(position sensitive detector), Quadrant PSD, Reflective sensors and Charge coupled device (CCD) camera.

2.1.1.1 Lateral effect PSD

Lateral effect PSD [7] works on the principle of photo electric effect and is basically a modified photodetector. A photodetector is a device that produces electric current called photo current when a light is projected on its surface. The magnitude of this current is directly proportional to the intensity of the incident light. In

the lateral effect PSD, the modification includes a thin layer of current resistive material of non uniform thickness across the photovoltaic cell surface. This non uniform resistive layer makes the photo cell to produce non uniform photo current depending on the location of the incident beam. If the beam is positioned at the surface where the resistive material has larger thickness then the resulting photo current will be smaller. Similarly if the light is positioned at the thinner part of the resistive material layer then the photo current will have greater magnitude hence the photo current will be sensitive to position of the incident light beam.

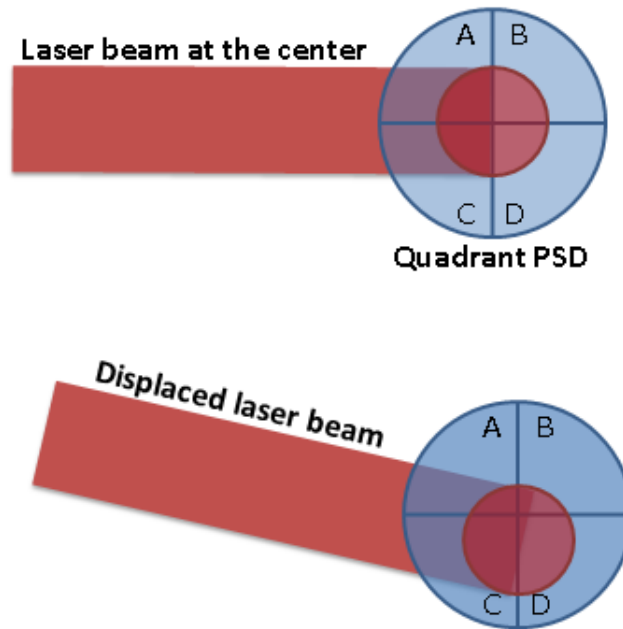


Figure 2.1: The quadrant position detector)

2.1.1.2 Quadrant PSD

The Quadrant PSD contains four photo detectors placed very close together such that it makes a quadrant cell. The four detectors are physically separated by a very small distance, typically in the order of tens of micro meters as shown in Figure 2.1. Initially the light beam is focused in the middle of the detector such that all the four detectors namely A,B,C and D will produce equal amount of photo current. The deviation in the position of the beam will result in one or more quadrants having more light projected towards them than the other quadrants. For example in the displaced laser beam, shown in Figure 2.1, the quadrant C and D has more light projected on it. Hence, the quadrant C and D will produce more photo current than the other quadrants. The two dimensional positioning, naming X and Y, can be approximately mapped with the help of the following equations

$$X = \frac{(b + d) - (a + c)}{a + b + c + d} \quad (2.1)$$

$$Y = \frac{a + b - (c + d)}{a + b + c + d} \quad (2.2)$$

where a,b,c and d represents the magnitude of the photo currents of the quadrants A,B,C and D respectively. X and Y represent the magnitude of the two dimensional positioning of the beam relative to the currents a,b,c and d. The quadrant PSD doesn't have a resistive layer and only contains four conventional photo detectors placed tightly together.

2.1.1.3 Reflective sensor

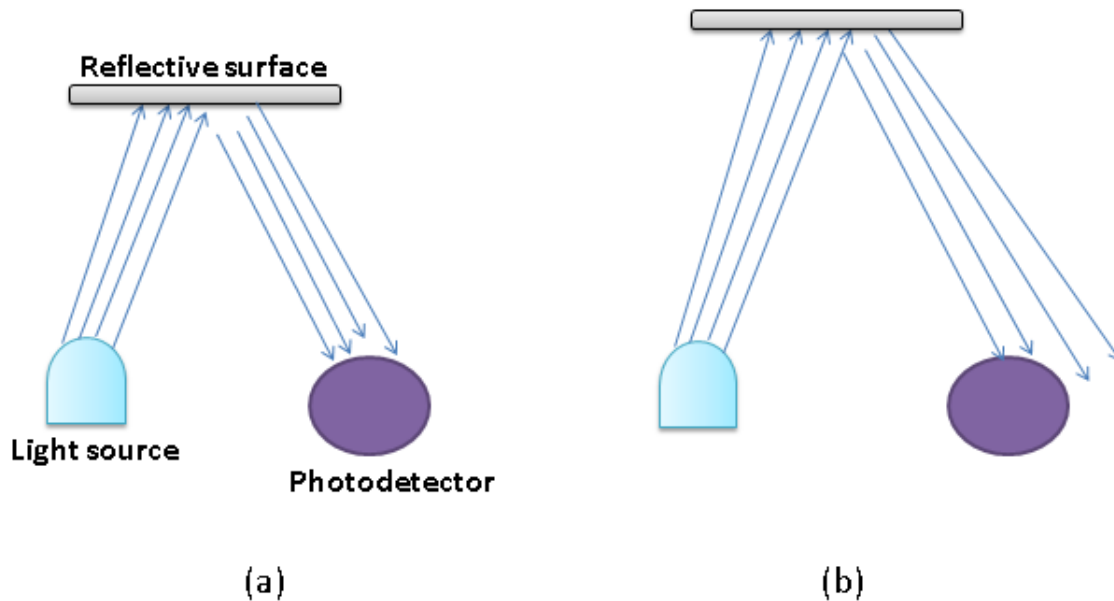


Figure 2.2: The Reflective sensor. (a) Reflective surface at short distance, having detector receiving more light. (b) Reflective surface at longer distance, having detector receiving less light.

The reflective sensor also referred as proximity sensor contains one light source and one photo detector placed adjacent to each other as shown in Figure 2.2. A reflective surface is placed near to the sensor and the reflected light is detected by the photo detector. The magnitude of the photo current produced by the photo detector directly depends on the distance between the reflective surface and the sensor.

2.1.1.4 CCD camera

The simplified diagram of charged couple device (CCD) is shown in Figure 2.3. The CCD makes use of an array of hundreds of small charge carrying capacitive

bits embedded on a thin sheet. The amount of charge directly depends on the intensity of the incident light and an intensity profile over the entire sensitive area of the CCD device can be made to track the position of the incident beam [7].

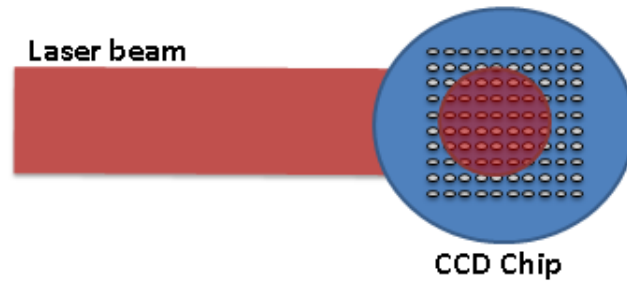


Figure 2.3: CCD chip with an array of photo sensitive sensors.

Each kind of detector has its advantages and disadvantages. The performance of the quadrant detector is dependent on the diameter of the incident beam. If the diameter is too big then the detector will have very short detection range and will suffer from non linearity. On the other hand it has low noise with high dynamic range typically in the order of 100 KHz. The lateral effect PSD has extra noise due to the resistive layer but is less dependent on the beam diameter. Although less expensive, the reflective sensor has a very low range of displacement detection and is less sensitive than the other sensors. The CCD camera has very good sensitivity but the device itself needs an embedded system to communicate with large array of sensor bits.

2.1.2 Mechanical sensors

The most common mechanical sensors include Gyroscopes and Accelerometers, both of these sensors are very small, micro electro-mechanical system (MEMS) devices. They are often packed in a single integrated chip with the integrated electronics. They are very commonly used in modern cell phones to detect the position and orientation of the device. The gyroscope is helpful in detecting the orientation of the attached device in three dimensions, namely the three angles roll, pitch and yaw. It works on the principles of angular momentum and contains three rotating mechanical wheels around a single referenced axis. Similarly the accelerometers measure acceleration and contain small spring like mechanical strips. The mechanical sensors are widely available and are very cost effective, small in size and easy to interface with the embedded controller. However, they don't have high sensitivity and at most can detect angular changes in the order of few milli radians where as the requirement for the project is to detect angular changes as small as 2 micro radians.

2.1.3 Inductive and capacitive sensors

The inductive sensor contains a current carrying electrical inductor excited at a specific frequency and works on the principles of electromagnetic interference. This current carrying inductor will generate a magnetic field around itself and when brought close to a metallic surface, will result in the change of inductor's inductance. The change is due to the electromagnetic interference of the magnetic field with the metallic surface. Normally the circuit contains a resistor and the inductor and is excited at a resonance frequency. This results in maximum voltage amplitude at the output. The voltage could be measured across the resistor and any change in the inductance value would lower the output magnitude. This output magnitude is directly proportional to the distance between the excited inductor and the metallic object.

The capacitive sensor works on the principle of parallel plate capacitor. The capacitance of the capacitor is inversely proportional to distance between the two conductive parallel plates. The sensor normally contains two electrodes where one electrode is tied fixed while the other electrode is attached to the movable object. This forms a parallel plate capacitor configuration. Any displacement in the movable object will result in the capacitance change. Like in inductive sensor this capacitive change can be detected by forming a resistor-capacitor resonance circuit.

Inductive and capacitive sensors are small in size and have very high sensitivity. However, any electromagnetic interference can immensely degrade the performance of these sensors. The fast steering mirrors make use of electromagnetic coils that induce large electromagnetic interference, making these sensors a bad choice.

2.2 Signal detection and noise filtration

Normally every signal from a sensitive sensor is accompanied by a noise. In some cases the noise may be more than the actual signal which makes it difficult to separate the signal from noise and some good technique must be applied to extract the signal. A straight forward naive approach is to add an amplifier with high gain to increase the output signal. However, doing this does not reduce the noise, which is amplified together with the signal. In fact an additional instrument noise of the amplifier is added to the signal which further increases the noise. Eventually the signal without any amplification seems to have better chance of detection. A somewhat better approach is to use some filter based amplification. To use filter based amplification you need to know the frequency of the actual signal along with the frequency range of the possible noise sources. There could be many sources of noise depending on the nature of instruments you are using and the surrounding environment. For example in a optical sensing system, one source of noise could be the shot noise coming from the photo detector and another could be an electromagnetic interference coming from the nearby electric power lines. The first step is to identify these noises and try to reduce them by taking appropriate

measures [23]. On the other hand, if you know the frequency of the actual signal then the next step is to design a filter based amplifier circuit. That circuit will amplify only the signal having the frequency of the actual signal while rejecting all other frequency signals (the noise). In practice making such an ideal band pass filter is not possible. The filter circuit does not completely reject all the noise frequencies and also does not amplify only a single frequency signal. With the conventional operational amplifier based band pass filters you could only achieve limited amount of performance in increasing the signal to noise (S/N) ratio.

2.2.1 Phase sensitive detection (PSD)

A more complicated and robust technique called phase sensitive detection or lock in detection can be used to recover signal buried in noise [12]. The technique offers much better performance over the wide range of frequencies. In this technique the first step involves modulation, where the sensing device producing the signal is modulated at some fixed frequency. In simple terms modulation means that the sensor is operated at some fixed frequency [13]. The sensor is sensing the operation of a device and its modulation frequency is related to the max operational frequency of this device. In the case of tip-tilt device the sensor is detecting the motion of the mirror. Most commonly every device has a maximum operable frequency for a certain application. For example to track the position of an object that doesn't change its position faster than 5 milliseconds, a tip-tilt devices is operated in a range of 0 to 200 Hz. That means the maximum operable frequency for this tip-tilt device is 200 Hz. The fixed modulation frequency of the sensor is always chosen to be much higher than this maximum operable frequency. The reason why this is the case, will be explained in the subsequent sections. Preferably the sensor is modulated by a sinusoidal of fixed phase and frequency. If the noise is ignored then the output of this modulated sensor will look like Figure 2.4 (a). If the accompanied noise is not ignored then the signal will look like Figure 2.4 (b). The goal is to maximize the signal strength buried in the noise which will lead to higher signal to noise ratio (S/N).

In the next step the noisy signal in Figure 2.4 (b) is multiplied with a clean, noise free sinusoidal signal. This clean signal must have exactly the same phase and frequency as of the modulation signal in Figure 2.4 (a). The resulting signal from the multiplication is passed through a low pass filter (an averaging filter) with a cutoff frequency a little higher than the maximum operable frequency of the device. The resulting output provides much higher signal to noise ratio with significant reduction in noise. The next section analyze the phase sensitive detection method and shows how it helps in reducing noise.

2.2.2 PSD Analysis

Lets consider an example of a sensor excited by a sinusoidal signal S_o at some higher frequency ω_o having phase ϕ_o , this excited signal is also accompanied by some random noise. Then, $S_o = A\sin(\omega_o t + \phi_o)$ where t is time and A is the

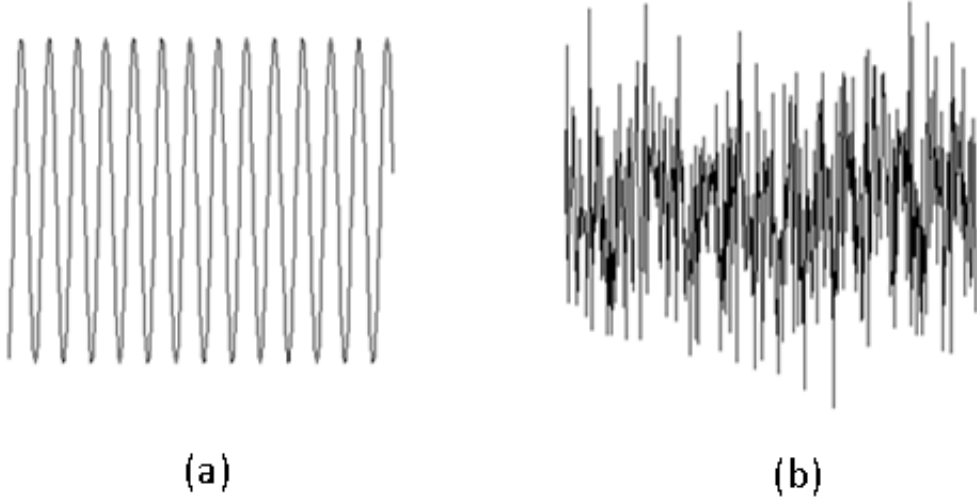


Figure 2.4: (a) A noise free modulated signal. (b) Modulated signal buried in noise.

amplitude, that defines the actual signal strength. Now lets assume a reference sinusoidal signal S_r of amplitude B having frequency ω_r and phase ϕ_r is multiplied with the modulated signal S_o ,

$$\begin{aligned}
 S &= A\sin(\omega_o t + \phi_o) \times B\sin(\omega_r t + \phi_r) \\
 &= \frac{1}{2}AB\cos([\omega_o - \omega_r]t + \phi_o - \phi_r) - \frac{1}{2}AB\cos([\omega_o + \omega_r]t + \phi_o + \phi_r) \quad (2.3)
 \end{aligned}$$

In the above equation 2.3, if the frequencies ω_o and ω_m are the same then it will simplify to,

$$S = \frac{1}{2}AB\cos(\phi_o - \phi_m) - \frac{1}{2}AB\cos(2\omega_o t + \phi_o + \phi_m) \quad (2.4)$$

The equation 2.4 has two components, the DC component $\cos(\phi_o - \phi_m)$ and higher frequency component $\cos(2\omega_o t + \phi_o + \phi_m)$. Now if the above signal is passed through a low pass filter then the higher frequency component will be filtered out and the resulting signal will have the following form

$$S = \frac{1}{2}AB\cos(\phi_o - \phi_m) \quad (2.5)$$

In the equation 2.5, the signal will have a maximum value when the two phases ϕ_o and ϕ_m have the same value (in-phase). The signal S will have a minimum value when the two multiplied signals have opposite phase (completely out of phase). From the equation 2.5 it can be deduced that any sinusoidal components having different phase and frequency would completely diminish or have lower magnitude than the sinusoidal of the same frequency and phase. The A will constitute an

amplitude from the sensor signal and B would be the multiplying gain. As the noise signal will mostly constitute random frequencies and phases, much of the overall noise signal, including that is represented in the equation 2.5, will be reduced. Hence, it is important for the multiplying signal to have the same frequency and the phase as of the modulated signal. If the frequencies are not the same then the equation 2.5 will not result in a DC signal and might contain frequency components that will be filtered out by the low pass filter resulting in lower amplitude [10].

2.2.3 Spectrum Analysis

As we know from the definition of the Fourier series, every periodic signal can be represented as the sum of shifted and scaled (having different phases and amplitudes) sinusoidals. For example, a noise signal from electromagnetic power line of frequency ω_j can be expressed as

$$S_j = \sum_{k=1}^K A_k \cdot \sin(\omega_j + \phi_k) \quad (2.6)$$

The equation 2.6 shows a general form representation of any periodic signal. Most of the noise signals are random and might not be completely periodic but they can be approximated to the equation 2.6 by considering short term periodicity [24]. Now if the signal shown in Figure 2.4 (b) is approximated in the form of Fourier series like the equation 2.6. This approximation will contain sinusoidals of many different frequencies. To find out the strength/amplitude of these sinusoidals, present in the signal, at different frequencies, a Fourier transformation is used. A Fourier transform shows a frequency spectrum of a signal and has the following generalized mathematical form

$$F(\omega) = \int f(t)e^{-j\omega t} dt \quad (2.7)$$

where $F(\omega)$ represents the frequency spectrum of the time domain signal $f(t)$.

Now if we draw the frequency spectrum of the noisy signal shown in Figure 2.4 (b) then it will look something like Figure 2.5. The spectrum shows the signal strength at various frequencies during a specific time interval. The spectrum in Figure 2.5 (a) is taken during one time interval from t to $(t + \tau)$ and the spectrum in figure 2.5 (b) is taken at another time interval from $t + \tau$ to $t + 2\tau$. In Figure 2.5 (a), let's take the signal at frequency ω_o to be the actual signal from the sensor, the signal at frequency ω_k to be from a constant noise source (electromagnetic interference from 60 Hz power line) and signals at ω_i , ω_n and ω_m from random noise sources. It should be noted that the noise signal at ω_i has more amplitude than the actual signal at ω_o during the time interval from t to $(t + \tau)$. Now the spectrum in Figure 2.5 (b) shows that the amplitudes of the random noise at ω_i , ω_n and ω_m is different from Figure 2.5 (a). Whereas the amplitudes of the constant noise source and the actual signal at ω_k and ω_o are the same. The difference is due to the random nature of the noise, which produce different spectrum at different

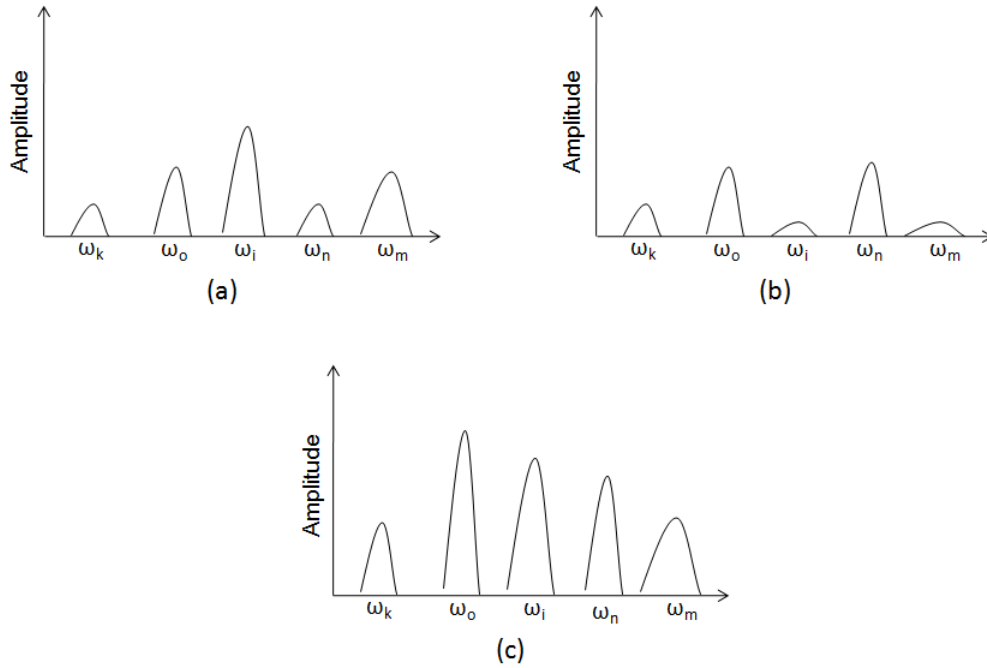


Figure 2.5: Fourier spectrum of the modulated noisy signal. The horizontal scale represents the frequency and the vertical scale represents the amplitude (signal strength). (a) Spectrum during time interval t to $(t + \tau)$. (b) Spectrum during time interval $(t + \tau)$ to $(t + 2\tau)$. (c) The resulted spectrum after adding (a) and (b).

time. Lets add the two spectra in Figure 2.5 (a) and (b), the resulted spectrum is shown in Figure 2.5 (c). The resulted spectrum shows that the signal amplitudes at ω_o , ω_k has doubled while for the rest of the amplitudes the behavior is random, some have increased and some have decreased. If we take many such spectra at different time intervals then summing them all together will increase the signal amplitude linearly, making the strength of the signal much higher than the rest of the noise. Where as due to random nature of the noise, its amplitude will only increase by the square root of the total number of spectra added [25]. This shows that overall strength of the signal compared to the noise will increase resulting in much higher S/N. The overall effect of summation of the signal is achieved by the low pass filter, also referred as averaging filter.

2.2.4 Low pass filter

In general the low pass filter has the following mathematical form

$$S_{out} \approx \frac{1}{t} \int_0^t S dt \quad (2.8)$$

In the equation 2.8, it is desirable to keep the integration time t as high as possible to achieve higher average sample. The longer average sampling will result

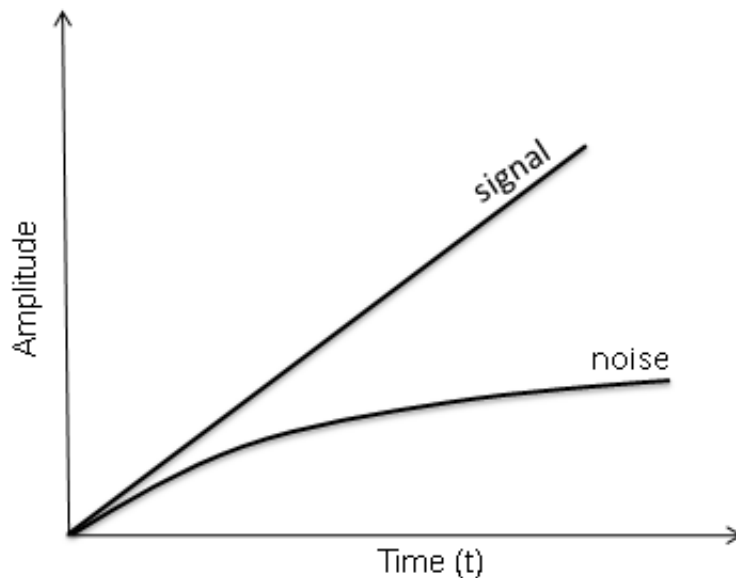


Figure 2.6: The effect of the low pass on the signal and noise. The strength (amplitude) of the signal increases linearly with time while the strength of the noise increases only by the square root of the time.

in higher signal to noise ratio. Figure 2.6 shows the effect of the integration time on the signal and noise amplitude. The signal's amplitude increases linearly with time compared to square root times increase in noise. However, if the relative integration time is too long then it will also average out the actual low frequency changes in the original signal. This is the reason that the modulation frequency f_{mod} is chosen to be much higher than the max operable frequency f_{signal} of the device such that the relative integration time $t = 1/f_{filter}$ could be higher, $f_{signal} < f_{filter} \ll f_{mod}$. By relative, it means relative difference between the reciprocal of the max operable frequency $t_{signal} = 1/f_{signal}$ and the reciprocal of the modulation frequency $t_{mod} = 1/f_{mod}$ such that $t_{signal} > t \gg t_{mod}$. In other terms, higher modulation frequency will generate more cycles that could be summed up in order to increase the signal strength [11].

2.3 Feedback control system

The final goal of the project is to develop a feedback control system for the tip-tilt device. Figure 2.7 shows the tip-tilt system with a feedback control. The current position of the tip-tilt mirror is sensed and fed back to the differential block. The differential block takes in the user input for the desired position (set point) and subtract it from the current position to generate an error signal. The error signal is processed by the control block and an appropriate control signal is generated.

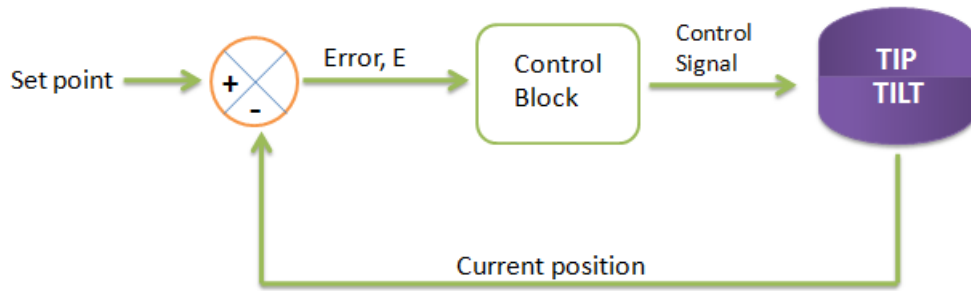


Figure 2.7: Basic structure of the system with feedback control.

The control signal drives the tip-tilt device such that the error signal is minimized as quickly as possible. To develop a good control-block, various approaches are followed. A rigorous approach is to first come up with a theoretical model of the tip-tilt device and then develop a control algorithm based on that model. On the other hand a very well known and much simpler PID control approach could be used [27].

Figure 2.8 shows the implementation of a PID control-block. In the PID approach, the error signal is dealt in three ways to generate a suitable control signal. First, the error signal is simply multiplied by the proportional gain P , second, the error is integrated and then multiplied with the integral gain I and third, the error is differentiated and then multiplied by the derivative gain D . All three results are added to generate the final control signal that will drive the tip-tilt device in minimizing the error. The response of the control system solely depends on the values of these P , I and D gains. To achieve a best response these parameters are rigorously tuned to suitable values.

Figure 2.9 shows some general response of the control signal based on different values of P , I and D . The response has some useful characteristics that are important to discuss. The time it takes for the system to reach the set point i.e, reducing the error to zero, is referred as the rise time. It is desirable to reduce the rise time to minimum to get fast response from the system. However, reducing the rise time comes at the cost of overshoot. The overshoot is the amount by which the systems exceeds the set point. In Figure 2.9, there are three typical responses shown, underdamped, critically damped and over damped. Underdamped is the state when the system has very low rise time but provides some overshoot and oscillates around the set point before settling down. On the other hand, the over damped system has very large rise time but does not have any overshoot or suffers from oscillations. Whereas the critically damped system has intermediate response, with moderate level of overshoot, rise time and oscillations. In general, high values of integral gain I and proportional gain P lead towards the underdamped response. The differential gain D helps in mitigating the oscillations. At the end, normally a trade off is made between these values, depending on the system's need. Sometimes it is more desirable for the system to have minimum rise time with some tolerable

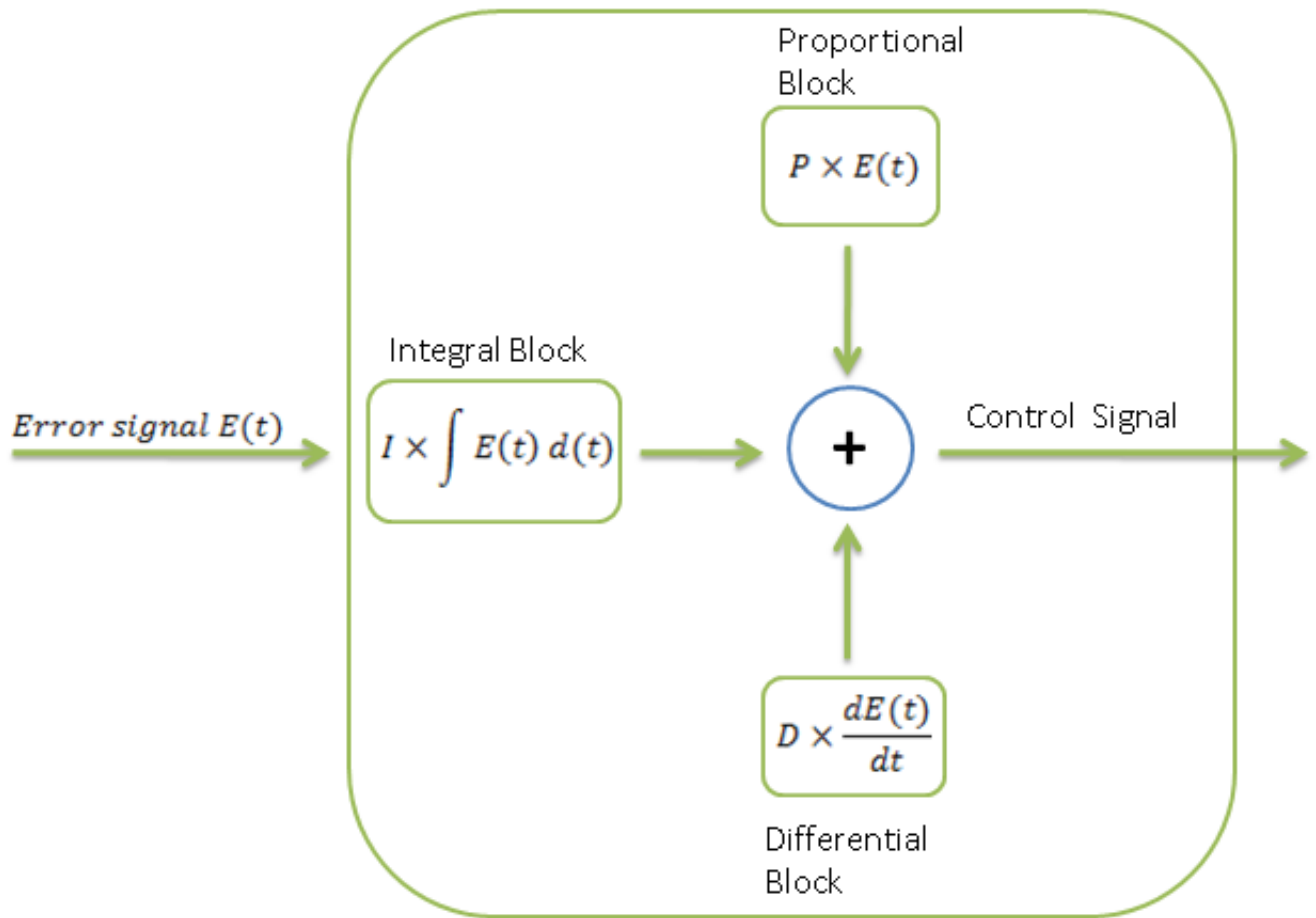


Figure 2.8: PID control block.

overshoot, in other cases opposite might be required. Normally the PID values are tuned in real time, one parameter at a time, starting with P then I and finally D. The response of the system is constantly observed till the desire values are found.

2.4 Embedded Controller and Interfacing

At the heart of every embedded system there is a powerful digital embedded controller, that is responsible for all the controls, calculations and making all the intelligent decisions. The embedded controller could consist of a field programmable array (FPGA), a digital signal processing (DSP) chip, an ARM processor or any 8-bit AVR micro controller. The choice solely depends on the required needs for the processing power and capabilities of the embedded controller. Higher capabilities and processing power comes at a cost of higher budget, hence it is very important to choose the controller that exactly fits with the requirements and needs.

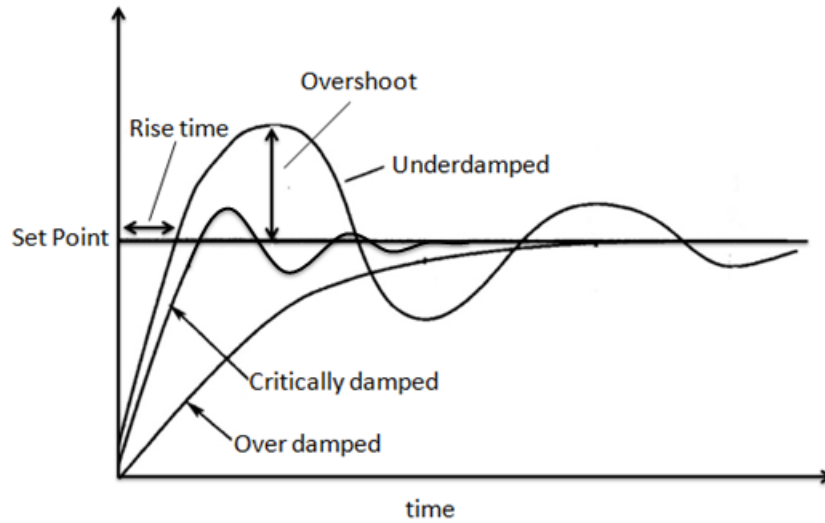


Figure 2.9: Typical response of PID control.

The current need is for a suitable device that can perform all the necessary calculations required for the implementation of phase sensitive detection. A fast analog to digital converter (ADC) with a good resolution of 14 bits. At least two output channels for digital to analog conversion, that can provide the control for two dimensional motion of the mechanical actuator. A suitable USB communication support and some good internally calibrated clock oscillators to produce accurate reference clock for modulation. As there is not much need for many input-output general purpose digital ports and to keep the size of the controller small, the selected controller should have as less number of pin counts as possible. The general purpose digital I/O pins are the ones that are not connected with any specific MCU's peripheral (ADC, DAC, timers etc.). Also, having a high number of pin count leads to a tight pin packaging that adds further complications in the manufacturing of the printed circuit board. As the fast steering mirror device has a dynamic range of about 200 Hz, a modulation frequency of about 10 kHz is a good choice. Any ADC with a sampling rate above 500 ksp/s will suffice for the two dimensional control of the mirror device. However, for all the signal processing and fast filter implementation, a slightly higher MIPS (million instructions per seconds) value for the execution speed of the controller is required, roughly a 32 bit micro-controller running at least 60 MHz clock. Also the tip-tilt device uses a standard 12 Volts 500 milliamps power adapters and the embedded system is required to share its power needs from this adapter. A low power consumption of the embedded system is also a requirement.

There are many micro controller manufacturers, and the most common ones are Texas Instruments, Atmel, NXP semiconductors, ST Microelectronics, Toshiba and Energy Micro. Almost all of them produce microcontrollers having similar kind of capabilities with slight differences. Also every manufacturer has its own development boards and supported software. The writer had a prior experience and training in working with Atmel and Texas instruments devices so the available

devices offered by these two manufacturers were explored initially. The TI 32 bit Piccolo[18] micro-controller(MCU) series offers very suitable features having low power consumption with high MCU operating frequency, ranging from 40 to 90 MHZ. The Atmel Sam3S[19] MCU series has an operating frequency of 64 MHZ and offers similar kind of features as the TI Piccolo series. In all the MCU devices offered by the TI with the device pin count between 44 to 60 pins provided basic functionality requirements of fast ADC, timers and high CPU clock. However, the facility of at least 2 channels digital to analog converter (DAC) was missing. The MCU that provided the facility of 2 channels DAC and had a pin count in the range of 100 pins minimum. Whereas, some of the SAM3S devices are available with pin count of 64 pins offering all the required feature including 2 DAC channels. Hence, the preference is given to the Atmel MCU device.

2.4.1 Development board and supported tools

For the selected MCU device a development tool kit is normally required to perform all the testing and debugging prior to the deployment of the actual system. Generally a development kit involves a programmer/debugger device, a development board that has the MCU, along with testing peripherals and a supported development software. A programmer /debugger has a main functionality of writing the instruction program into the internal flash of the MCU device and the secondary functionality involves debugging the MCU device while it is operational. A development board also has some peripherals like a display LCD, communication connectors (USB, Ethernet, UART), testing buttons and small light emitting diodes attached to some I/O pins of the MCU. The development software provides a suitable environment to develop the program for the chosen MCU device and includes all the necessary libraries and a compiler tool chain to support C programming.

Atmel provides many development boards but they are quite expensive. Another vendor, OLIMEX, also provide some suitable development boards that are much affordable and support some Atmel MCU devices. The Olimex SAM3-P256 development board shown in Figure 2.10 comes with the Atmel SAM3S4B[20] MCU device and provides easy peripheral interface. The SAM3S4B MCU is 64 pins device with 32 bits ARM Cortex-M3 processor architecture running at 64 MHZ. The ARM Cortex-M3 is equipped with many advanced features like memory protection unit (MPU), low power consumption and provides high level 32 bit processing power. The MCU device is equipped with internal calibrated RC oscillators and embedded UART/USB bootloader code in separate 16 KB ROM to support easy device programming using USB/UART interface. The main supported features of the MCU are listed in the table 2.1.

The common supported development software tools are Keil-uVision, IAR and Atmel Studio. The Keil-uVision and IAR are professional tools that support wide range of devices from many different manufacturers and provide a user friendly development environment. However, these tools are not freeware and are expensive to buy. The Atmel Studio is a freeware development software provided by the

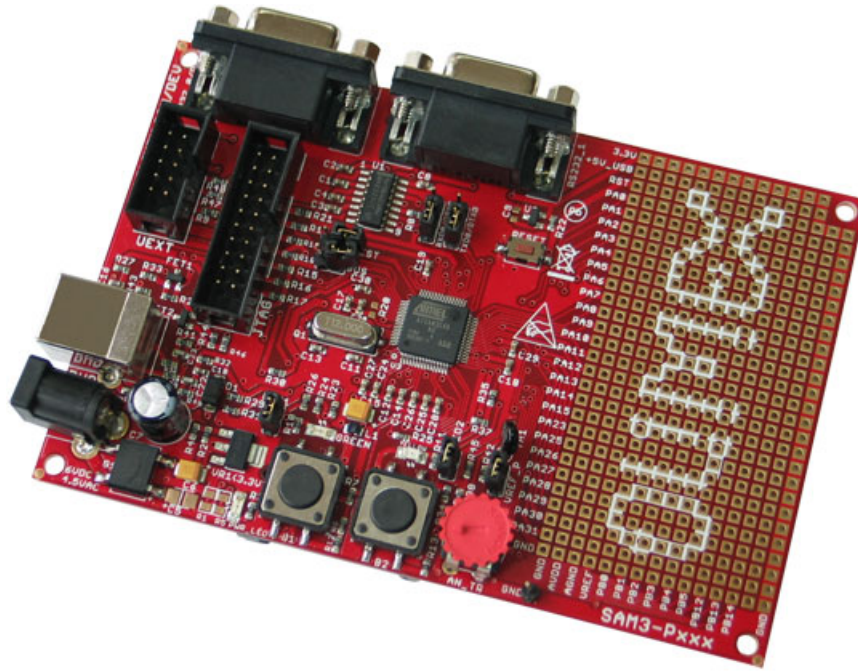


Figure 2.10: Olimex SAM3-P256 development board [16].

Parameter	Value	Parameter	Value
Max I/O Pins:	47	Analog Comparators:	1
USB Interface:	Device	USB Speed:	12 Mbps
ADC channels:	10	ADC Resolution (bits):	12
ADC Speed (ksps):	1000	UART:	4
DAC Channels:	2	DAC Resolution (bits):	12
DAC Speed kspS	2000	Hardware MPU	Yes
Timers:	3	PWM Channels:	4
Operating Voltage (Vcc):	1.62 to 3.6	Diff. ADC Inputs:	5

Table 2.1: SAM3S4B important features[20].

Atmel Inc. and is only limited to support Atmel devices. In this project, the Atmel Studio 6.2 will be used for all MCU software development.

2.4.2 Electronics Interface

In general, micro controller(MCU) I/O pins can supply or sink very little amount of current and lacks driving capability for many simple external electronics. Other than that, the analog to digital converter (ADC) has a specific input voltage range. A signal only in that range can be converted to digital data. If the input voltage falls outside the ADC range then it will possibly damage the device. Similarly, the digital to analog converter (DAC) can output analog voltage in a certain range. It might be often the case, that this range doesn't fulfill the output requirement of your design. Also for UART type serial communication, a standardized voltage signal of dual polarity that can range to ± 10 volts is required, where as MCU

digital pins are only capable of generating voltage from 0 to 3.3 volts. To overcome all these limitations some good, low noise suitable external electronics components are required. This electronics interface will provide a smooth transition of MCU signals to the external system.

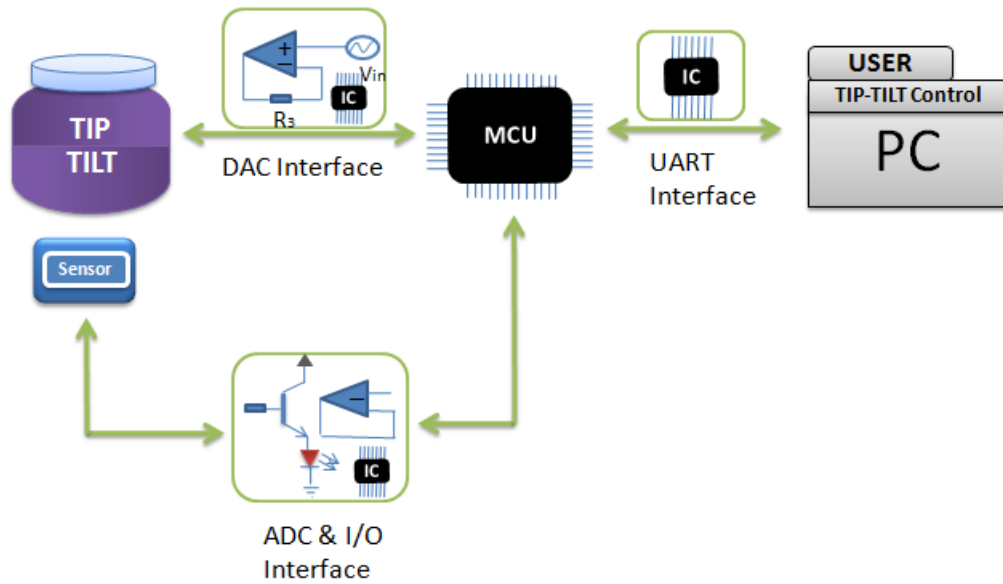


Figure 2.11: Different types of electronics interface, DAC, UART, ADC and I/O required at different stages of the embedded system.

Figure 2.11 shows the external electronics interface at different stages of the embedded system. The DAC interface normally requires some operational amplifiers to amplify and adjust the voltage levels according to the need of the tip/tilt inputs. The I/O interface contains some discrete transistors to drive the sensor. The ADC interface makes use of some low noise amplifiers to adjust the voltage levels. The UART interface uses an integrated circuit that converts the MCU communication signals to standardized UART voltage signals. The exact design and details of these electronics circuits are discussed in the next chapter.

2.4.3 Communication Interface

To connect and control the tip-tilt device by the user software running on a computer, a suitable communication interface between the embedded system and the computer is required. The SAM3S4B MCU provides a universal asynchronous / synchronous (USART/UART) and USB full speed device interface. UART/USART or USB both are suitable for developing communication interface with the computer. However, both have their advantages and disadvantages. The SAM3S4B supports a device USB interface, where the MCU will be connected to a computer (host) via USB as a device. Just like a USB mouse or keyboard device is connected to a computer. The big advantage of USB interface is that it can provide really

fast data rate, upto 12 Mbps. Also the USB interface doesn't require a need of any external interface electronics, like in the case of USART/UART. Further, a modern computer no longer provides USART/UART physical port.

The biggest issue using USB interface is the intense complication involved in writing a driver interface. The USB is designed to provide a single universal interface to connect a vast range of different devices. This puts a burden on the software side to write driver support that has a long , very complicated protocol to accommodate many different kinds of devices. The devices could include large data transfer external storage devices and flash drives, or slow devices like keyboard and mouse that require quick response but less data or intermediate speed devices like printers or scanner. On the other hand USART/UART provides a max communication speed of 230.4 Kbps. It also requires some external electronics interface to convert MCU signals to standardized USART/UART voltage signals. However, the driver interface for USART/UART is much simpler, there are many library supports including windows API , hyperterminal etc. Moreover the USART/UART RS232 serial protocol[46] is much simpler than the USB[17], making its software implementation simpler.

Once the communication interface USB or USART/UART has been developed between the embedded system and the computer, a complete user software is required. The software sends user specific commands to operate the tip-tilt device, mostly consisting positioning coordinate data. More details of the communication interface and software will be discussed in the chapter 4.

Chapter 3

Proposed Approach and Design

This chapter discusses in detail, the approach and design choices that will be followed during the project implementation. From the literature study of sensors it can be concluded that the inductive sensors are not feasible to use in voice coil mirror setup due to strong electromagnetic interference and mechanical sensors do not comply with the required resolution. The rest of the sensors are too expensive to deploy and go beyond the budget requirement for the embedded system. Instead, a novel approach in devising a sensing mechanism is proposed. Based on this mechanism, some initial small experimental tests were performed that provided promising results to pursue further with this new approach. However, this sensing approach suffers from large noise and needs good signal processing technique like the phase sensitive detection in order to achieve reliable sensing output. The next section discuss this sensing approach in details.

3.1 Sensing technique

In this approach, four small surface mount (SMD) package light emitting diodes (LEDS) are grouped together on a small sheet in a configuration shown in Figure 3.1 (a). The LEDS emit red light of wavelength 639 nm and have a rectangular shape with the dimensions of 0.8 x 1 mm [21]. The photo detector[22] with its light sensitive area, shown in Figure 3.1 (a), is used to detect the intensity of light. This photo detector is attached to the mechanical actuator whose displacement is to be sensed. The LEDS are placed on top of the photo detector in such a way that about half of each LED stays outside the sensitive surface of the photo detector and the half directly shines on the sensitive surface as shown in Figure 3.1 (b). The distance between the LEDs and the photo detector is kept at about 1 to 2 mm. Now, if the actuator moves towards left in the horizontal direction, the attached photo detector will also move along and the the left most led will have more light falling on the photo detector than the right most LED, as shown in Figure 3.1 (c). Similarly, if the actuator move in upward direction then the top most LED will have more light falling on the detector than the bottom most LED. If the detector is able to differentiate between the light from all the four LEDS separately then

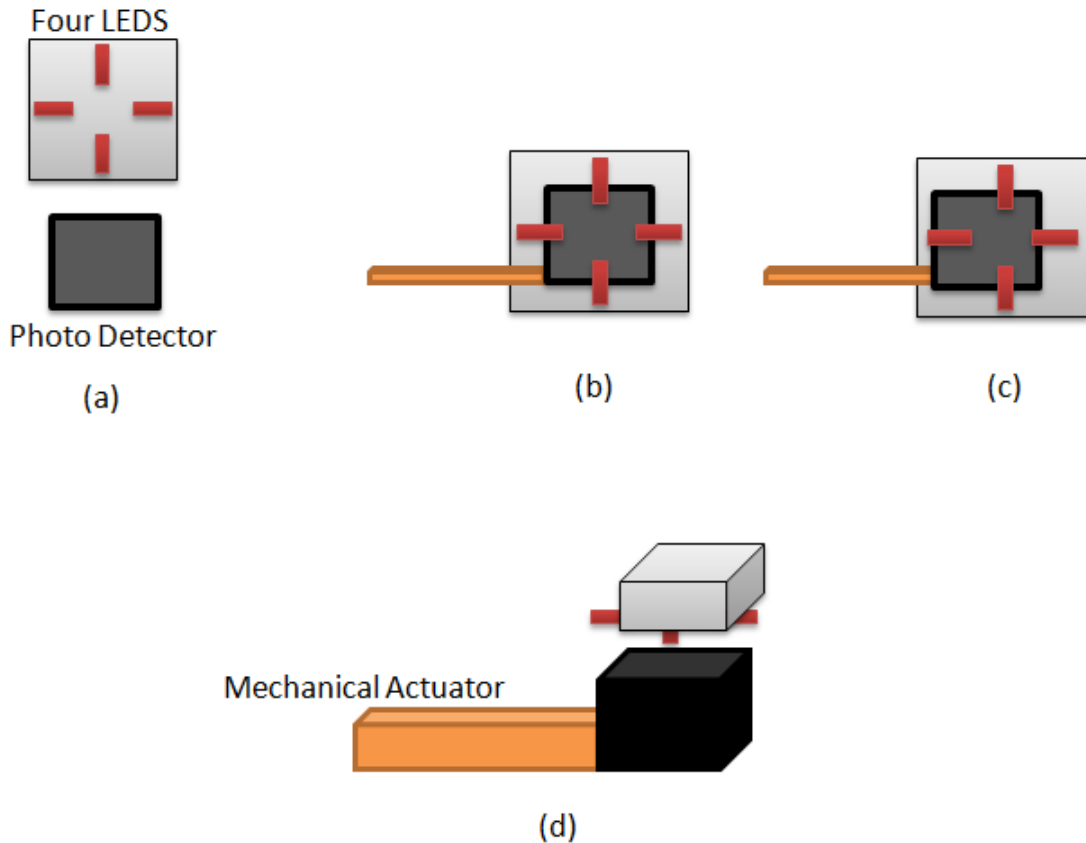


Figure 3.1: (a) Four red SMD LEDs mounted on sheet holder along with the photo detector. (b) Photo detector attached with the mechanical actuator placed in front of the mounted LEDs. (c) The mechanical actuator is displaced to the left. (d) Side view of the assembly.

the two dimensional motion of the mechanical actuator can be detected accurately. This is achieved by driving each LED separately with a 10 kHz 90 degrees out of phase square wave.

Figure 3.2 shows the driving square wave for each LED, namely LED 1, LED 2, LED 3 and LED 4. These four square waves are out of phase from each other such that only one LED is lit at a time and each square wave has a duty cycle of 20% i.e, the time the signal is at high level. The 20% duty cycle means that each LED will emit light only 20% (20 usec) of the total time period (100 usec) of the 10 kHz square wave. During the 5% relaxation gap, no LED will lit, this gap is used to provide some margin for the signal rise time and fall time, as in reality the signal cannot jump from low to high or high to low instantaneously. Now, it is known that which LED will lit at a specific time and by using the technique of phase sensitive detection each signal can be singled out, extracting the information from each LED separately. To apply phase sensitive detection in this specific scenario, the output signal from the photo detector will be multiplied with the same square waves shown in Figure 3.2 having the same frequency and phases. For example, to extract an information from LED1, a square wave of frequency 10 kHz having

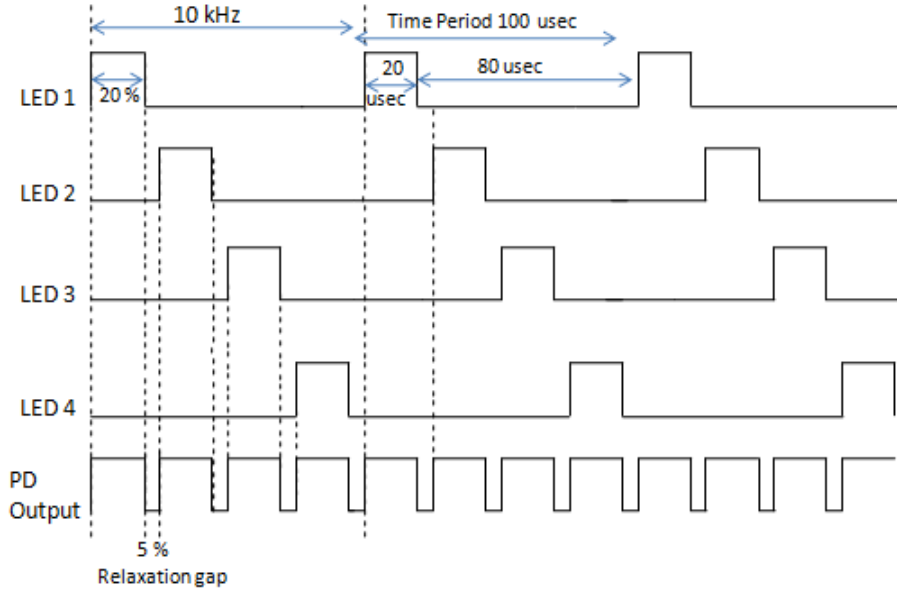


Figure 3.2: The driving signal for the four LEDs and the resulting signal of photo detector (PD). The high state in the signal is considered to turn ON the LED and the low state to turn OFF the LED, the resulting photo current profile is shown in the PD Output waveform.

the same phase as of LED1 modulated signal is multiplied with the PD output, as shown in Figure 3.3 (a).

It should be noted that Figure 3.3 shows more practical PD output with the addition of signal and noise on the carrier wave. After the multiplication, the resulted output will represent the actual information only from the LED1 displacement. Similarly, the displacement information from the LED2, LED3 and LED4 can be extracted by multiplying the PD signal with their respective modulated signals. One important thing to consider is that the multiplying signal should exactly have the same frequency and phase as of the modulated signal. If that is not the case then the resulted output will mix up with other signals and will provide wrong information. As shown in Figure 3.3 (b), the multiplying signal to extract LED1 information has a wrong phase, which leads to mixing of LED2 information and relaxation gap. Finally the extracted output will go through a low pass filter (integrator), to perform the final step of the phase sensitive detection. This will increase the signal strength, leading to better signal to noise ratio. The above proposed approach have many advantages over the conventional use of available sensors. The major advantage is that the hardware assembly is extremely cost effective. Second, it makes the use of modulation and phase sensitive detection a necessary part of the scheme which greatly benefits in noise elimination. However, this approach requires a fast processing power capabilities to perform all the necessary calculations of the phase sensitive detection in time. Also, a fast enough ADC along with good timing control to have reference phases intact and perfectly

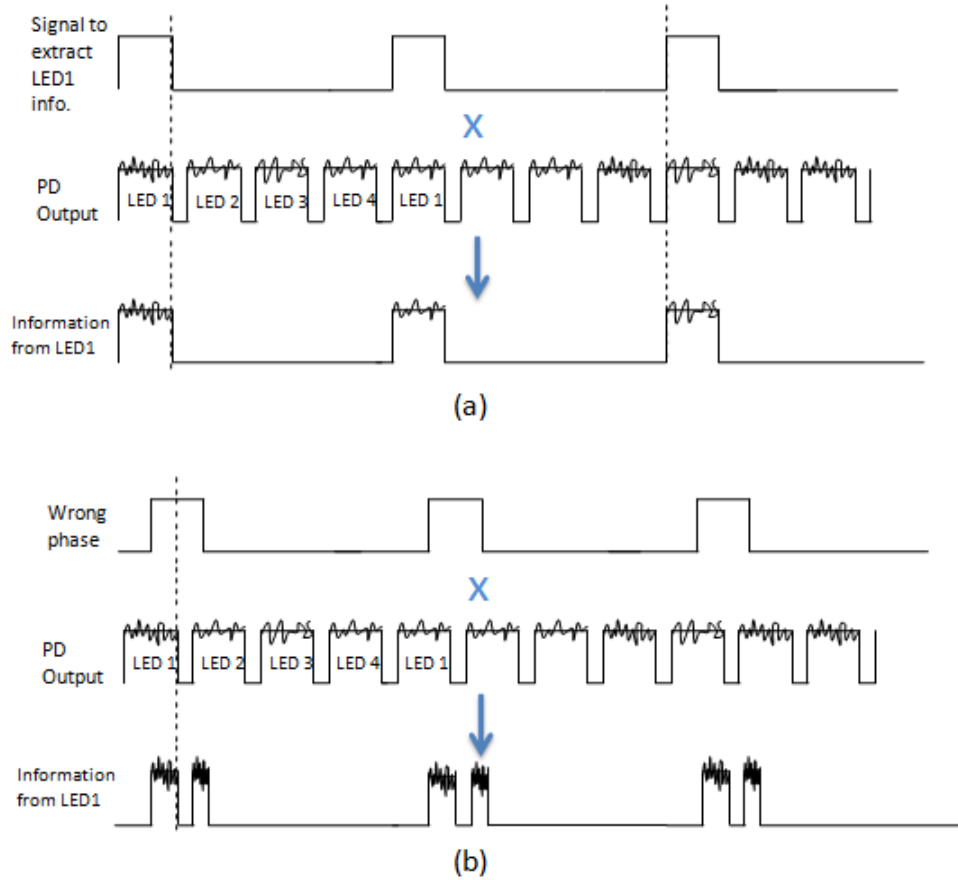


Figure 3.3: Signal extraction from individual LED sources. (a) Extraction of displacement information from LED1 by the multiplication of the PD output with the LED1 modulated signal. (b) The modulated signal having wrong phase, leading to wrong extraction of LED1 information.

synced with the LEDs modulating signals.

3.1.1 Modulated signal

It might have been noticed that the proposed modulated signal for LEDs is a square wave. Where as, in the section 2.2, the suggested modulated signal was a pure sinusoidal. The use of sinusoidal modulated signal led to the equation 2.5, which suggested how the interference signal (noise) of any other frequencies and phase would result in lower amplitude than the actual signal. The reason to use square wave to modulate LEDs instead of a sinusoidal is to reduce complexity. Lets see how the phase sensitive detection can be implemented in electronics circuitry. The more conventional method would be to follow analog circuitry that mainly consists of an analog multiplier and a reference sinusoidal generator. However, the analog circuit majorly suffers from a phase drift and harmonic distortion and a correction of which requires expensive and complicated additives [10]. The phase can drift over time and could lead to wrong multiplication results, like the case

in Figure 3.3 (b). On the other hand a digital approach could be used, which will require a fast high resolution analog to digital converter. In order to generate four separate modulated signals for the LEDs, a fast, high resolution 4 channel digital to analog converter will be required. Also, the generation of four sinusoidal that are exactly 90 degrees out of phase is a quite challenging task, as embedded controllers do not provide separate peripheral for it. On top of that, a more complicated electronics interface (subsection 2.4.2) will be needed to transfer this sinusoidal signal unharmed, to the LEDs. Where as it is much more easier to generate square waves, as the embedded controller provides separate peripherals for square wave generation, discussed in more details in the chapter 4.

Now, lets see if the square wave is used then how it will transform the equation 2.5 and affect the performance. The Fourier spectrum (section 2.2.2) of a square wave with a fundamental frequency of ω_o is shown in Figure 3.4. Figure 3.4 shows that there will be a main sinusoidal component (harmonic) of the fundamental frequency ω_o along with sinusoidals at odd multiples of ω_o (odd harmonics). The sinusoidal at ω_o has a higher amplitude compared to the odd harmonics. The odd harmonics fade away as we move farther from the fundamental frequency. Hence, from Figure 3.4 it can deduced that the major part of the square wave is formed out of pure sinusoidal of the same frequency as the square wave, which will lead to the same solution as of equation 2.5. However, the odd high frequency harmonics present in the square wave will mostly be filtered out, they will slightly contribute in lowering the overall signal strength. In conclusion, tolerating some signal degradation while using simple square wave is still a better trade off.

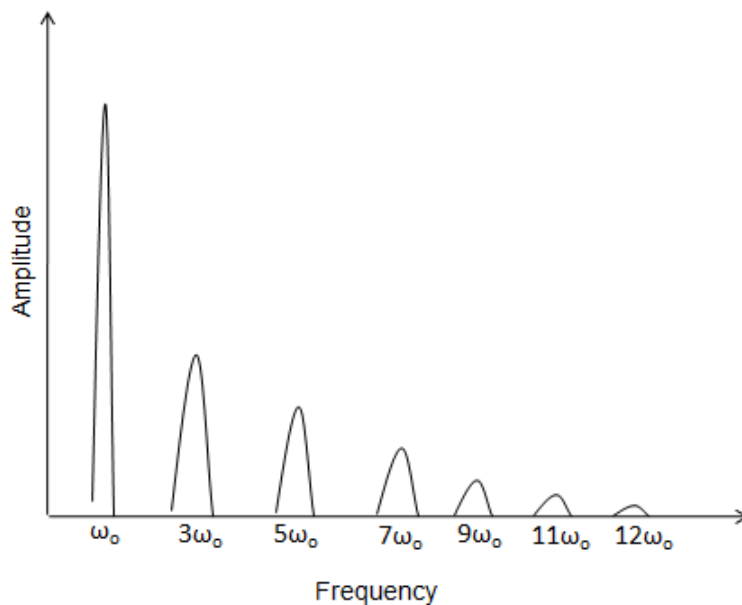


Figure 3.4: Fourier spectrum of a square wave of frequency ω_o .

3.1.2 Moving average filter

The low pass filter can be implemented in certain ways depending on the implementation of phase sensitive detection. Here the phase sensitive detection will be implemented in digital domain, hence an appropriate digital filter will be needed. The most commonly used low pass filter is the moving average filter that provides best performance[26]. This filter is directly deduced from the principle of convolution. Mathematically it has the following form

$$y[i] = \frac{1}{M} \sum_{j=0}^{M-1} b_j x[i + j] \quad (3.1)$$

where y is the output signal, x is the input signal, b_j is the weight and M is the number of points in the average. Each $x[i+j]$ represents the digital sample and b_j is the associated weight with that sample. As the filtration is used to average out the noise and due to random nature of noise all samples should be given equal weight for best performance. Hence, the b_j is chosen to be 1 to get the best results. The main performance parameter for the moving average filter is M , i.e, the total number of points in the average. More points lead to better performance in reducing the noise. However, the M should be within the limits of the max operable frequency of the device (section 2.2.4).

3.2 Analog electronics

This section will discuss the design approach for interfacing all electronics components. Including, the exact components to be used, the reason for their choice, detailed usage and limitations.

3.2.1 Photodetector

One of the main component in the sensor composition is a photodetector. A photodetector is a device that generates electrical current (photocurrent) when a light is fallen on its surface. The magnitude of the photocurrent is directly proportional to the intensity of the incident light. The generated photocurrent is usually very small, in the order of microamperes. The photodetector is generally followed by a very high gain transimpedance amplifier to convert this small photocurrent into voltage. The quality of this voltage signal highly depends on the performance of the amplifier. Choosing a good amplifier design is of utmost importance and it depends on the configuration modes the photodiode is operated. There are generally two photodetector modes, photovoltaic and photoconductive .

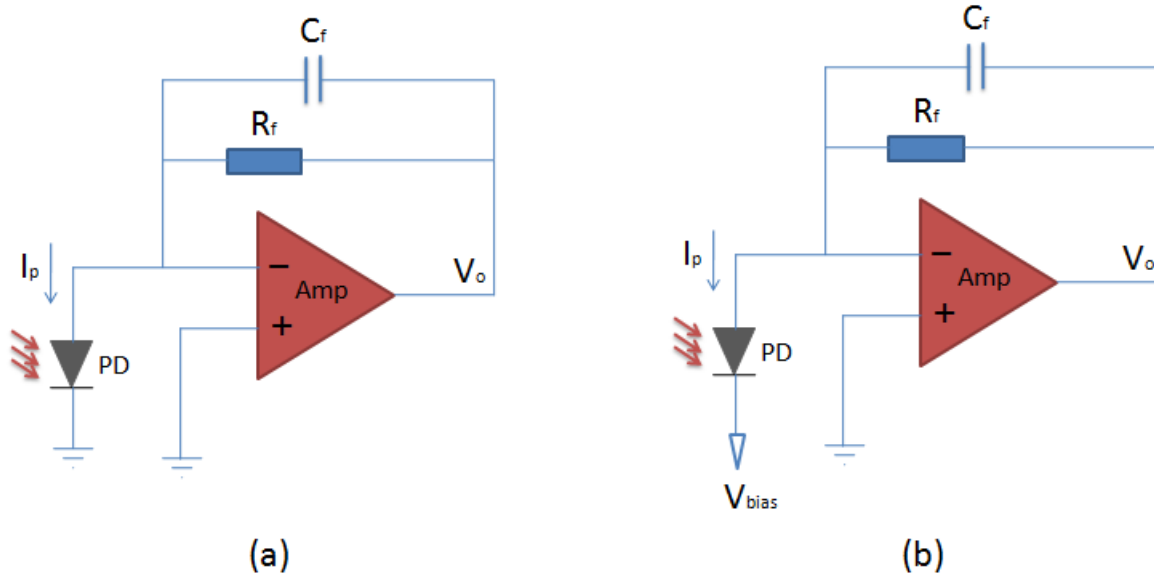


Figure 3.5: (a) Photodiode configuration in photovoltaic mode. (b) Photodiode configuration in photoconductive mode.

3.2.1.1 Photovoltaic mode

In this mode the anode of the photodetector is directly connected to the inverted terminal of the operational amplifier while the cathode is grounded. A large feedback resistor, in the order of megaohms, is used to convert small photocurrent to voltage as shown in Figure 3.5 (a). The output V_o is given by $R_f \times I_p$, where I_p is the photocurrent. The main advantage of this mode is its simplicity and low noise. However, the photodetector exhibit a junction capacitance which is maximum in this configuration. The large junction capacitance means that the photodetector will have a slow response (low bandwidth).

3.2.1.2 Photoconductive mode

In this mode the cathode of the photodetector is reversed biased by an external voltage as shown in Figure 3.5 (b). This will increase the width of the depletion region and reduce the junction capacitance of the photodiode, leading to faster response time, hence a high bandwidth. However, this configuration suffers from higher electron noise. Also, due to increase in the width of depletion region the amount of dark current noise is more than the photovoltaic mode [29].

3.2.1.3 OPT101 Photodiode

To reduce electronics noise due to long wire leads, instead of using an external amplifier, an integrated photodetector with amplifier is chosen. The Texas Instrument OPT101 shown in Figure 3.6, comes with an integrated transimpedance amplifier in standard 8 pins DIP packaging with a transparent top surface. The photodetector has a light sensitive area of 2.286 x 2.286 mm. In this project, due to high requirement of low noise, the photovoltaic mode will be used.

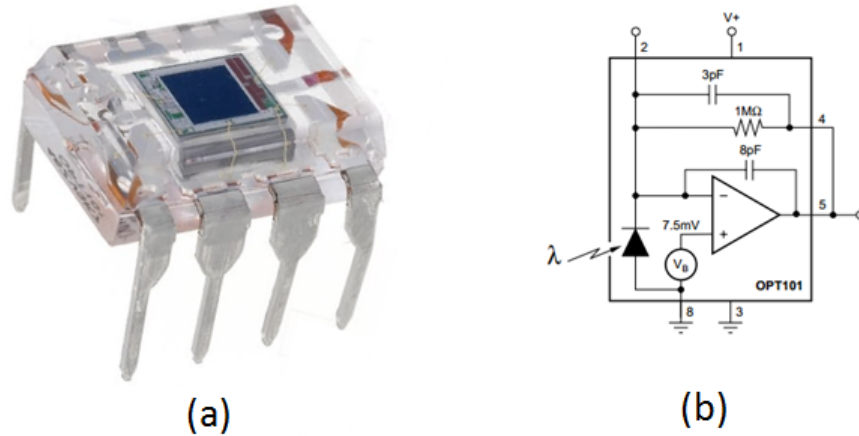


Figure 3.6: Texas instruments OPT101, photodiode integrated with transimpedance amplifier [30].

The internal configuration of OPT101 shown in Figure 3.6 (b) has an internal feedback resistor of 1 MΩ. The value of this feedback resistor can be adjusted by connecting an external resistor in parallel, between the terminal 2 and 5. This will reduce or increase the overall gain of the amplifier. The terminal 8 provides the option of diode operational mode, photovoltaic, if connected to ground, photoconductive, if connected to external bias voltage.

Figure 3.7 shows the OPT101 in photovoltaic mode with external components R_{ext} and C_{ext} . The table shows the effect on the bandwidth for various selection of R_{ext} . It could be seen that by increasing the gain resistor R_{ext} the available bandwidth decreases. As for the modulation frequency of 10 kHz for each LEDs, the PD output signal in Figure 3.2 has a frequency of 40 kHz. So the amplifier should be able to have a bandwidth of at least 40 kHz, which will restrict the value of R_{ext} to be less than 0.1 MΩ (100 kΩ).

3.2.2 LED interface

The chosen LEDs are of red color, emitting light with a center wavelength 625 nm. The spectrum for the responsivity of the OPT101 photodetector and reflective intensity of the LED is shown in Figure 3.8 (a) and (b) respectively. Figure shows

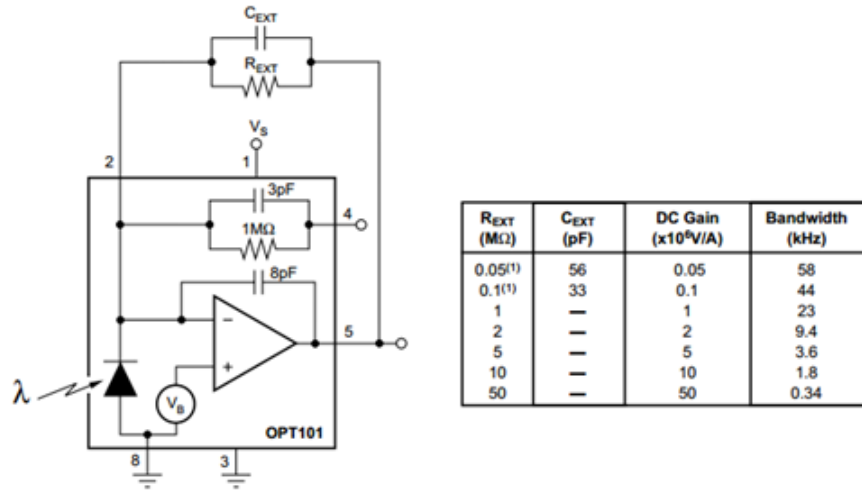


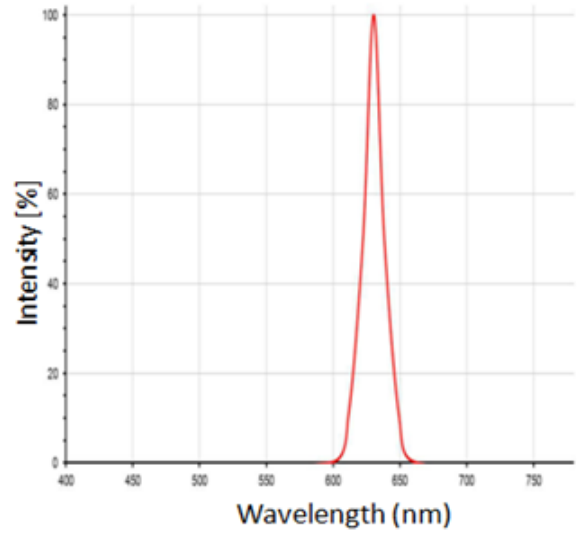
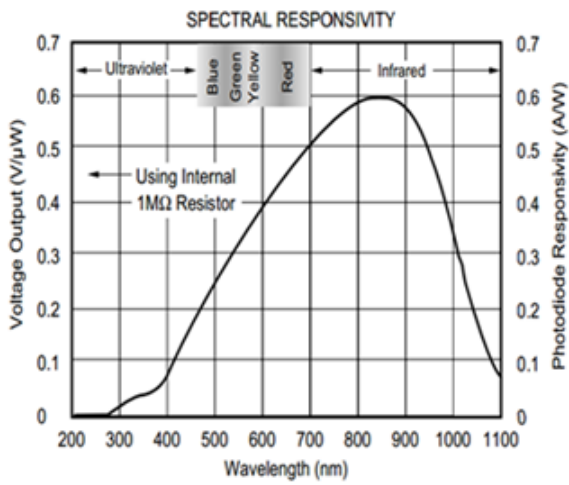
Figure 3.7: OPT101 recommended external component values according to gain and bandwidth characteristic in photovoltic mode [30].

that maximum emitted light from the LED centers at about 625 nm. The photodetector has a responsivity of about 0.43 A/W (72 %) to the 625 nm light. The signal strength can increase if the photodetector has a maximum responsivity of 0.6 A/W (100 %) at 625 nm or if the LED emits light with the center wavelength of about 840 nm . However, with the available cost effective components this is not possible, exploiting 72 % of photodetector responsivity is a better trade off with cost.

The sensor’s four LEDs in Figure 3.1 will be driven by the 10 kHz wave signal in Figure 3.2. This signal will be directly generated from the I/O pins of the SAM3S4B embedded controller. As discussed in the section 2.4.2, this signal lacks the capability to directly drive the LEDs and require an external electronics interface. The single LED has a recommended maximum driving current requirement of 30 mA. Figure 3.9 shows the electronics interface attached to each of the four LEDs. The interface has two main components, the npn transistor and a 30 mA led driver. The PDTC143 npn transistor [32] comes with internal resistors R_1 and R_2 and is capable of delivering max 100 mA of current . The PDTC143 turns the LED, OFF and ON based on the input waveform (high or low), and is optimized for fast switching that can operate at frequencies as high as 230 MHz. The NSI45030AT1G [33] 30 mA led driver is a constant current source. It makes sure that every time the LED is turned ON, only 30 mA current flows through it. The led driver and transistor both come in a small SMD package of dimensions 1.6 x 2.69 mm and 1.8 x 0.9 mm respectively, making them an ideal choice.

3.2.3 DAC interface

The output of SAM3S4B MCU’s digital to analog converter (DAC) has specific electrical characteristic that are listed in the table 3.1.



(a)

(b)

Figure 3.8: (a) Responsivity of the OPT101 photodetector to the incident light[30]. (b) Reflective intensity of emitted light by the LED [31].

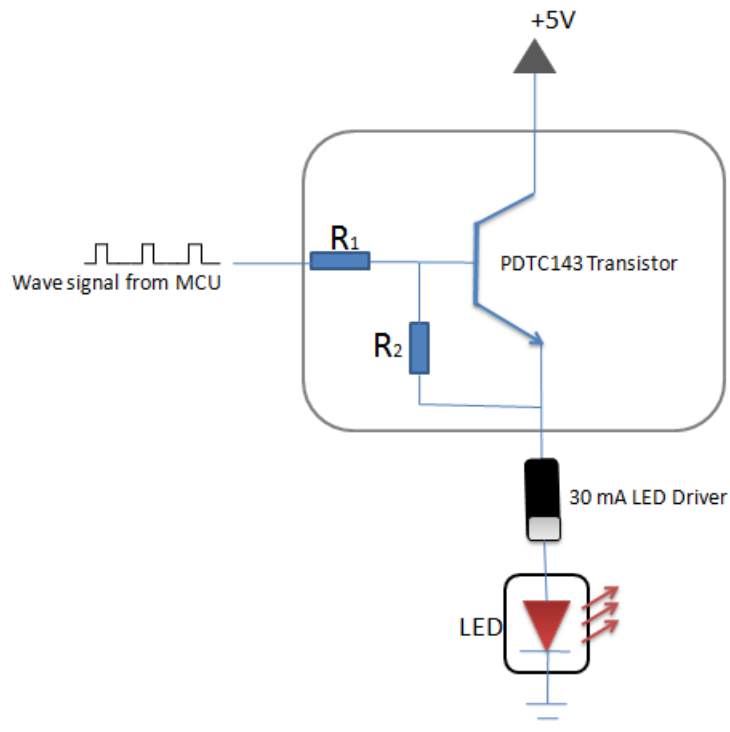


Figure 3.9: Electronics interface for the LEDs, here, $R_1 = 4.7 \text{ k}\Omega$ and $R_2 = 10 \text{ k}\Omega$

Parameter	Min	Typ	Max	Units
Voltage Range	$(1/6) \times V_{ADVREF}$		$(5/6) \times V_{ADVREF}$	V
Output Current	-	-	0.9	mA

Table 3.1: Electrical characteristic of output voltage for the MCU's DAC [20]

The table 3.1 shows that for the 12 bit DAC, at the minimum digital value of 0, the corresponding analog voltage will be $(1/6) \times V_{ADVREF}$ and at the maximum number 4096 (12 bit) the corresponding analog voltage will be $(5/6) \times V_{ADVREF}$. The maximum allowed value for V_{ADVREF} is 3.33 volts, which means the lowest analog output will be $(1/6) \times V_{ADVREF} = 0.555\text{volt}$ and $(5/6) \times V_{ADVREF} = 2.775\text{volts}$. The required output voltage range for the tip-tilt device is 0 to 5 volts, where as the DAC can only provide voltage in the range of 0.55 to 2.775 volts. An external component is required that can map 0.55 - 2.775 volts to 0 - 5 volts. Pulling output from 0.55 volts to 0 is a difficult task if there is no negative voltage supply available. As everything in the embedded system is powered up by single +12 volts adapter, there is no negative supply available. There are some complicated solutions available that could help in generating a negative supply reference from positive 12 volts supply [35]. However, with some trade off, a simple solution is provided by the circuit shown in Figure 3.10. The circuit consist of MC33078, a low noise operational amplifier[34], configured as an inverting amplifier with positive offset. The output V_o is given by the following equation,

$$V_o = \frac{12(R_f + R_i)R_2}{(R_1 + R_2)R_i} - \frac{V_{DAC}R_f}{R_i} \quad (3.2)$$

The term $\frac{V_{DAC}R_f}{R_i}$ defines the inverting gain of the amplifier and the term $\frac{12(R_f+R_i)R_2}{(R_1+R_2)R_i}$ defines the positive offset. The gain term amplifies the 2.775 - 0.55 = 2.275 volts to 5 - 0 = 5 volts providing a gain of $5/2.275 = 2.197$. Hence, $R_f = 5\text{ k}\Omega$ and $R_i = 2.2\text{k}\Omega$. Now after this gain stage the $V_o = - (0.55 \text{ to } 2.775) \times 2.197 = - (1.21 \text{ to } 6.09)$ volts. This -1.21 to -6.09 needs to be brought at 0 to 5 volts, hence a positive offset of + 6.09 is required. The values of R_1 and R_2 are calculated as $\frac{12(R_f+R_i)R_2}{(R_1+R_2)R_i} = 6.09$. One important thing to note is that by adding this positive offset to $(-1.21 \text{ to } -6.09) + 6.09$ leads at 0 to 4.88 volts range. Hence a little adjustment in the values of gain resistors (R_f , R_i) and offset resistors (R_1 , R_2) is required to perfectly map the output at 0 to 5 volts. This adjustment can be performed by selecting the variable resistors and tuning them in real time. As the resistors normally come with 5% tolerance, hence for perfect mapping of DAC voltage, using tunable resistors is an appropriate choice. The only problem with the circuit in Figure 3.10 is that the output V_o will never completely go to zero and will always have an offset of about 200 mV. This is due to the reason of using only a single positive supply to power up the operational amplifier with the lack of negative supply. One solution to overcome this problem is to use a little expensive rail to rail precision amplifier that has a lower offset of about 20 mV [36]. Another solution, to completely remove the bias voltage, would be to use a low noise negative bias generator like LM7705 that provides -0.23 volts reference. The negative bias can be connected to the negative supply of the amplifier [37].

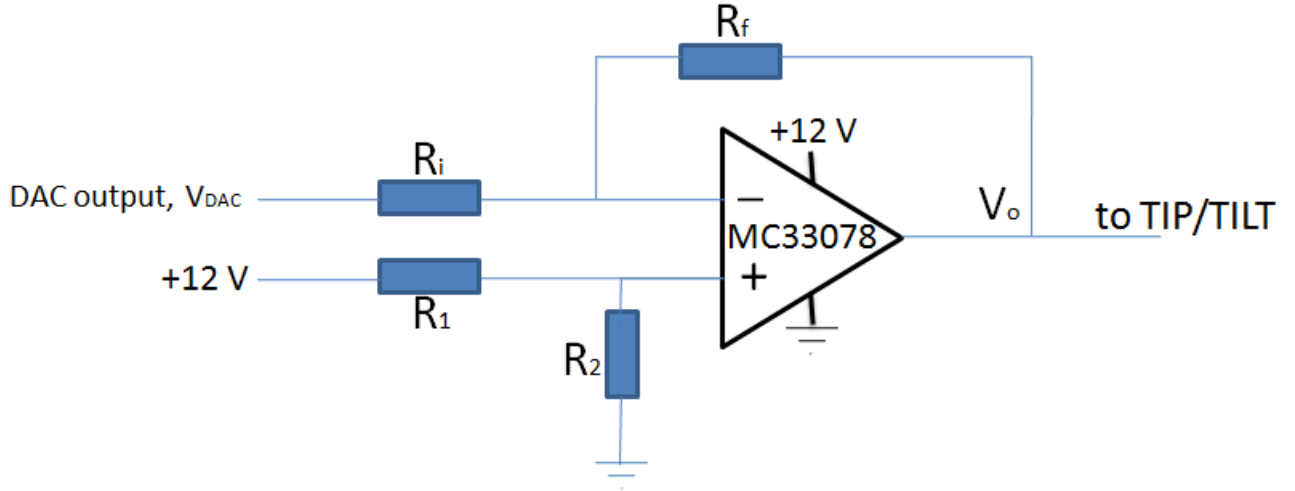


Figure 3.10: Electronics interface for the DAC.

3.2.4 ADC interface

The SAM3S4B ADC unit can convert input voltage in the range of 0 to V_{VREF} to a digital number with a 12 bit resolution at a sampling rate of 1 Mega samples per second. Where V_{VREF} can have a maximum value of 3.3 Volts. It is important to discuss the choice for the value of V_{VREF} as it directly affects the precision of the voltage. The minimum voltage change that can be precisely resolved by the 12 bit ADC is given by the following equation.

$$V_{min} = \frac{V_{VREF}}{4096} \quad (3.3)$$

The equation 3.3 shows that the V_{min} can only be reduced by choosing a low value for V_{VREF} or by increasing the resolution of the ADC. However, reducing the V_{VREF} also reduces the dynamic range of the input voltage. The appropriate value for the V_{VREF} depends on the output range of the voltage signal coming from the photodetector OPT101. According to the sensor configuration (figure 3.1), there will always be some light projecting on the photodetector, giving a non zero offset voltage at the OPT101 output. So the output of the OPT101 will have a voltage range from V_{off} to V_{disp} , where V_{off} will be offset voltage and V_{disp} will be the maximum output swing depending on the gain resistor of OPT101. To map this voltage range V_{off} to V_{disp} at 0 to V_{VREF} , similar kind of circuitry as in Figure 3.10 (DAC interface) will be required.

The limitation of 12 bits resolution leads to quantization error [38], reducing the ADC sensing precision. The fast sampling rate of ADC can be utilized to increase the resolution by the technique of oversampling [39]. Figure 3.11 shows the ATMEL Inc. [40] demonstration of quantization error due to limited resolution of 12 bits and how by using the oversampling technique the resolution is increased to 14 bits. According to this technique the input signal is over sampled and an average over

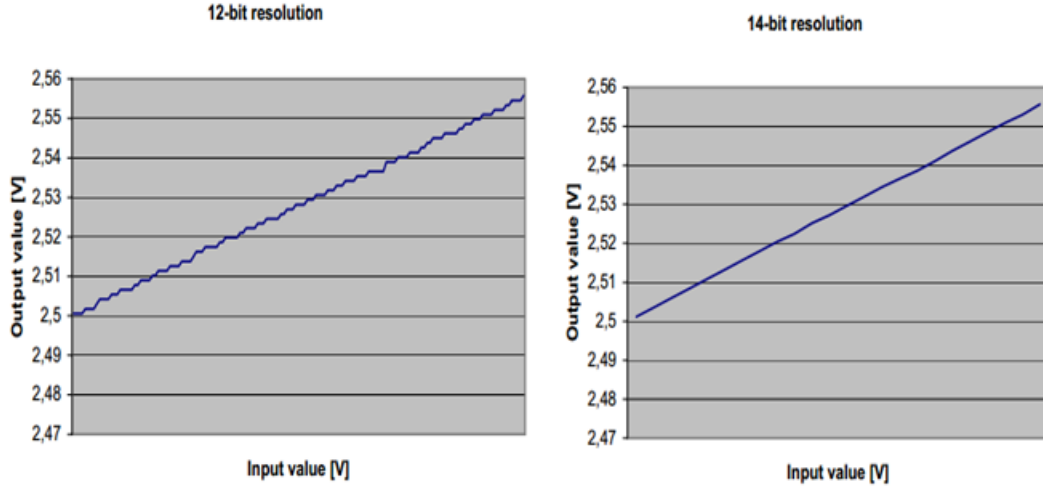


Figure 3.11: Reduction of quantization error due to increase in resolution from 12 bits to 14 bits by the oversampling technique[40].

these extra samples is reduced to higher resolution bits. The oversampling rate required to achieve each extra bit b resolution, is given by the equation 3.4.

$$f_{os} = 4^b f_s \quad (3.4)$$

The b is the extra number of resolution bits desired, f_s is the original sampling rate and f_{os} is the sampling rate required. For example, suppose a sensor produces one reading every one second which is sampled by a 12 bit ADC. To increase the resolution of this ADC from 12 bits to 14 bits, instead of one 12 bits sample, sixteen ($f_{os} = 4^2 \times 1 = 16$) 12 bits sample are taken every second. These 16 samples are added up together and then divided by $2^b = 4$, the resulting average will have 14 bits resolution. Although the resolution is increased by 2 bits, the overall ADC sampling rate is decreased by 16 times. Higher resolution comes at the cost of a decrease in the over all sampling rate of the ADC. Here SAM3S4B's ADC unit can take 1000 kilo samples per seconds, and oversampling by a factor of 16 to increase the resolution to 14 bits will be a good approach. One important thing to consider is that this oversampling techniques has some limitations and only works if the sampled signal is accompanied by some random noise, which is definitive case for the proposed sensor signal. To read more about the theory behind the use of oversampling in increasing the ADC resolution, see the reference [39].

Chapter 4

Implementation

This chapter will include the implementation of the purposed design discussed in the previous chapter. Also the chapter will discuss some deviations from the purposed approach and adapting to new solutions. The implementation also includes programming the SAM3S4B MCU, which includes configuring the specific registers in the MCU. Here, to build an overall conceptual understanding of the current implementation, only a few important register configurations are discussed. For more details on MCU registers and possible configurations consult the MCU datasheet [20].

4.1 Modulated square waves

One of the most important task for the embedded system is to generate four modulated square waves, shown in Figure 3.2, that have the same frequency and are exactly 90 degrees out of phase. There are three possible ways to do that, first is to program four general purpose digital I/O pins of the MCU. Second is to use MCU's PWM peripheral and configure them in such a way that can generate the required square waves. The third way is to use MCU's wave generation peripheral controlled by three independent 16 bits timers.

The first approach of using I/O pins is very much prone to errors. Programming the four individual I/O pins in the main program of the MCU, will not guarantee exact timing delays due to which exact phase synchronization is not possible. The most suitable technique would be to use some independent MCU peripheral, that once programmed, can run independently without any interference from the main program. The second and third option of using PWM peripheral and wave generation timer peripheral provide that facility. Both peripherals can run independently and provide, in some sense, a parallelism with the main program of the MCU. The pulse width modulation (PWM) peripheral is designed to generate pulses, whose duty cycles can be controlled in real time. It is less suitable to generate waves of fixed duty cycle with different phases. On the other hand, the MCU's wave generation timer peripheral is very much suitable for that kind of tasks and will be the best choice for the modulated square waves implementation.

4.1.1 Timers/Counter peripheral

The SAM3S4B MCU has a timer/counter peripheral, containing three independent 16 bits timers. The timer can have a maximum count from 0 to 65535, each count is made by the tick (high or low transition) of the input clock. The block diagram of the peripheral is shown in Figure 4.1. The three timer/counter modules are represented by channel 0,1 and 2. Each channel can be operated separately by its own input clock. Also each channel has two output connections namely TIOA and TIOB, this means three timer/counter modules can generate wave patterns on six different outputs. The state (high, low or tristate) of these outputs depends on how they are configured in their control registers.

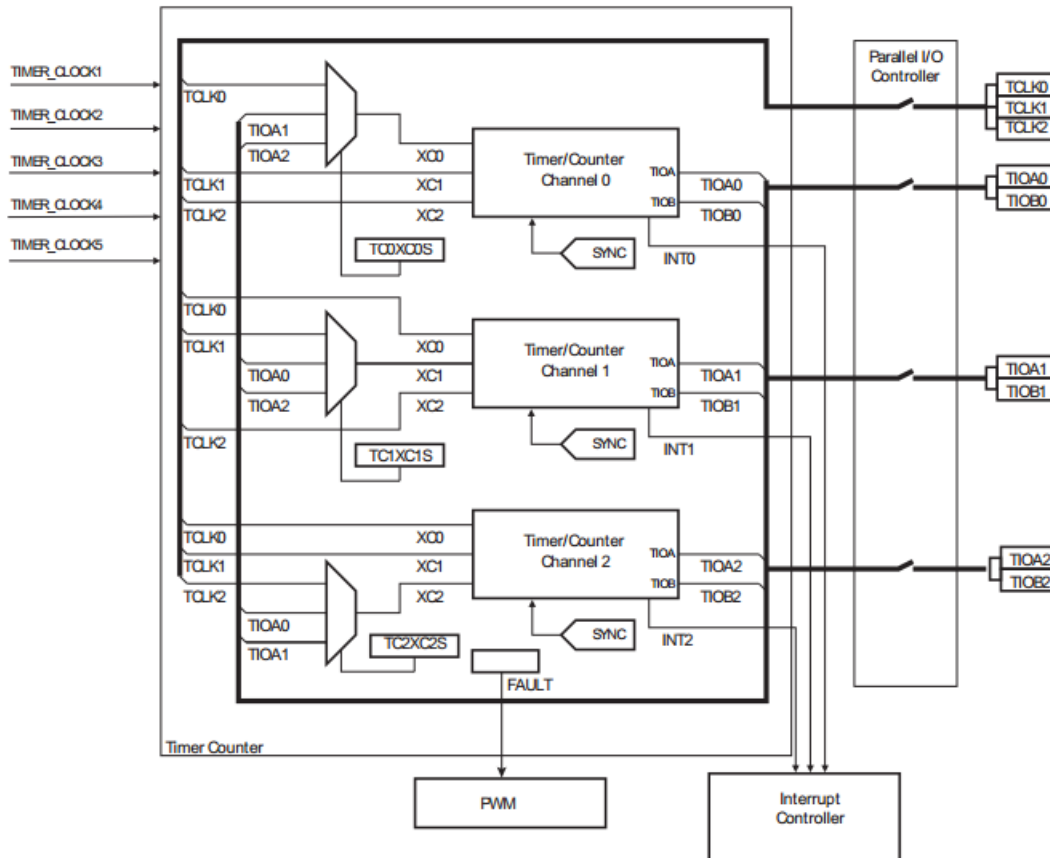


Figure 4.1: Timer/counter peripheral block of the SAM3S4B MCU[20].

4.1.1.1 Input Clock

The three timers can run either by internal clock or external clock. The external clock can be connected to the external pin TCKL, mentioned on the right side of the block diagram, in Figure 4.1. The use of external clock is only chosen when the internal possible clock options are not suitable to the requirement. In our case for the generation of 10 kHz square wave the internal clock option was optimal. The possible clock selection is shown in Figure 4.2. This clock selection can be made

by TCCLKS bits in the Channel Mode Register of the MCU. The MCK represents the main master clock of the MCU, in our case the MCK is 64 MHz. To generate a 10 kHz wave a suitable clock choice for all timers is TIMER_CLOCK1 i.e, 32 Mhz. At this choice, the minimum rate at which the timer/counter can control the state of the associated output pins TIOA/TIOB can be $32/65536 \approx 488$ Hz and maximum rate can be 32 Mhz.

Name	Definition
TIMER_CLOCK1	MCK/2
TIMER_CLOCK2	MCK/8
TIMER_CLOCK3	MCK/32
TIMER_CLOCK4	MCK/128
TIMER_CLOCK5	SLCK

Figure 4.2: Clock selection for each timer channel.

4.1.1.2 Trigger and clock control

Each timer can be disabled, enabled or trigger at demand. When trigger happens the associated timer/counter resets and starts its clock. Figure 4.3 shows the block diagram of the clock control unit for the MCU timers. The timer clock can be disabled by the disable event, or temporarily stopped by the stop event or reset by the trigger event. These events can occur internally by the software control or externally by the external source, depending on the clock configuration. For our case, only the internal trigger event is of importance. There are three types of trigger events, software trigger, SYNC trigger and Compare RC trigger. In the present implementation only SYNC trigger is used. The SYNC trigger is common to all three timers, once this trigger is initiated all three timers are reset. The SYNC trigger can be initiated by setting the TC_BCR bit in the Block Control register of the MCU.

4.1.1.3 Timer modes

The timers can be configured to operate in two modes: Capture and Waveform mode. The waveform mode provides wave generation and capture mode provides measurement on external digital signal. Only the waveform mode is implemented and discussed here.

In general, if four different waveforms are required then there is also a need for four timers but the SAM3S4B MCU has only three timers. However, each timer/counter can be configured to generate waveforms on two different output pins TIOA and TIOB. So the goal is to exploit only two timers, controlling in total four output pins (TIOA0, TIOB0, TIOA1 and TIOB1) to generate four waveforms

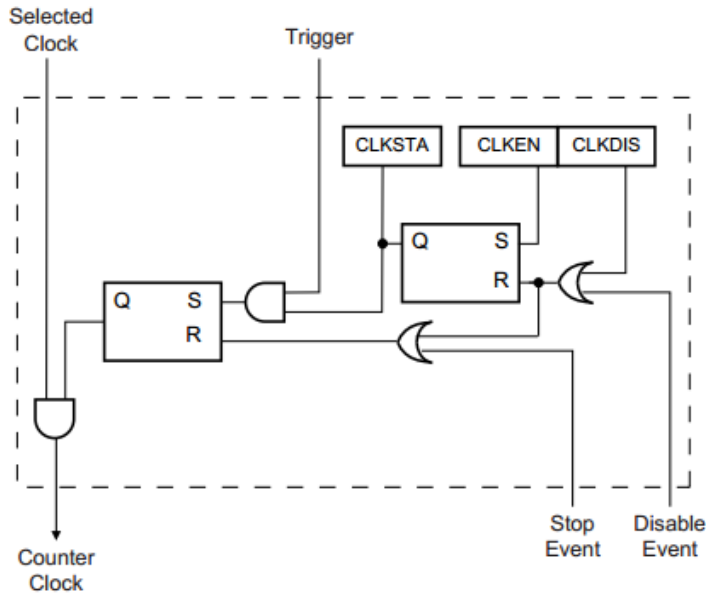


Figure 4.3: Timer/counter trigger and clock control block.

of 10 kHz with exactly 90 degree phase differences. We will see that with proper approach such a configuration is possible within the capabilities of the MCU timers. Figure 4.4 shows the operational features of the timer in the waveform mode. The waveform mode provides a very flexible way to configure the control of the output pins with the help of the three 16 bits registers namely, RA, RB and RC. Three registers can be loaded with custom values. The register RA is associated with the TIOA pins, RB is associated with TIOB pins and RC is associated with the both TIOA and TIOB pins of the timers. The current value of the timer/counter is stored in a register TC_CV, that updates its value at every clock cycle of the chosen timer clock(32 MHz). At every clock cycle(32 MHz) of the timer, these registers are compared with the current value of the TC_CV. On a match with the registers, some specific action can be taken on the timer operation.

Four different actions are possible on the timer operation depending on the value of the WAVSEL bits in the TC Channel Mode Register of the MCU [20]. Here only WAVSEL = 00 operation is implemented. In this condition the timer/counter counts from 0 to 65536 and then resets itself. Figure 4.5 shows the behavior of the timer/counter when WAVSEL = 00. The timer is always influenced by the trigger event regardless of WAVSEL chosen value. Figure 4.5 (b) shows the effect of SYNC trigger, the timer is reset in the middle when the SYNC trigger event is detected.

The state of the output pins PIOA and PIOB can be controlled separately when a match of RA, RB and RC with the TC_CV occurs. By setting the value of ACPA, ACPB and ACPC bits (in the TC Channel Mode Register of MCU) according to the table 4.1, the state of PIOA pin is configured for the match of RA, RB and RC respectively. The state of PIOB can only be altered during the match of RB and RC and is configured by the BCPB and BCPC bits respectively.

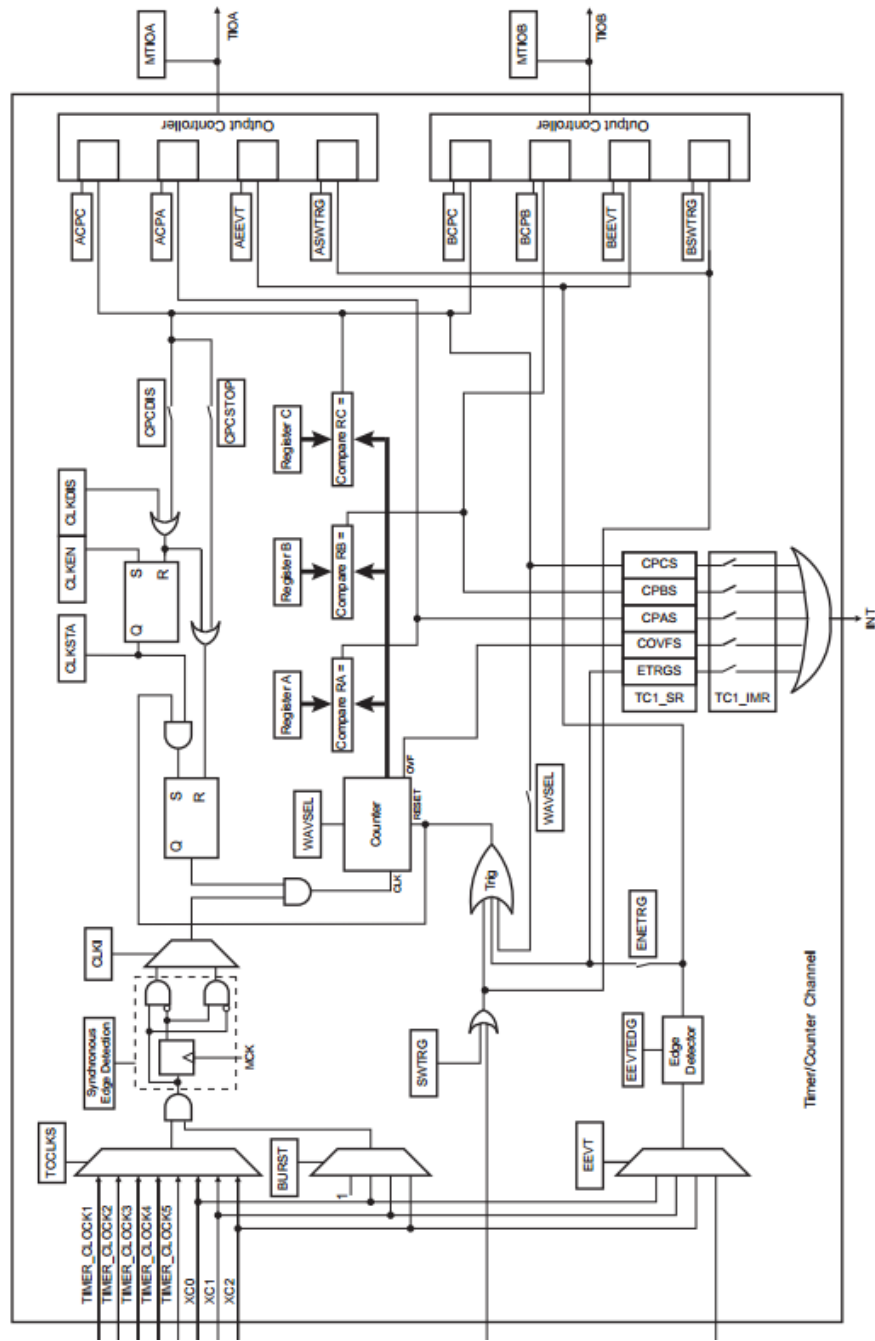


Figure 4.4: Timer/counter functional diagram in waveform mode [20].

4.1.1.4 Waveform mode configuration

The table 4.2 shows the implemented configuration values of several bits. The description column tells the possible meaning of the configured value. The register column tells which associated register match will be effective. The Timer channel and output pin tells the associated timer and effective pin respectively.

Figure 4.6 shows the behavior of the output pins TIOA and TIOB, based on the configuration in the table 4.2. The two timers, timer 0 and timer 1 have separate

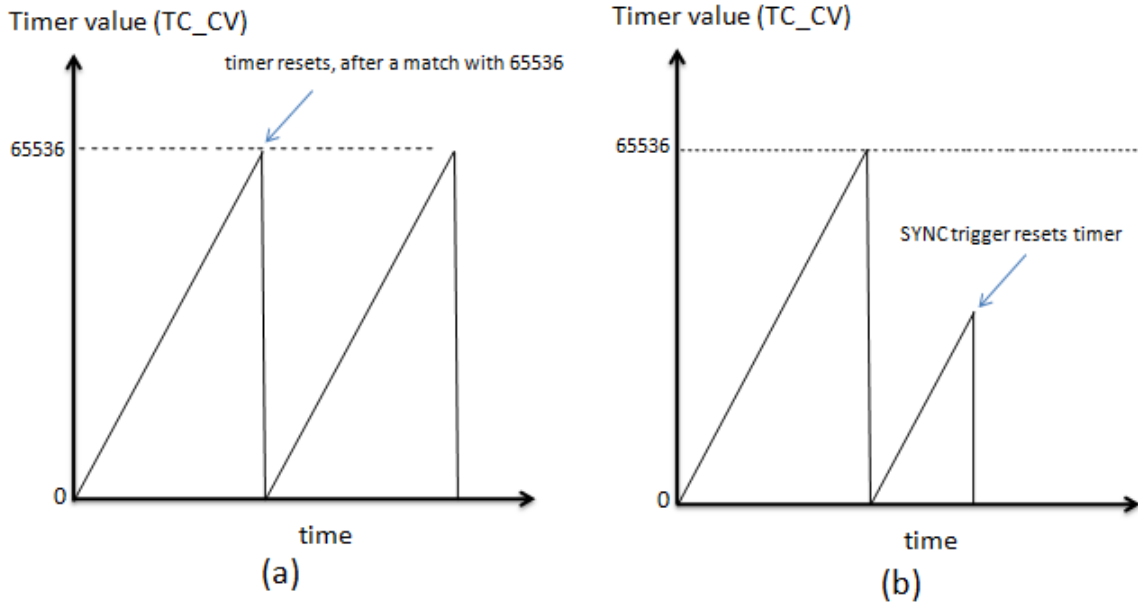


Figure 4.5: Timer operation in WAVSEL = 00. (a) Without initiation of any trigger. (b) With the initiation of SYNC trigger.

Value	Description
0	None
1	Set
2	Clear
3	Toggle

Table 4.1: Possible actions on the state of PIOA and PIOB

counting value that increases with time. The RA register match with the timer 0 turns TIOA0 low and TIOB0 high. Similarly, the RA match with the timer 1 turns TIOA1 high. Note that each timer timer0 and timer1 has separate set of comparison registers RA, RB and RC even though they are named the same. In the same way RB match of timer 0 turns TIOB0 low and RC match of timer 1 turns TIOA1 low and TIOB1 high. Later, the SYNC trigger is initiated that will reset both the timers, turning TIOA0 high and TIOB1 low, and then everything starts over. This process continues and the change in the states of TIOA and TIOB pins results in the four 10 kHz square waves, exactly 90 degrees out of phase. As can be seen that the initial state of output pins is different. In the current implementation, after a SYNC trigger event, the PIOA0 pin is configured as high state while the rest of the pins PIOB0, PIOA1 and PIOB1 are configured as clear (low state). The initial state of the PIOA and PIOB pins after a trigger event, can be controlled by configuring the BSWTRG bits. These bits can be configured according to the table 4.1.

One important thing to note here is that there is no relaxation gap like the one shown in Figure 3.2. With the current configuration capabilities of the MUC

Bits	Value	Description	Register	Timer Channel	Output Pin
ACPA	2	Clear	RA	0	TIOA0
ACPB	0	None	RB	0	TIOA0
ACPC	0	None	RC	0	TIOA0
BCPB	1	Set	RB	0	TIOB0
BCPC	2	Clear	RC	0	TIOB0
ACPA	1	Set	RA	1	TIOA1
ACPB	0	None	RB	1	TIOA1
ACPC	2	Clear	RC	1	TIOA1
BCPB	2	Clear	RB	1	TIOB1
BCPC	1	Set	RC	1	TIOB1

Table 4.2: Configuration values for the generation of four modulated waves.

wavemode timers, it is not possible to generate the waves with relaxation gap. The simple solution to implement the relaxation gap, is to just ignore some initial samples in ADC operation. This will be discussed later in the ADC implementation section.

4.1.1.5 Compare register values

Each of the four waveforms has a frequency of 10 kHz with a duty cycle of 25 %. This means an ON cycle time will be 25μ sec. One count of the 16 bit timer running at 32 MHz, provides a delay of $1/32 = 0.03125 \mu$ sec. Hence, for 25μ sec delay a count value of $25/0.03125 = 800$ will be required. This will be the value loaded in RA compare register of the timer 0 to generate 25 % duty cycle of 10 kHz pulse at the pin TIOA0, as shown in Figure 4.6. In a similar way the value for the other compare register will be chosen. The implemented values of all the compare registers are shown in the table 4.3.

Register	Value	Timer
RA	800	0
RB	800	0
RC	1600	0
RA	1600	1
RB	3200	1
RC	2400	1

Table 4.3: Implemented compare registers values

4.1.1.6 Timer interrupt

Once the waveform mode timers are configured and set to run, the waves will be continuously generated at the associated output pins, independent of the main MCU program. However, it is important to keep track of the state of the generated modulated waves. By knowing the current state of the wave, helps the ADC to

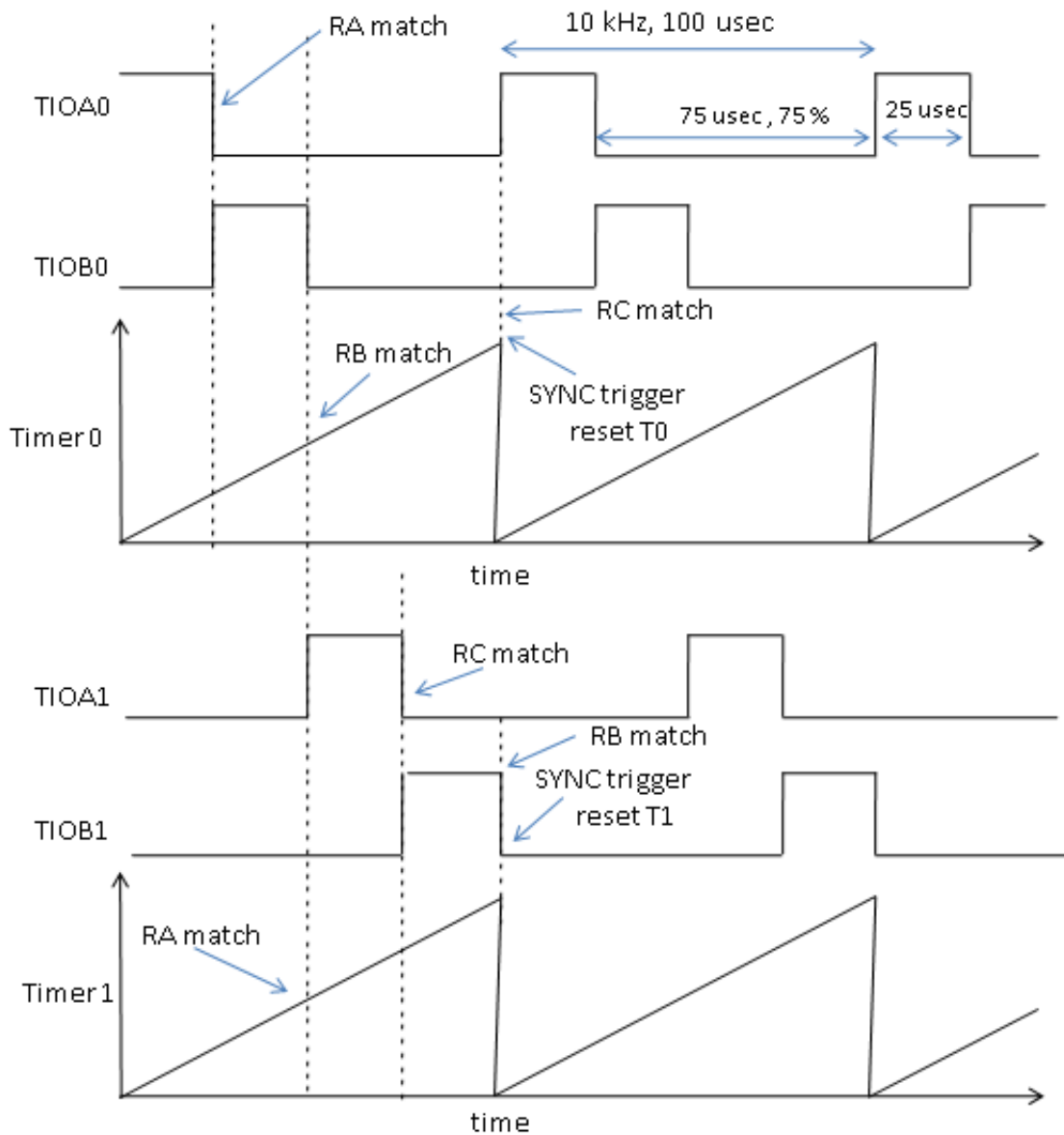


Figure 4.6: The wave generation at the output pins, according to the timers configuration.

track the correct samples from each LED separately. The timer interrupts can be configured to occur at several possible events. Here, the timer 0 interrupt is configured to occur at RA and RB register match. Similarly the timer 1 interrupt is configured to occur at RC and RB register match. It can be noticed in Figure 4.6 that these register match occurs only when the modulated wave, change its state form low to high or high to low. Also at a time, only one of the four waves is at high state, which means only one LED is lit. By knowing which of the four waves is currently at the high state, tells us exactly which one of the four connected LEDS is lit at the current moment. The interrupt event helps tracking this information correctly.

4.2 Analog to Digital Converter (ADC)

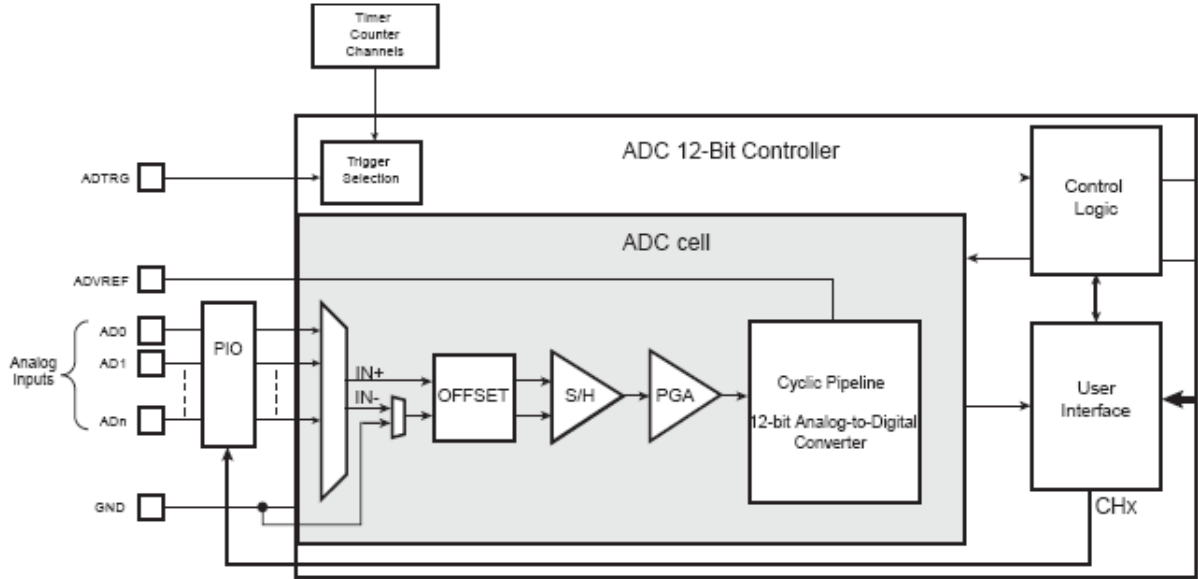


Figure 4.7: The block diagram of the MCU's ADC unit [20].

The SAM3S4B ADC unit is shown in Figure 4.7. The ADC provides 14 analog input channels multiplexed on a single line, with an option of external trigger ADTRG. The reference voltage for the ADC cannot be selected internally and must be provided by the external pin ADVREF. The ADC will convert the analog voltage at the input channel to a 12 bits digital number. The analog input voltage is limited within a range of 0 to ADVREF, where ADVREF can has a maximum value of 3.3 Volts. The maximum achievable sampling rate is 1 mega samples per second (1 Msp/s). This rate is only achievable under certain conditions for ADC operation, otherwise the rate will always be less than 1 Msp/s. The exact sampling rate is also subjected to the way in which the ADC is configured. If more than one ADC channels are used then the sampling rate S_c for each channel is given by the equation.

$$S_c = \frac{S_{max}}{N} \quad (4.1)$$

The S_{max} is the maximum ADC achievable sampling rate and N is the total number of channels used. For example, if four ADC channels are used then the maximum sampling rate for each channel $S_c = \frac{1Msp/s}{4} = 250$ ksp/s. In some cases this S_c could be lower, depending on the ADC mode of operation. Hence, to achieve max sampling rate of 1 Msp/s at one input, it is favorable to use only a single ADC channel. The ADC sampling rate is also affected by the selected ADC clock. Slower ADC clock will result in lower sampling rate. The possible ADC clock selection is given by the equation 4.2.

$$ADC_Clock = \frac{MCK}{(PRESCAL + 1) \times 2} \quad (4.2)$$

The MCK is the master clock of the MCU (64 MHz) and PRESCAL is an 8 bit number ranging from 0 to 512. The 0 PRESCALE value will result in maximum ADC_Clock value of $MCK/2 = 64/2 = 32$ MHz, leading to max ADC rate of 1 Msps. Any lowest ADC_Clock value will lower the sampling rate accordingly e.g, an ADC_Clock value of 16 MHz will lower the max sampling rate to 500 ksps.

There are four modes in which the ADC can operate. Timer trigger mode, external trigger mode, manual software trigger and free run mode. When a trigger event is detected, the ADC starts its conversion and once the conversion is completed, it stops and wait for another trigger. In timer trigger mode, an internal 16 bit timer is configured with a specific value which generates periodic triggers to the ADC. In external trigger mode, the ADC only converts when an external trigger pulse is detected at the pin ADTRG. In software trigger, the ADC is triggered internally by setting the START bit in the Control Register(ADC_CR) of the MCU. In all of these three modes, the ADC is slowed down by 2 MCK cycles, due to asynchronous handling of the trigger signal. Hence the max achievable rate of 1 Mbps is slightly slowed down by the amount of 2 MCK cycles. The free run mode is the simplest and fastest ADC operational mode. In this mode the ADC will continuously perform conversions , one after another, without any subsequent delays. In the current implementation, only one ADC channel is used and the ADC is operated in the free run mode, achieving max rate of 1 Msps. Lets see how by choosing this ADC configuration it helps us in achieving the desired functionality.

Figure 4.8 shows the ADC operation and the sample handling. The ADC is configured to operate at 1 Msps in free run mode with only one channel enabled. The ADC will take a 12 bits sample of analog input from the OPT101, every $1 \mu sec$. This means in $25 \mu sec$ period, the ADC will have 25 samples taken. Out of these 25 samples, first 5 and last 4 samples are discarded while the the remaining 16 samples are added up and then divided by 4. The discarded samples provide the relaxation gap discussed in Figure 3.2. The averaged resulting number will be of higher resolution (14 bits) as discussed with the oversampling technique in the previous chapter. This resulting number will be stored in the respective LED buffer.

As discussed in the previous section (4.1.1.6), the timer interrupt routine keeps track of the current states of the wave signals at the pins PIOA0, PIOB0, PIOA1 and PIOB1. This tracking information helps separating the ADC samples and storing them in the correct buffers. The buffer LED1 BUFF shown in Figure 4.8 contains information from the LED1 signal. Similarly, the LED2 BUFF, LED3 BUFF and LED4 BUFF contain information from the LED2, LED3 and LED4 respectively. These LED buffers are implemented as circular buffers of size 32. A 32 points moving average filter operation is performed on these buffers to provide the functionality of the low pass filter discussed in the section 5.4. Figure 4.9 shows the pin connections that helps in understanding the operation of the signals in Figure 4.8. It shows how the wave signal drives the LEDS and the resulting

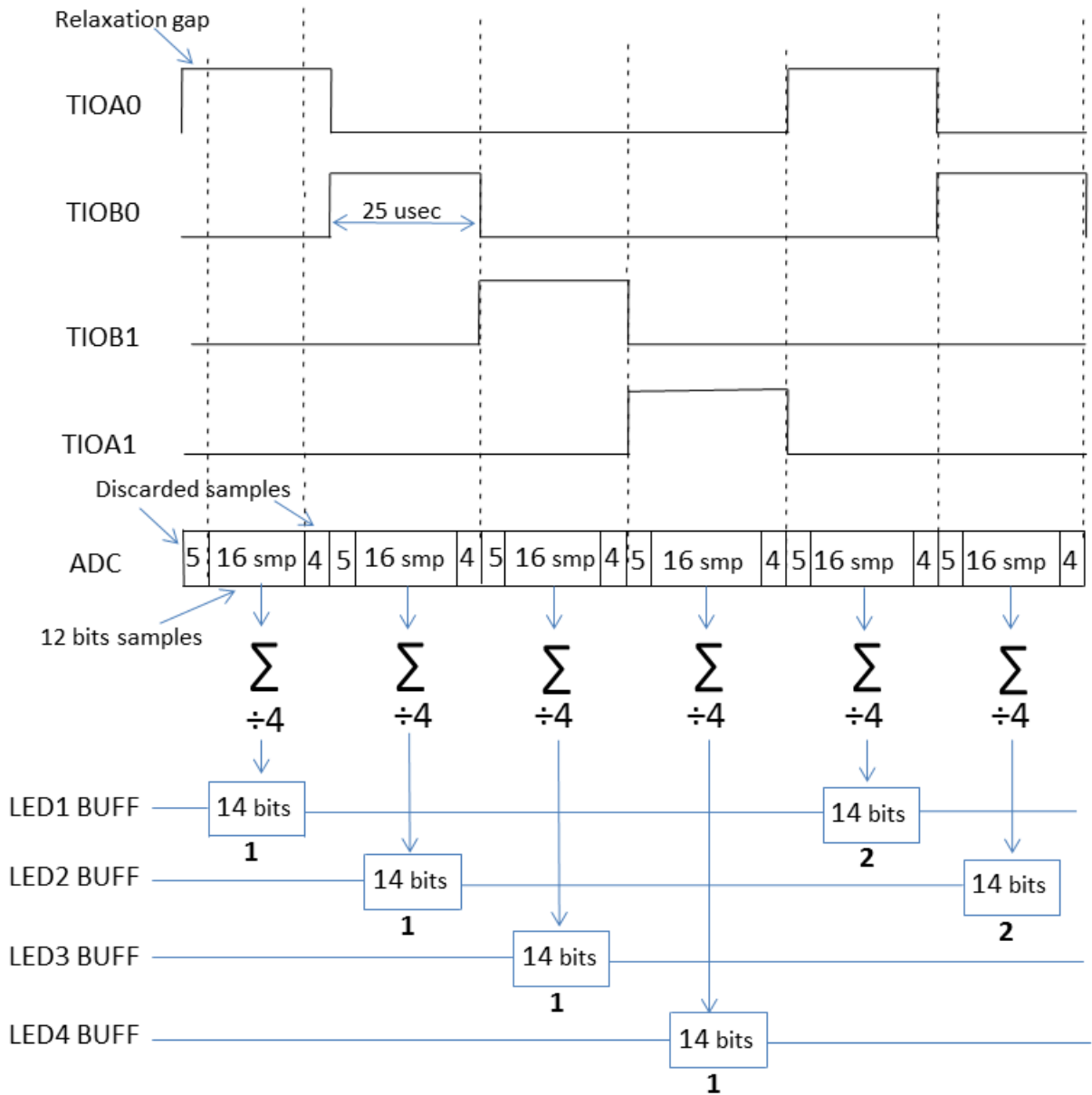


Figure 4.8: The ADC operation and samples handling.

photodetector (OPT101) output is sampled by the ADC.

The final thing to understand is that, by just taking the digital samples (ADC) and later separating them in the respective LED BUFFERS, performs the square wave multiplication discussed in Figure 3.3. All the above operations completes the implementation of the phase sensitive detection discussed in the previous chapter. The following points summarize the overall operation

- The four out of phase modulated signals that drive the LEDs are generated by the timer/counter peripheral.
- The timers interrupts are used to keep track of each LED state.

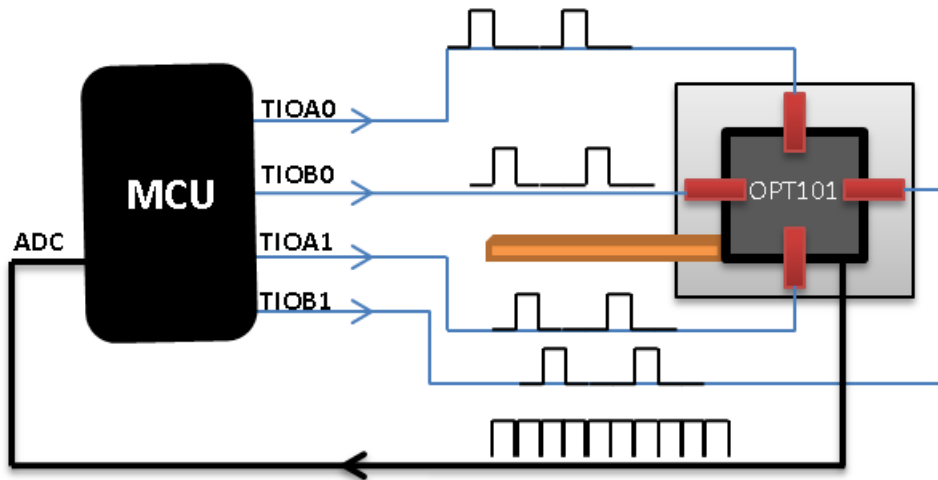


Figure 4.9: The ADC and wave pins connections.

- Based on this tracking, the ADC samples are separated for each respective LED. This separation essentially performs the square wave multiplication discussed in the phase sensitive detection technique.
- Some ADC samples are ignored to provide the relaxation gap mentioned in the 3.2.
- The oversampling is performed and the extra 16 samples are averaged out to increase ADC resolution to 14 bits.
- The resulted 14 bits samples are stored in their respective buffers of size 32. The 32, 14 bits stored samples are passed through the operation of moving averaging which completes the final step of low pass filtration in the phase sensitive detection technique.
- The resulted signals from these four buffers, after the averaging operation, contain the final information from each LED.

Now, one should be able to clearly relate the theory of the purposed technique discussed in the previous chapters with the current implementation.

4.3 Digital to Analog converter (DAC)

The DAC unit shown in Figure 4.10 has two output channels DAC0 and DAC1. It can convert a 12 bits number into an analog voltage. If the both channels are used, then each channel can has a conversion rate of 1 Msps, otherwise a single channel can operate at 2 Msps. The DATRG pin provides the functionality of

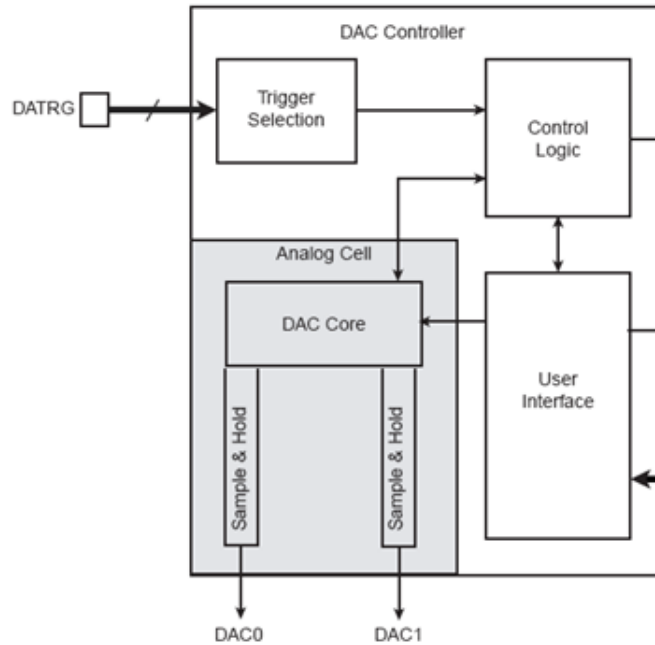


Figure 4.10: The SAM3S4B DAC module.

external trigger in the same was as the ADC external trigger ADTRG. The tip-tilt operation is controlled by the two DAC channels, providing two dimensional control of the device.

The DAC configurations are much simpler than the ADC. The DAC is configured to operate in a free run mode (max speed mode). In this mode whenever two 12 bits numbers are written in the MCU DACC_CDR register, they are converted to analog output. The only thing to be aware of is the DACC_CDR register should not be written at a rate faster than 1 mega times per second. This can be ensured by checking the ready flag TXRDY bit (DAC mode register) before writing the DACC_CDR register.

In the current implementation, there is no need to configure the DAC interrupt, the value is directly written to the DACC_CDR register which is converted to the analog output. The DAC_CDR is a 32 bit register and is written in a specific order. The first 12 bits of DACC_CDR[11:0](DD1) and the 12 bits at DACC_CDR[27:16] (DD2) are used to write two 12 bits conversion values. The 2 bits at DACC_CDR[13:12] are used to specify the corresponding DAC channel where the DD1 will be put. 0 means DAC0 channel and 1 means DAC1 channel. Similarly, the 2 bits at DACC_CDR[29:28] are used to specify the output channel for DD2 data. In the current implementation DD1 is put at DAC0 channel and DD2 is put at DAC1 channel. One important thing to configure is the refresh rate of the DAC output voltage. The analog voltage at the DAC output channels will start to lose its state after $20 \mu sec$. To stop this from happening, a DAC refresh period is configured in the DACC mode register of the MCU [20]. Last but not least is to configure the slew rate of the DAC analog output. The slew rate is the rate at which the DAC output voltage changes with time. In the current configura-

tion the max slew rate of $11 \text{ V} / \mu\text{sec}$ is set. In the max slew rate configuration, the MCU consumes a little more power but provides faster response to the requested analog voltage change.

4.4 Universal asynchronous receiver transmitter (UART)

Figure 4.11 shows the UART interface. The baud rate is generated from the MCU's master clock MCK. The 4.11 (b) shows the baud rate selection mechanism. The baud rate selection is done by the following relation, $BaudRate = \frac{MCK}{16 \times CD}$, where CD is the 16 bit value written in the MCU's UART_BRGR (Baud Rate Generator Register). In this implementation a baud rate of 256 kbps is used. This is the maximum baud rate that is supported by the windows API serial programming, used on the connected computer. The two MCU's pins, UTXD and URXD are used to transmit and receive data respectively. To transmit data on UART port is very simple, the Atmel studio compiler provides a library support to use the C *printf* function. This function directly output any the data on the transmit UTXD pin. The *printf* works in exactly the same as the standard C function. However, to receive data on URXD pin, the standard C *scanf* function doesn't work.

Every byte received on URXD must be dealt manually. This is done by first enabling the receiver interrupt. The interrupt will be initiated by the MCU, every time a byte is received on the URXD pin. Second, a communication protocol is defined to extract meaningful information from each received byte. Figure 4.12 shows the structure of the communication packet. Each packet has four different markers, recognized by the characters *s*, *n*, *c* and *e*. The character *s* identify the start of a packet and tells that subsequent bytes would contains information about the set point for the X-coordinate (horizontal position) of the tip-tilt mirror. Similarly, the marker *n* identifies the end of X-coordinate information and the start of the Y-coordinate information in the subsequent bytes. The character *c* identifies the end of Y-coordinate data and indicates the start of configuration information in the next byte. Finally, the *e* character marks the end of the packet. The packet is decoded in the URXD interrupt service routine and the respective data is put into the appropriate buffers. The configuration byte contains information for specific functionality, listed in the table 4.4. If the configuration byte contains a value 2 then it means that the Integral gain parameter of the PID controller will be increased by 0.001. Similarly, the functionality of the values 3,4,5,6,7 and 8 can be deduced from the description given in the table 4.4.

The MCU only transmits certain kind of information to the connected computer. This information can be selected by the configuration byte value 9,10 and 11, *Print Y info.*, *Print X info.* and *Print current PI parameter values* respectively. If *Print Y info.* is chosen, then the MCU will only send information about the Y coordinate i.e, the current set value for vertical (Y) position , the current Y position read by the sensor and the current output value after the PID calculations. The *Print PI current values* will send the current values of the PID gain

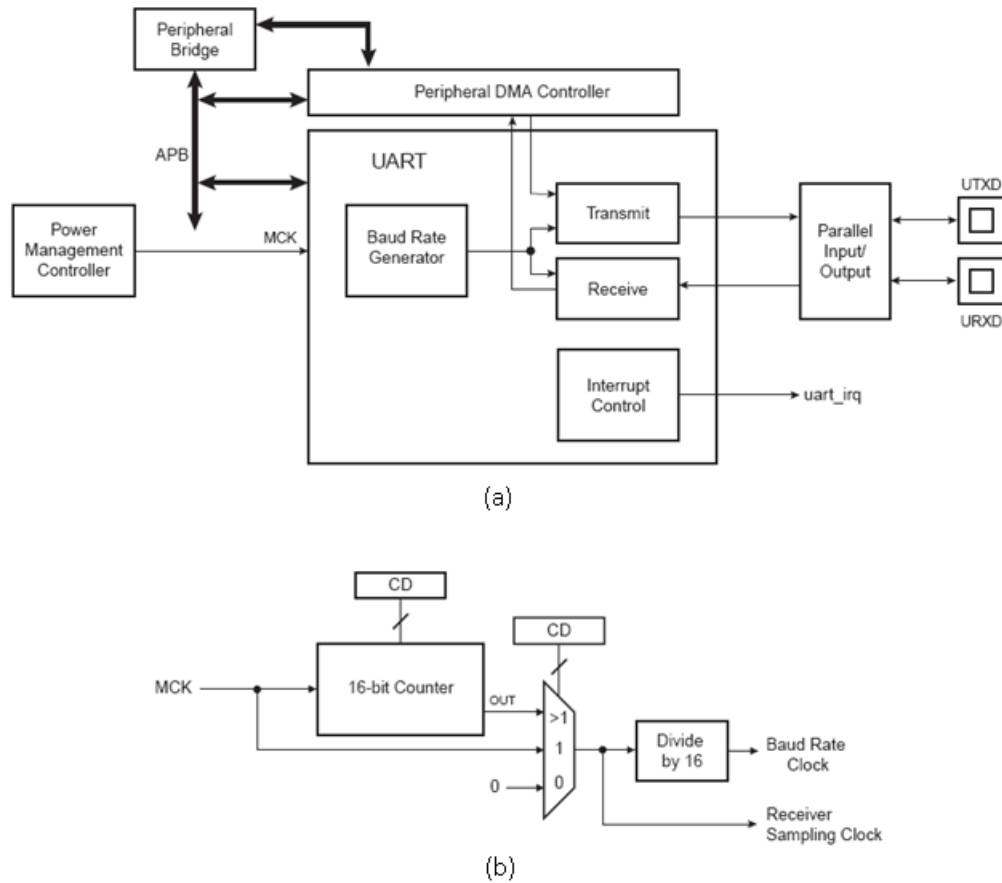


Figure 4.11: (a)UART block of the MCU. (b) Baud rate selection from the master clock(MCK)[20].

parameters P and I.

The UART also supports byte level parity check as an error detection mechanism. If the parity check fails on a byte then it is discarded. The complicated error correction/detection mechanism like Cyclic redundancy check (CRC) check was considered but not implemented. Because all the packet decoding was done in the interrupt service routine (ISR), hence it was desirable to keep the packet length short and avoid extra calculations.

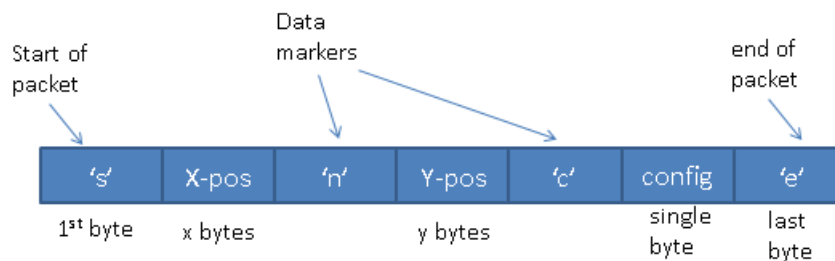


Figure 4.12: Structure of the communication packet.

Value	Function
2	I+0.001
3	I-0.001
4	P+0.01
5	P-0.01
6	Reset P and I to initial values
7	PID OFF
8	PID ON
9	Print Y info
10	Print X info
11	Print PI current values

Table 4.4: Configuration value with its defined functionality.

On the computer side, there is no serial port available. A FTDI US232R-100[45], USB to serial converter, shown in Figure 4.13 is used to provide the serial interface from the computer side. The US232R-100 converter comes with the supported driver that creates a virtual serial communication port in the operating system. This virtual communication port acts like a normal standard serial port. The windows application interface (API)[46] provides an easy programming interface to establish serial communication via this virtual port. That's how a two way serial communication between the computer and the embedded system is established.



Figure 4.13: FTDI US232R, USB to serial converter .[45].

4.5 PID Controller

The PID controller implementation performs operation of the feedback control system discussed in the section 2.3. The main program of the MCU performs only two tasks, PID calculations and putting resulted values in DAC unit.

The following code lines extracts the current position information from the LED signals stored in the buffer after the low pass filtration step (4.2).

```
Xpos = buff_led1 - buff_led0 - offsetX;
```

```
Ypos = buff_led3 - buff_led2 - offsetY;
```

The *Xpos* stores the current tip-tilt position in horizontal direction. Similarly, the *Ypos* stores the current position in the vertical direction. The *offsetX* and *offsetY* are used for calibration to remove any initial offsets.

```
errorX= setX - Xpos;

errorY= setY - Ypos;
```

The *setX* contains the user input for the horizontal position and *errorX* stores the difference between the current (*Xpos*) and the required position (*setX*). Similarly, the *errorY* stores the difference for the vertical position.

```
Xsum = Xsum + errorX;

Ysum = Ysum + errorY;
```

The *Xsum* performs the integration step in the PID control block (section 2.3). It sums up the *errorX* with its previous value.

```
outX = Pgain*errorX + Igain*Xsum ;

outY = Pgain*errorY + Igain*Ysum ;
```

Finally the *outX* will contain the control signal for the horizontal position control. The *Pgain* and *Igain* are the P and I gains of the PID algorithm (section 2.3). The differential gain D is omitted in the current implementation as only the P and I were enough to get good control response. These *outX* and *outY* control signals are fed to the two DAC channels that will control the motion of the tip-tilt device.

4.5.1 Fixed point implementation

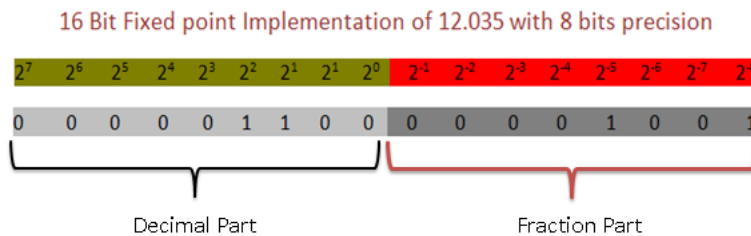


Figure 4.14: Fixed point implementation with 8 bits precision by using 16 bits integer.

In order to have good performance from the PID control, a fixed point arithmetic support is required. The *Pgain* and *Igain* require floating point (fixed point) values and all the calculations should be done in fixed point arithmetic. The

SAM3S4B architecture does not provide fixed point arithmetic support and only supports 32 bit integer arithmetic. Figure 4.14 shows an example of fixed point implementation of 12.035 using a 16 bits integer. Out of these 16 bits, 8 bits are used to represent the fraction part(.035) and the other 8 bits are used to represent decimal part(12). For more information on the fixed point implementation see the reference [28].

In the current implementation a faster technique that make use of shift operation is used to provide the approximated support for fixed point arithmetic. The following code shows the currently used fixed point implementation

```
Pgain = 12; // 0.012 = 12/1000
Igain = 3; // 0.003 = 3/1000
FIXED_POINT = 10;

outX = (Pgain*errorX + Igain*Xsum); // Integer arithmetic

outX = (outX>>FIXED_POINT); // shift right or divide by 1024

outY = (Pgain*errorY + Igain*Ysum); // Integer arithmetic

outY = (outY>>FIXED_POINT); // shift right or divide by 1024
```

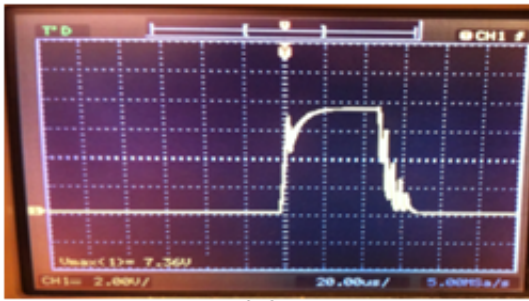
The *Pgain* and *Igain* contain integer values of 12 and 3 respectively, where as the intended values are 0.012 and 0.003. After the integer arithmetic operations the final result will be in the *outX* and *outY*. Now if *outX* and *outY* are divided by 1000 then the resulting number will be approximately the same as if the calculations were done with the *Pgain* and *Igain* having values 0.012 and 0.003 respectively. Here the division is achieved by shifting the integer bits towards the right by an amount of 10. This will result in a division by 1024, which is quite close to 1000. The reason to use shift operation is that it is much faster than the normal integer division. This fixed point implementation has less precision but has a major advantage of providing high speed performance.

4.6 Modifications

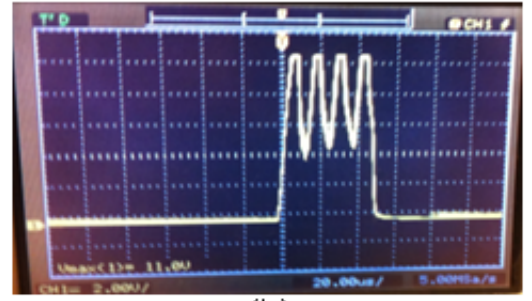
During the implementation, few issues were revealed and appropriate modifications were made. This section discusses these issues and respective modifications.

4.6.1 Photodetector

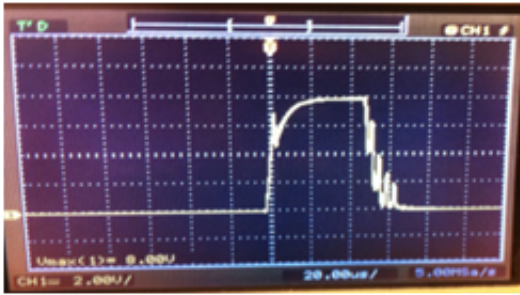
Figure 4.15 shows the response of the OPT101 device. Six different responses are shown based on the values of *R_ext* and *C_ext*, discussed in the previous section 3.2.1.3. It can be seen in Figures 4.15 that all the responses suffer from some oscillations. Figure 4.15 (b) response is without any capacitor and shows maximum



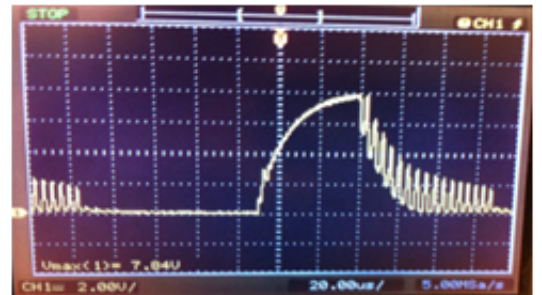
(a)



(b)



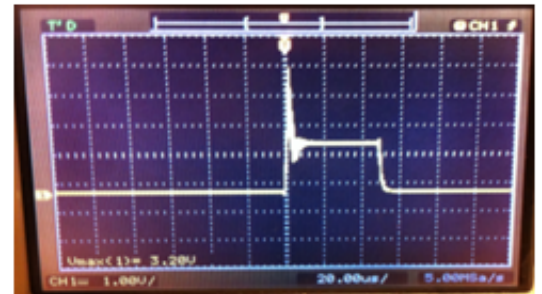
(c)



(d)



(e)



(f)

Figure 4.15: The photodetector OPT101 response for different values of feedback resistor and capacitor. (a) $R_{ext} = 13 \text{ k}\Omega$ and $C_{ext} = 390 \text{ pF}$ (b) $R_{ext} = 13 \text{ k}\Omega$ with no capacitor. (c) $R_{ext} = 14.33 \text{ k}\Omega$ and $C_{ext} = 390 \text{ pF}$ (d) $R_{ext} = 14.33 \text{ k}\Omega$ and $C_{ext} = 1 \text{ nF}$ (e) $R_{ext} = 3 \text{ k}\Omega$ and $C_{ext} = 1 \text{ nF}$ (f) $R_{ext} = 3 \text{ k}\Omega$ and $C_{ext} = 390 \text{ pF}$

oscillations. Figure (d) shows a response with high value for the C_{ext} with no oscillations in the beginning but having a very slow response with the high rise and fall times. But the falling edge of the signal has significant oscillations. Figure (e) and (f) has less gain with low value of R_{ext} . Figure (e) has the fastest response due to the low value for C_{ext} but it also has high overshoot in the rising edge. Overall, the response of the OPT101 suffers from oscillations with very low quality output. This is not suitable for the current application where high resolution is required.

4.6.1.1 Transimpedance amplifier and VBP104S photodiode

Due to low quality response of OPT101, an alternative solution is implemented. In this solution a separate good quality opa381 transimpedance amplifier [44] with a separate VBP104S photodiode[22] is deployed. Figure 4.16 shows the OPA381 internal circuitry and its connections with the photodiode. The external R_f resistor is used to define the gain of the amplifier. The OP3A81 with VBP104S photodiode has much better response than the OPT1010, the response will be discussed in detail in the chapter 5 (Results). Apart from having a better response, the combined OP3A81 with VBP104S is much less expensive than the OPT101, which makes the design more cost effective. Also both parts are available in small SMD packaging, making it suitable for compact assembly.

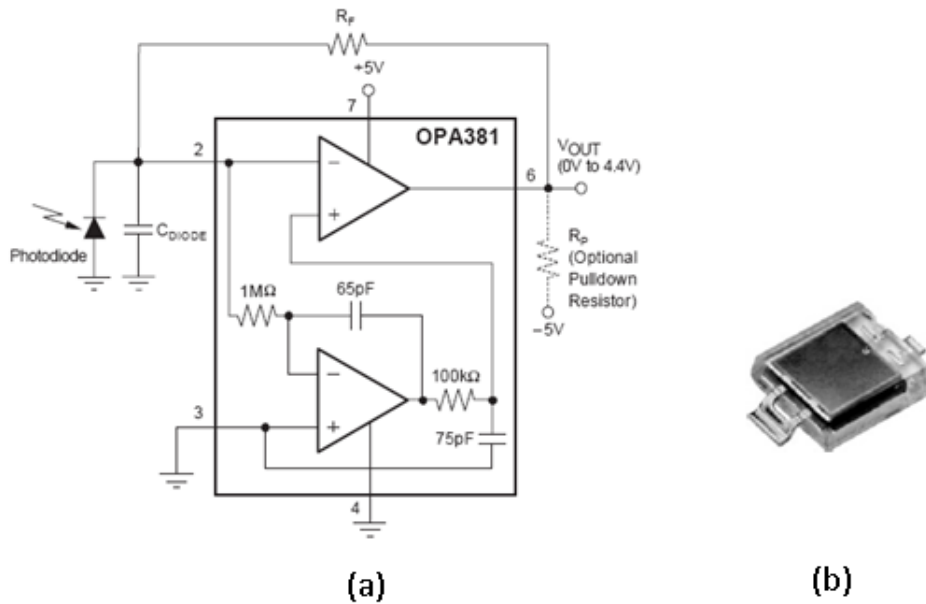


Figure 4.16: (a) OPA381 transimpedance amplifier. (b) VBP104S photodiode.

4.6.2 Enhancing the optical gain

The best way to increase the signal strength, without an addition of noise, is to increase the optical gain of the sensor. The optical gain is increased by increasing the light intensity of the four LEDs. More intensity means that the photodiode will produce more photocurrent. The transimpedance amplifier that converts this photocurrent to the voltage signal, will produce more voltage for the same value of the gain resistor R_f . Keeping the R_f value low, reduces the voltage gain but enhances the signal quality [29]. Low R_f means that the electronics noise from the amplifier is amplified less and contributes less to the main signal. Furthermore, the low R_f value increases overall bandwidth of the amplifier which results in faster response, leading to low rise and fall times. So, its in best interest to keep the R_f value low while enhancing the photocurrent by increasing the light intensity. The

current LED is being operated by the 30 mA constant current source. This is due to the maximum rating of the LED [31]. One way to increase the light intensity is to use a LED with high current rating. However, the SMD LED with similar dimensions, was only available with max rating of 30 mA, so currently getting a higher rating LED was not possible.

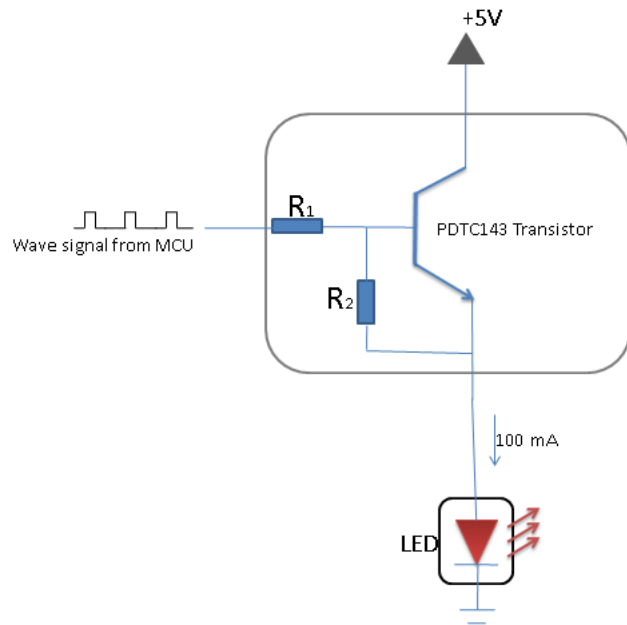


Figure 4.17: Modified LED driver circuit.

One interesting thing to note about the LED driving signal is that it is a modulated wave of 10 kHz with a duty cycle of 25 %. This means the LED is only turned ON for the 25 % of the time of its operation. Hence the average current consumed by the LED is only $30/4 = 7.5$ mA. This means that the average current can be increased by 4 times. Now by operating the LED at $30 \times 4 = 120$ mA with a square wave of 25 % duty cycle will lead to the average current of $120/4 = 30$ mA, this current is within the limits of the max rating of the LED. This means that the optical gain can be increased by four times without damaging the LEDs. However there is an extra limit, the LED manufacturer also recommends that the peak current at any instant should not be more than 100 mA [31]. This means that instead of 120 mA, only 100 mA can be fed to the LED. To increase the LED current also requires a constant current source of 100 mA. Unfortunately, with small smd package of same dimensions as of 30 mA current source (previously used), is not available. One solution could be to use 3 such current sources in parallel to provide a current of 90 mA. On the other hand a better solution would be to omit constant current source completely and exploits the max current capability of the PDTC143 transistor, already used in the design (figure 3.9). The PDTC143 transistor has the ability to provide a maximum of 100 mA current [32]. If the transistor is exploited to draw more current, the transistor will limit its output to restrict the current at 100 mA, this way it can act as a constant current source of 100 mA. Now, Figure 3.9 can be modified with a better design that can provide high optical gain. Figure 4.17 shows the modified circuit for the LED driver. This circuit is

more simpler and omits the extra constant current source. One important thing about the optical gain is that it should not be too high, such that it saturates the photo detector. The VBP104S photodiode has a saturation current limit of 50 mA [22] and in the current implementation it does not saturate.

4.6.3 Slowing down the frequency

The ADC of the MCU was configured to operate at 1 Mbps. This means that every 1 μsec there will be an ADC interrupt. The ADC interrupt service routine (ISR) executes some code to handle the sample. This execution takes some time and on top of that, the timers interrupts and serial port interrupts also execute some code. All the interrupts, the timers, the ADC and the USART interrupt are implemented with the same priority. This means that at a time when one ISR is being executed and if other interrupt occurs then the executing interrupt will not be preempted. The other interrupt will wait till the previous ISR finishes its execution. This choice is made in order to avoid a critical section problem [47]. Some important values are being updated in an ISR and these values are being used by another ISR, so preemption is avoided to ensure consistent values. The MCU is running at 64 MHz, which provides an execution of 64 (assembly level) instructions in 1 μsec . Now if the ADC ISR is to be executed every 1 μsec then there is a room of only 64 assembly instructions to be executed before the other ADC ISR execution request occurs. This means there is a room of only 64 instructions between the two consecutive ADC interrupts. It turned out that this room of 64 instructions is not enough for the MCU to finish execution of first ADC ISR before the second ADC ISR occurs. If the second ADC ISR occurs, before the first ISR execution is not finished, then the ADC interrupts requests will start to accumulate and the MCU will not be able to perform any other tasks and might get stalled. Despite adding some tricks to reduce the programming instructions, this problem was not solved. At the end, the overall ADC speed was reduced, by half, to 500 ksps. This also resulted in reducing the 10 kHz modulation frequency to 5 kHz. The overall effect of this change was not that much significant. The 5 kHz modulation frequency with 500 ksps ADC was still enough to perform all the purposed methodologies in the chapter 3. Also the oversampling to achieve 14 bits resolution and 32 points moving averaging was done in the same way as purposed in the chapter 3.

Chapter 5

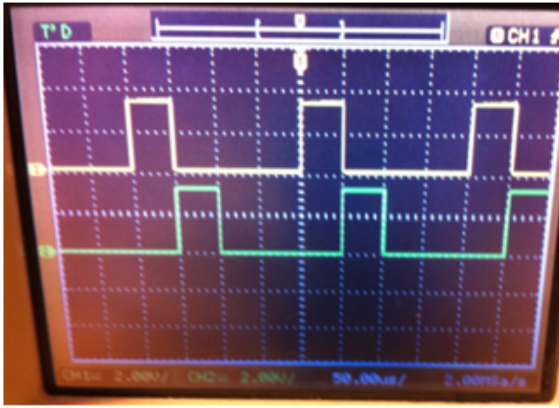
Results

5.1 Modulated waves

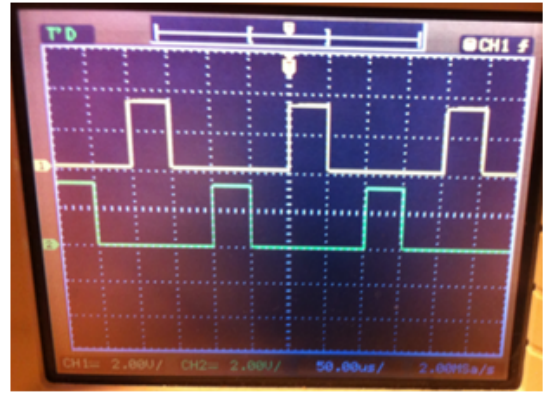
Figure 5.1 shows two-channels oscilloscope screenshots of the modulated waves generated by the MCU. Figure 5.1 (a) shows two modulated waves at the top and at the bottom. The top one is generated at the pin TIOA0 controlling LED0 and the bottom one at the pin TIOB0 controlling LED1. Similarly, in Figures 5.1 (b) and (c) the top wave generated at the pin TIOA0 is taken as a reference and the corresponding waves at the pin TIOA1 (controlling LED2) and at the pin TIOB1 (controlling LED3) are shown at the bottom. As can be seen in the Figure 5.1, the time scale is $50 \mu\text{sec}$ and each wave has a duty cycle of 25 %, lasting for exactly $50 \mu\text{sec}$. This leads to a wave frequency of exactly 5 kHz. Also, all the waves are exactly 90 degrees out of phase without any noticeable jitter.

5.2 DAC output

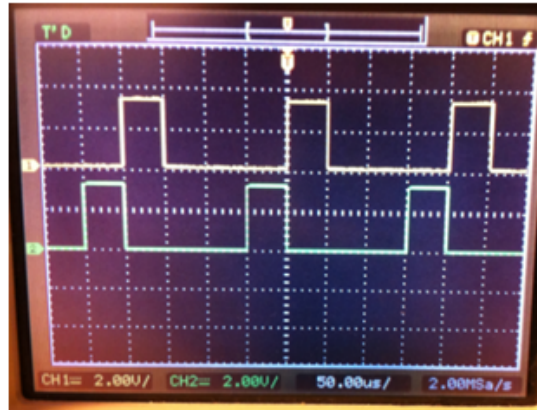
Figure 5.2 shows the output of the digital to analog converter (DAC). In Figure 5.2 (a), the DAC is driven with a digital input ranging from 0 to 4000. The corresponding DAC output will range from 0.56 to 2.76 volts. This output was required to be mapped to a range of 0 to 5 volts with the help of the interface electronics, as previously discussed in the section 3.2.3. Figure 5.2 (b) shows the output of the DAC voltage after the interface electronics. The output now has a voltage range form 0.2 to 4.8 volts, as indicated by the oscilloscope measurements $V(\text{min})$ and $V(\text{max})$ at the bottom of Figure 5.2 (b). This range can be further tweaked to 0 to 5 volts range with the help of some extra circuitry and negative supply (section 3.2.3), but for practical purposes this range was good enough.



(a)



(b)

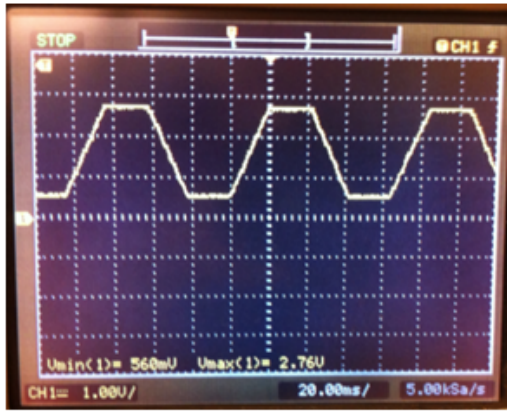


(c)

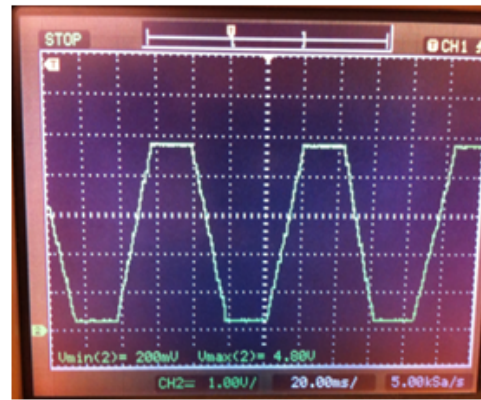
Figure 5.1: Modulated waves to drive the four LEDs. (a) The top wave at pin TIOA0 of the MCU. The bottom wave at the pin TIOB0. (b) The top wave at the pin TIOA0 and the bottom wave at the pin TIOA1. (c) The top wave at the pin TIOA0 and the bottom wave at the pin TIOB1.

5.3 Photo detector response

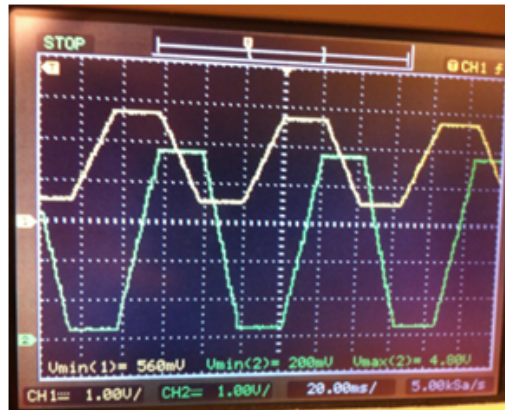
Figure 5.3 (a) and (b) show the photo detector response of the VBP104S photodetector after the transimpedance amplifier OPA381. Figure (c) and (d) shows the best response achieved from the OPT101 photodetector. The response is shown after a LED is modulated by the 5 kHz wave, generated by the MCU. The light from the LED is projected on the photodetector (VBP104S or OPT101) and the resulted voltage is shown on the oscilloscope. It can be seen that the response from the OPA381 is much better than the OPT101. OPA381 shows no oscillations and the output is much cleaner. Whereas the OPT101 severely suffers from oscillations and has higher noise level.



(a)



(b)

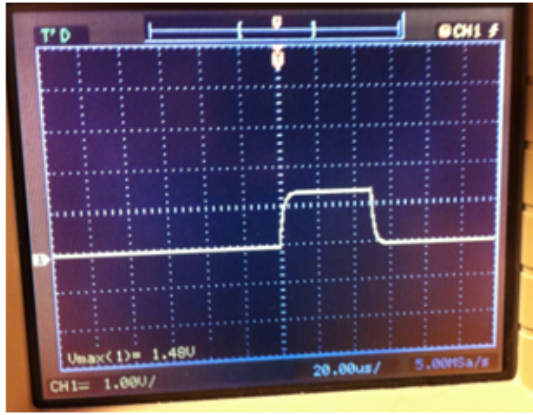


(c)

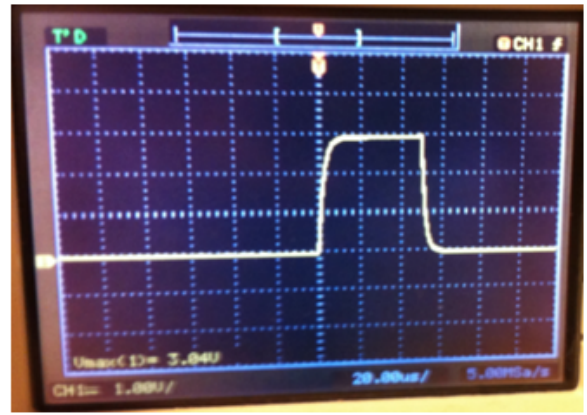
Figure 5.2: DAC output profile for the digital input range of 0 to 4000. (a) DAC output voltage without electronics interface. (b) DAC output voltage after the electronics interface. (c) Combined outputs, before the electronics interface (the top) and after the electronics interface (the bottom).

5.4 Moving average filter

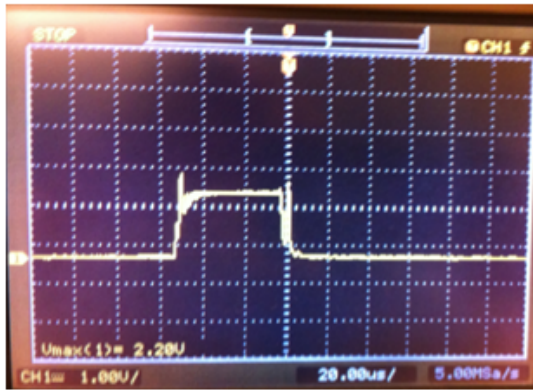
Figure 5.4 shows an output of the moving average filter for 16, 32 and 64 points. A DC voltage (with small inherent noise) of about 2 Volts was fed to the MCU ADC and moving average filtration was performed at 16, 32 and 64 points. The table 5.1 shows the analysis done on the gathered data. The data of about 300 samples from the filter output was taken. The second and third columns in the table 5.1 shows the minimum and maximum value in the samples. The fourth column shows an absolute deviation between the min and max values. The fifth column shows the standard deviation of all the gathered samples from the filter output. It clearly shows that by increasing the number of points in the averaging filter the standard error has reduced.



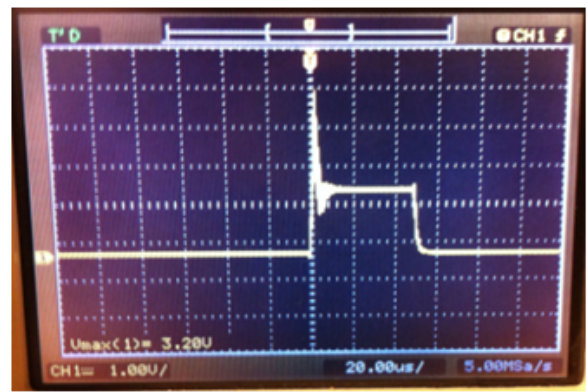
(a)



(b)



(c)



(d)

Figure 5.3: Photo detectors response from the modulated LED. (a) VBP104S response after the OPA381 amplifier. (b)VBP104S response after the OPA381 amplifier with higher optical gain. (c) OPT101 response. (d) OPT101 response with lower feedback capacitor and higher optical gain.

5.5 User Interface

An external computer is connected with the tip-tilt embedded system. User software on this computer sends operational commands to the embedded system via serial communication. Figure 5.5 shows the keyboard interface of the user software. The keyboard interface provides specific functionality based on the KEY pressed. Depending on which KEY is pressed, a data packet is formed according to the communication protocol discussed in section 4.4. This packet is sent to the embedded system via serial interface. The packet is decoded by the MCU and an appropriate action is taken. The KEYS R, I, P, J, L, Z, X, C, V and B provide the functionality discussed in the table 4.4 (section 4.4). The labels under these KEYS also provide a short description of their functionality. The KEYS T and F, increase and decrease the horizontal (X) position of the tip-tilt mirror from its initial position by the amount of jmp (a constant number) respectively. Similarly, the KEYS Y and G increase and decrease the vertical position respectively. The

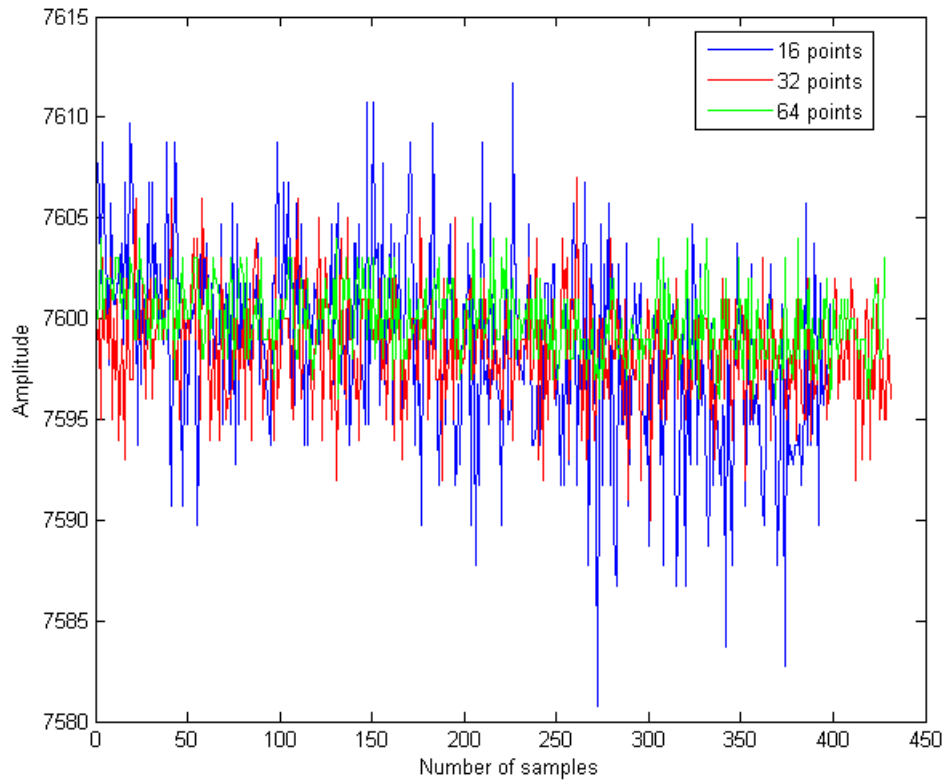


Figure 5.4: Moving average filter output for 16,32 and 64 points.

No. of points	Min. Value	Max. Value	Deviation	Std. Dev.
16	7580	7611	31	4.99
32	7590	7607	17	2.79
64	7596	7605	9	1.81

Table 5.1: Moving averaging filter analysis.

KEY U brings the tip-tilt mirror to its initial position. The KEYS O and K, enable or disable a shape formation. This functionality will be discussed more in the section 5.7.

5.6 Tip-tilt mirror and the displacement sensor

Figure 5.6 shows the tip-tilt device along with the feedback sensor. Figure 5.6 (a) shows a two-axis linear translation stage with micrometer screw gauges to control the displacement in horizontal and vertical direction. A sensor lever containing the four LEDS (Figure 5.6 (d)) is attached with the two-axis stage. The photo detector (Figure 5.6 (d)) is mounted on the actuator lever. The actuator lever is connected with the tip-tilt mirror and strictly follows the mirror's current position. The four LEDS of the sensor lever are placed under the mounted photo detector.

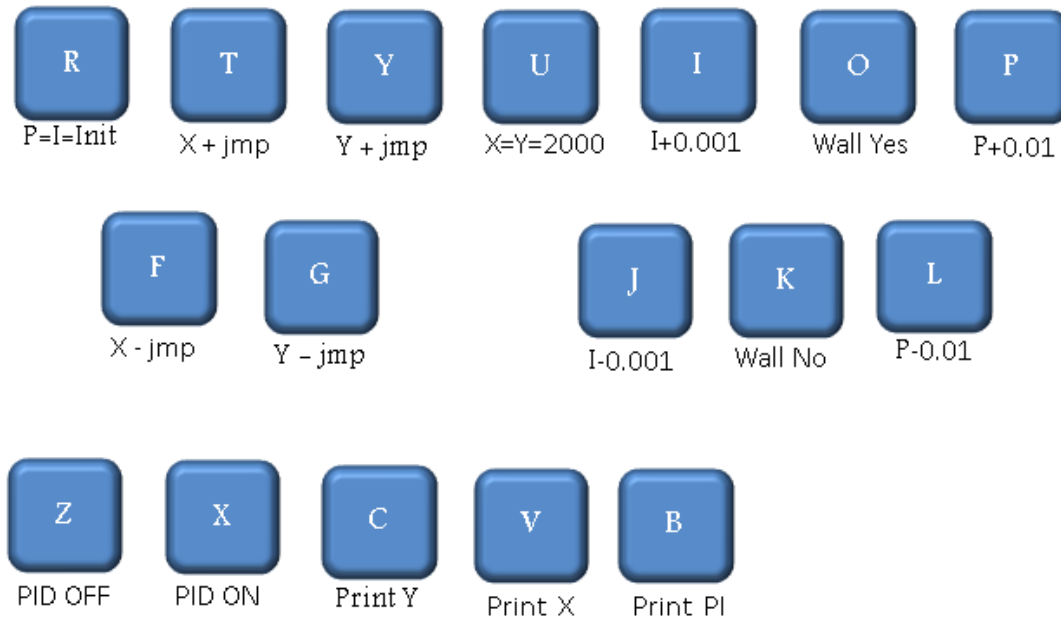


Figure 5.5: Keyboard interface for user control .

This will form a position sensor discussed in the section 3.1 (Figure 3.1). The two-axis stage is only used to perform testing and to check the response of the feedback sensor. In the final assembly there will be no two-axis stage and the four LEDs will be integrated inside the tip-tilt device. The sensor output from the photo detector is shown in Figure 5.6 (b). It shows signals from the four LEDs, LED0, LED1, LED2 and LED3 separately. In this state the sensor is balanced (calibrated to zero) and the LED0 and LED1 signals representing the X position are at an adjacent level from each other. Similarly, the LED2 and LED3 signals representing the Y position are also at an adjacent level from each other.

Now if the X-position of the LEDs is displaced towards the right by rotating the X-position micrometer counterclockwise then the LED0 and LED1 signal will not be at the adjust level. The LED0 signal will go down and the LED1 signal will go up. This is shown in Figure 5.7 (a) and (b). Similarly, if the micrometer is rotated clockwise, the LED0 signal will go up and the LED1 signal down as shown in Figure 5.7 (c) and (d). One thing to notice here is that there is a also a small change in the LED2 and LED3 signal. While the displacement is only in X direction, the Y direction signal associated with LED2 and LED3 will also experience slight change in its magnitude. This is referred as an interference. This interference, though quite small, needs to be corrected by the means of calibration. It should be noted that in the figures 5.7 and 5.8 the displacement effect is produced by the means of the two-axis translation stage. The same displacement effect is produced by the two dimensional motion of the tip-tilt mirror. In that case the translation stage is in static state and the tip-tilt mirror position is directly set by the user software. For example if the KEY T (X+ jmp) in the user software (section 5.5) is pressed then the mirror will move towards the right and will produce the same sensor output as of Figure 5.7 (b).

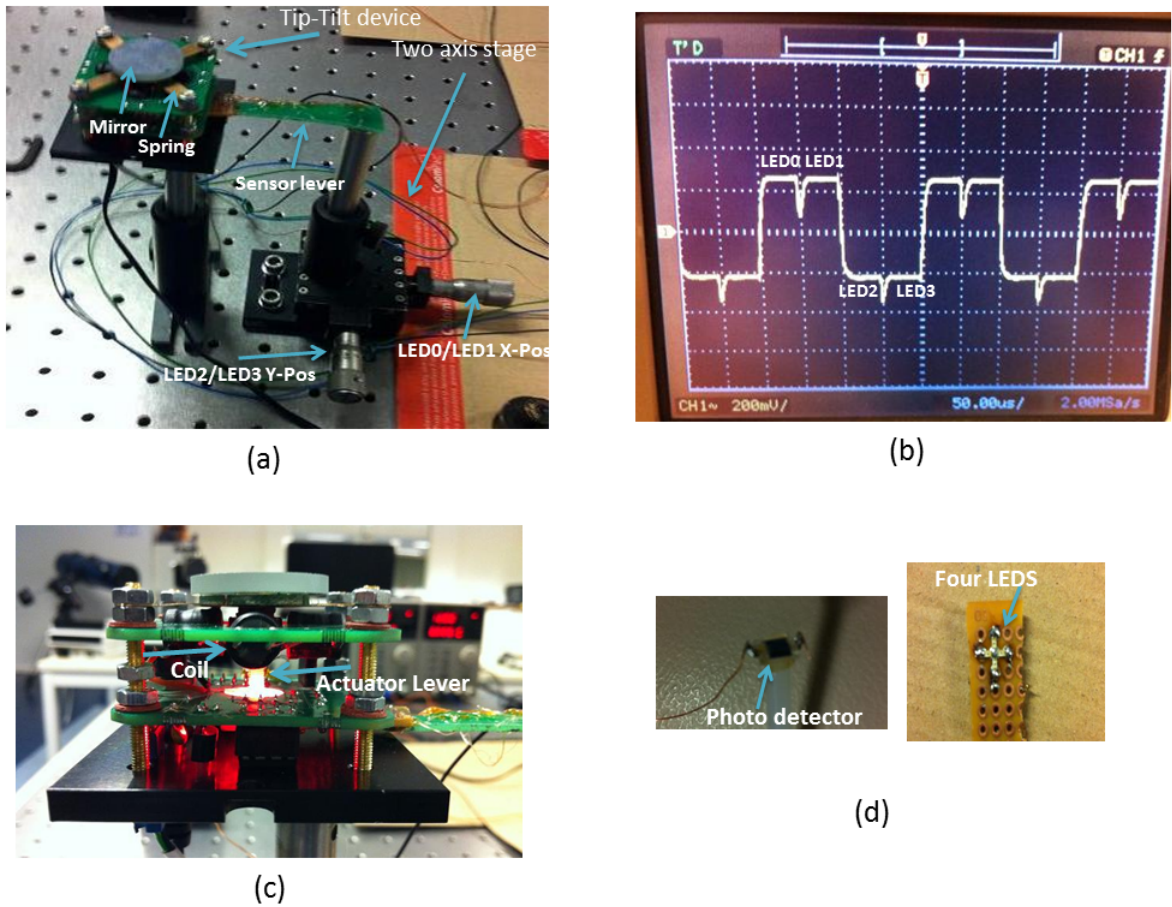


Figure 5.6: (a) Fast steering mirror. (b) Sensor output from the four LEDs. (c) A close up of the actuator lever and inductive coil. (d) The photo detector and the four LEDs .

5.6.1 Interference Calibration

Figure 5.9 shows the sensor output for horizontal and vertical displacement. The vertical position of the tip-tilt mirror is raised linearly from its initial position to maximum position, while the horizontal position is not changed at all. The interference in horizontal position due to this vertical displacement can be easily observed in the graph. It can also be noted that the interference response is approximately linear with respect to the linear change in the vertical position. In Figure 5.9, the initial and maximum positions in both vertical and horizontal outputs are marked by the data points. The maximum change in horizontal and vertical positions can be calculated by these data points. The maximum change in the vertical position (full scale reading) is $3879 - (-2256) = 6135$. The corresponding maximum change in the horizontal position due to interference is $1021 - 310 = 711$. Hence, the full scale change in the vertical position induces $\frac{711}{6135} = 11.58\%$ of interference in the horizontal position. This quantifiable interference will be constant throughout the operation of the device. Once the interference is quantified, it can be easily removed. This is done by first calculating the interference magnitude relative to the current vertical position and then subtracting it from the horizontal position.

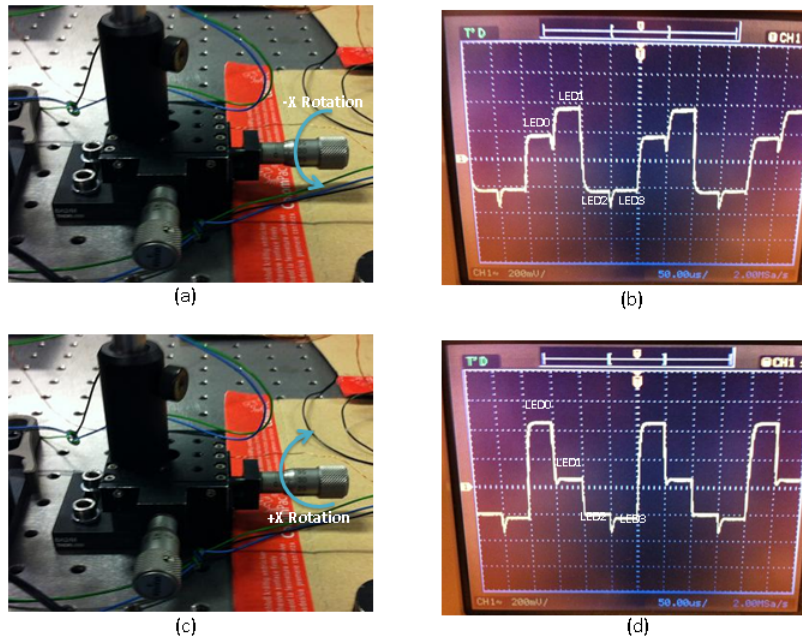


Figure 5.7: The position sensor response. (a) and (c) A displacement in the horizontal X direction by the rotation of the micrometer. (b) and (d) Corresponding effect of the displacement on the sensor output.

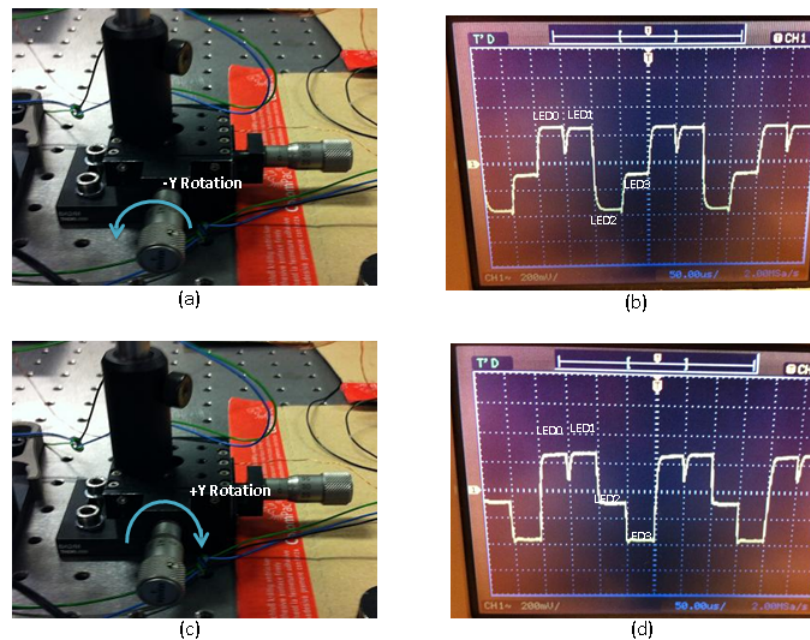


Figure 5.8: (a) and (c) A displacement in the vertical Y direction by the rotation of the micrometer. (b) and (d) Corresponding effect of the displacement on the sensor output.

In a similar way an interference in a vertical position due to the change in the horizontal position can be quantified and removed.

The interference in the sensor output is mainly caused by the wide spread of the LEDS light. The interference can be reduced by decreasing the distance between the LEDS and the photo detector. This will confine the spread of the LEDS light strictly to one position on the photo detector.

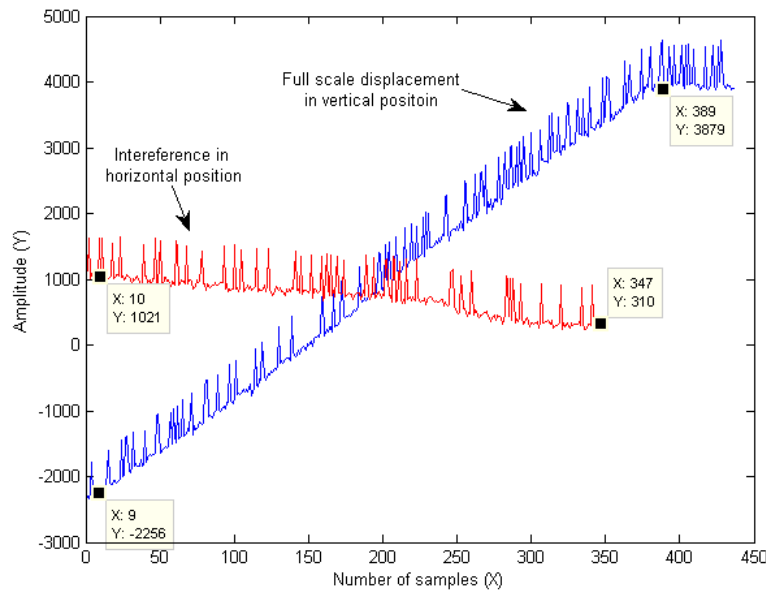


Figure 5.9: Interference in horizontal sensor data due to vertical displacement.

5.6.2 Output response with an active feedback

In the previous section, the sensor output response was shown with the PID feedback turned OFF. The disturbance in the displacement was added by the micrometers and this disturbance was reflected in the sensor output. Now, the PID feedback is turned ON and the device will correct any external disturbances. Figure 5.10 shows this phenomenon. The current X and Y positions are set to be at an adjacent levels. Any disturbance in their position added by rotating the micrometers clockwise or anticlockwise did not show any effect on the output. Because any added disturbances were instantly corrected by the PID feedback control. However, this correction ability of the feedback control is limited by two things. The speed or frequency of the external disturbances and the overall displacement range of the tip-tilt device. If the speed at which the disturbances are added is too high than the overall response of the feedback control might be too slow to correct the disturbances. This will lead to slow response for correction and some small fast disturbances will be visible in the response. One solution to this problem is to implement faster feedback control. This means faster sensor response, faster ADC and faster MCU clock speed. The second limitation could be due to the limited displacement range of the device. If the added disturbance is too large that it surpasses the maximum displacement range of the tip-tilt device then the complete correction is not possible.

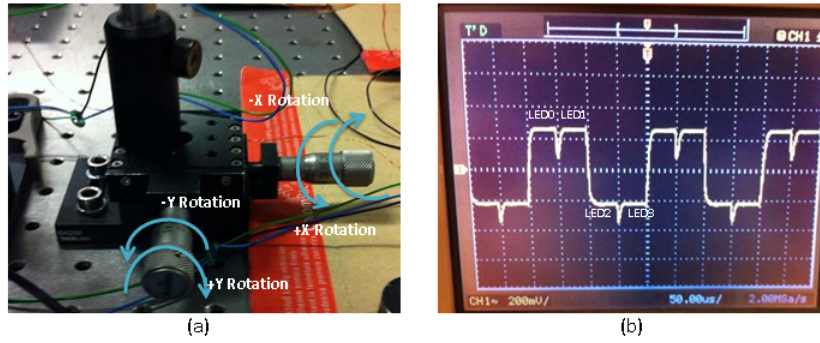


Figure 5.10: Output response with an active feedback.

5.6.3 Sensor resolution

The approximate sensor resolution can be calculated with the help of the micrometers screw gauges. In the current implementation, with respect to the full scale displacement of the tip-tilt mirror, the sensor value can range from -4000 to 4000. The currently used screw gauge has the minimum scale reading of 10μ meters. This means a minimum step of 10μ meters displacement can be accurately taken. Now by taking the 10μ meters step in the horizontal position (X-pos) by rotating the screw gauge and noting the change in the X-position data (LED0 and LED1 signals), an approximated resolution of the sensor can be determined.

Figure 5.11 shows the outputs of the sensor measuring horizontal position (X-pos) of the mirror. There are two output signals, the bottom signal shows the output at the mean position (initial) position. The upper signal shows the output after the 10 micrometer displacement in the horizontal direction. The sensor output is an integer number with a minimum step of 1. The bottom signal has a mean value of 57 with a standard error of 9.8. After the $10 \mu m$ displacement the lower signal is raised to the upper level with the mean value of 557.8 having a standard error of 8.8. Now the total change in the mean values of the output for the given change of $10 \mu m$ in the displacement will be $557.8 \pm 8.8 - 57.0 \pm 9.8 = 500.8 \pm 18.6$. Dividing this value by 10 will lead to $\frac{500.8}{10} \pm 18.6 = 50.08 \pm 18.6$. The value 50.08 ± 18.6 gives the change in the sensor value with $1 \mu m$ change in the displacement. This means that in the extreme case with an error margin of ± 18.6 , the absolute change in the sensor value per μm will be $50.08 - 18.6 \times 2 = 50.08 - 37.2 = 12.88$. The minimum change in the integer output of the sensor is 1. Which shows that the output change of 12.88 per μm will result in overall resolution of the sensor to be less than $1 \mu m$.

5.6.4 Sensor response time

The maximum speed at which the changes in position of the tip-tilt mirror can be detected is related to the sensor response time. The minimum response time of the sensor can be calculated with the help of Figure 4.8 (section 4.2). Figure 4.8 shows

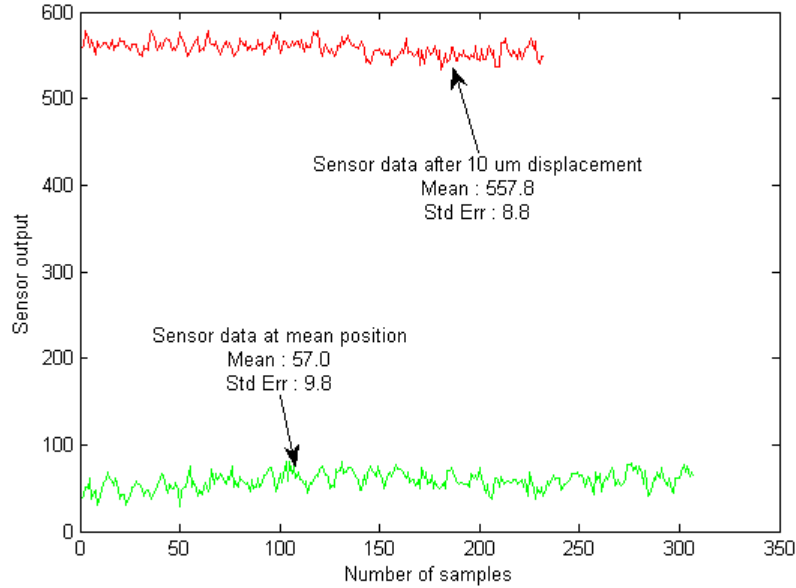


Figure 5.11: Sensor outputs at a mean position and after a 10 μm horizontal displacement.

that LED1 BUFF will be updated with new value every 100 μsec . In the current situation with 5 kHz modulation frequency the LED1 BUFF will be updated every 200 μsec . This updated value in LED1 BUFF will travel through the 32 points of the moving averaging filter. This means that the minimum response time of the sensor will be $200 \times 32 = 6400 \mu\text{sec}$. In this case, the maximum speed at which the mirror can change its position will be approximately $S_m = \frac{1}{6400} = 156 \text{ Hz}$. So the sensor response directly depends on the modulation frequency and the total number of points in the filter. A higher modulation frequency and lower points averaging in the filter will lead to faster response. However, higher modulation frequency requires faster embedded controller with higher CPU clock frequency as previously discussed in the section 4.6.3. Any changes in the mirror position that are faster than 156 Hz will not be detected by the current embedded controller.

Further more, the maximum speed at which the embedded system can response to the changes in the mirror position is related to the response time of the embedded controller. The response time of the embedded controller can be approximated as, Response Time = Sensor response time + PID calculations time + DAC Response Time . Here DAC is running at 1 Msps giving a response time of 1 μsec and sensor response time is 200 μsec . The PID calculations time depends on the execution time taken by the MCU to evaluate the PID expressions (section 4.5). The total PID expressions evaluation consists of about 8 C language instructions (section 4.5) which can be roughly converted into maximum of 200 assembly level instructions [20]. The current MCU can execute 64 assembly level instructions in 1 μsec [20]. So the execution of 200 instructions would roughly take about 4 μsec . This will lead to the embedded controller response time of *Response Time* = $6400 + 4 + 1 = 6405 \mu\text{sec}$ = . Here it can be concluded that the embedded system overall response time is strictly limited by the sensor response time. Lower sensor response time

will lead to faster response from the embedded system.

5.7 Shape formation

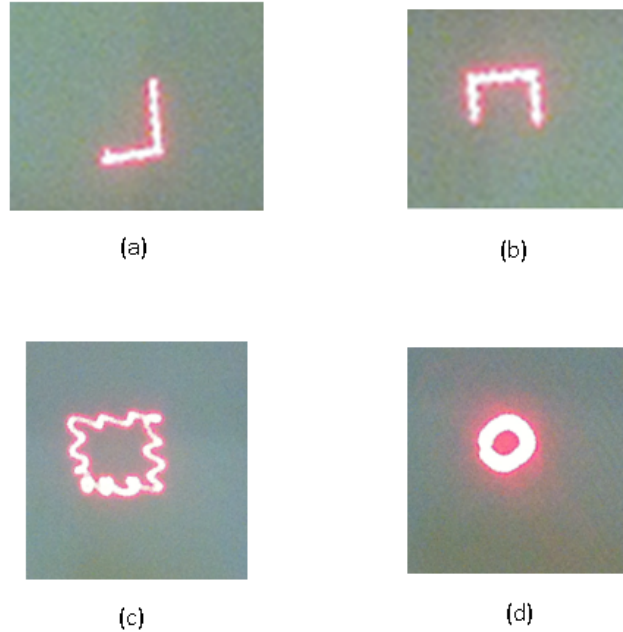


Figure 5.12: Tip-tilt mirror projecting formation of different shapes. (a) A laterally inverted L shape. (b) A half square. (c) A full square with fast nonlinear input, without feedback correction. (d) A full square with fast nonlinear input, with feedback correction.

A laser light can be projected on the tip-tilt mirror, and the reflected light from this mirror can be used to visualize the motion of the mirror. If the mirror is operated in a way that it continuously changes its position in a specific pattern then that pattern can be visualized by the projected laser. Figure 5.12 shows the projected laser while the tip-tilt mirror is operated to follow some specific patterns. Figure 5.12 (a) shows a laser pattern when the mirror is operated to form an L shape pattern. Figure 5.12 (b) shows a half square pattern and similarly different patterns can be formed. This kind of light projection helps in visualizing the operation of the tip-tilt device. Any non linearities or disturbances can be easily spotted. Although some non linearities can already be seen in Figure 5.12 (a) and (b) shapes, Figure 5.12 (c) shows a clear influence of non linearities in the square shape.

These non linearities are introduced by operating the tip-tilt mirror with an input containing fast non linear jumps in the data points. Figure 5.13 shows two types of input data streams that are used to drive the tip-tilt mirror. The non linear data stream has big jumps between the two consecutive data inputs. This

will result in a fast non linear changes in the position of the mirror. Where as the linear data stream has very low jumps between the two consecutive data inputs. This will result in smooth changes in the mirror position.

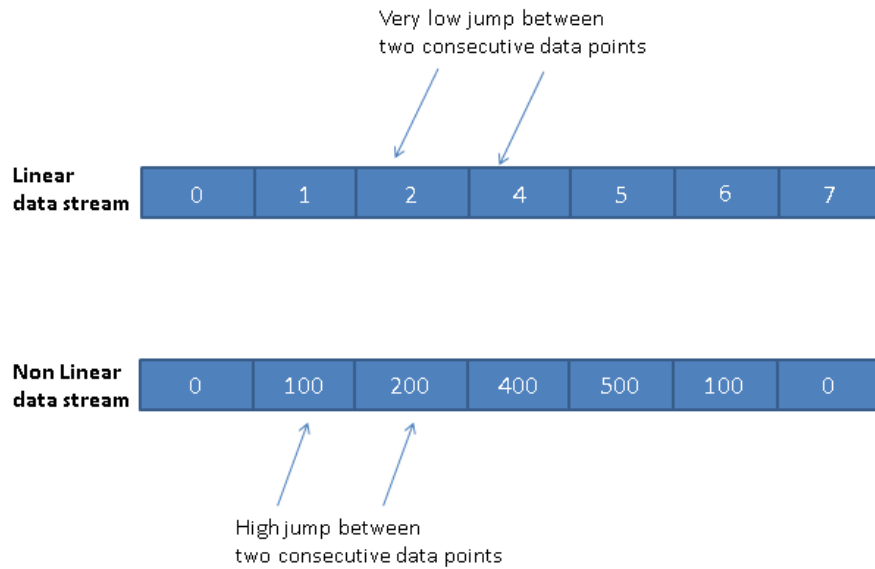


Figure 5.13: Input data to drive the tip-tilt mirror.

Figure 5.12 (c) shows the response when the tip-tilt is driven with a non linear input data stream. The tip-tilt mirror contains mechanical parts including springs, magnet and a mirror in its assembly (section 1.2). These mechanical parts, when driven by non linear input data stream, will exhibit a non linear response as shown in Figure 5.12 (c). Figure 5.12 (d) shows the response when the feedback correction is turned ON. The non linearities have been corrected by the feedback system but it has limited the overall dynamic range of the system. The overall shape is smaller and is bit transformed into a circle. There are no sharp corners like in the square shape. This is because of the slow feedback response (section 5.6.4) that cannot keep up with the fast changes in the mirror output. The feedback system can only respond to the changes slower than $6405 \mu sec$ (6.4 msec) (section 5.6.4). This adds a limitation on the speed of the non-linear disturbances that can be accurately corrected by the feedback system. The slow non linear changes/disturbances, as discussed in the section 5.6.2, are corrected without any performance degradation.

Chapter 6

Conclusions and Future work

6.1 Conclusions

Following conclusions can be made from this project.

- A unique method for the implementation of the position sensor, which makes use of robust signal processing technique supported by the embedded system, was proposed.
- The primary motive was to minimize the cost and size without significant performance deficiency.
- A phase sensitive detection mechanism was used to process the signal from the sensor.
- Four 90 degrees out of phase 5kHz square waves are generated from the MCU's timer peripheral. The accurate alignment of the four waves was ensured to avoid any interference.
- The oversampling method was exploited to enhance the ADC resolution from 12 bits to 14 bits.
- The two channels of the integrated DAC module of the MCU were used to control the two dimensional motion of the tip-tilt mirror.
- Appropriate electronics interfaces for the LEDS, DAC and serial port were deployed to overcome the limitations of the MCU.
- A resolution of less than 1 μm was achieved.
- A PID control algorithm was deployed to correct any positioning errors.
- A computer was connected to the embedded system via a serial interface. A communication protocol was deployed to ensure meaning full data transfer.
- A simplistic user software was made to facilitate easy control of the tip-tilt device from the keyboard KEYS.

- The overall prototype implementation was tested with successful results. The work will be presented in the scientific conference[48].

6.2 Future work

The overall performance of the system relies on three major things. The sensitivity of the sensor, the processing speed of the MCU along with the ADC resolution and the electronics interface. Several potential improvements can be made in these three areas. However most of these improvements come at some extra cost in terms of time and money.

The sensitivity of the sensor can be improved by increasing the optical gain of the LEDs or by using the correct wavelength LEDs. In the current scenario only 30 mA LEDs are used, higher current LEDs could easily increase the sensitivity. Second, the wavelength of the LEDs is not in a perfect match with the photo detector performance. Currently, the exploited photo detector efficiency is of 72 %. By choosing the 840 nm wavelength LEDs the efficiency can increase to 99 %.

The signal performance is enhanced if more points are used in the moving average filter. Currently only 32 points moving are used in the filter. This was due to the limitation of the MCU processing speed. Further, the full sampling speed of the ADC of 1 Msps was not exploited, instead 500 ksps was used. This was also because of the low processing speed of the MCU, the main program calculations were lagging in accommodating the new ADC samples coming after every $1\mu sec$. This is why that not only the ADC sampling rate was reduced but also the modulating frequency of 10 kHz waves was decreased to 5 kHz.

The interface electronics also plays an important role in increasing the dynamic range of the signal. Currently the sensor output cannot go to zero, it only swings between 2 to 3 volts. Whereas the ADC input can process a signal between 0 to 3.3 Volts. Mapping the sensor output perfectly to ADC processing voltages can significantly enhance the signal strength. The use of negative supply in the ADC interface electronics can achieve that. In the current implementation there is no negative supply available.

Lastly, the use of UART serial interface must be converted to USB one. This will eliminate the need of extra serial to USB converter.

Bibliography

- [1] Goldwasser, Sam. "Lasers in Consumer Electronics: The Optical Pickup." Optics and Photonics News, Vol. 22, Issue 2, pp. 12-13 (2011)
- [2] Zeman, Vlado. "Photonics—A Technological Revolution." Science Careers, From the Journal Science, 18 July 2003. Web. 03 Feb. 2015.
<http://sciencecareers.sciencemag.org/career_magazine/previous_issues/articles/2003_07_18/nodoi.14641300891300576094>.
- [3] Arba-Mosquera, Samuel, and Ioannis M. Aslanides. "Analysis of the effects of Eye-Tracker performance on the pulse positioning errors during refractive surgery." Journal of Optometry 5.01 (2012): 31-37.
- [4] Qingkun Z., Ben-Tzvi P., Dapeng F., and Goldenberg A. A., 2008, "Design of Fast Steering Mirror Systems for Precision Laser Beams Steering," 2008 IEEE International Workshop on Robotic and Sensors Environments, (October), pp. 144-149.
- [5] Physik Instrumente. "Capacitance Sensor, Measuring Nanometer Displacement, Nano-Metrology , Capacitive Gauge, Metrology, by PI." Capacitance Sensor, Measuring Nanometer Displacement, Nano-Metrology , Capacitive Gauge, Metrology, by PI. Web. 03 Feb. 2015.
<<http://www.capacitance-sensors.com/>>.
- [6] Measurement Specialties Inc. "Position Sensor " MR174B Linear Magnetic Field Sensors-Position Sensors-Magneto Resistive-Measurement Specialties". Web. 03 Feb. 2015.
<http://www.meas-spec.com/product/t_product.aspx?id=4791>.
- [7] Davidson, Andrew. "DETECTORS: CMOS Cameras Allow Robust Active Stabilization of Laser Beams." - Laser Focus World. PennWell Corporation, Tulsa, n.d. Web. 29 Sept. 2014.
<<http://www.laserfocusworld.com/articles/print/volume-47/issue-8/features/detectors-cmos-cameras-allow-robust-active-stabilization-of-laser-beams.html>>
- [8] "PSD Characteristics ", OSI Optoelectronics. Web. 2 Oct. 2014.
<<http://www.osioptoelectronics.com/application-notes/AN-Position-Sensing-Photodiodes.pdf>>

- [9] "Analog-to-Digital Converter in the SAM3S4." Atmel. 01 July 2011. Web. 2 Oct. 2014.
<<http://www.atmel.com/Images/doc11106.pdf>>
- [10] "About Lock-In Amplifiers." Stanford Research Systems. Web. 30 Sept. 2014.
<www.thinksrs.com/downloads/PDFs/ApplicationNotes/AboutLIAs.pdf>
- [11] Wolfson, Richard. "Phase Sensitive Detection" Web. 30 Sept. 2014.
<<http://www.csupomona.edu/~kvandervoort/Elec%20Lab%208.pdf>>
- [12] Chnical. "What Is a Lock-in Amplifier?" PerkinElmer Instruments. Signal Recovery. Web. 2 Oct. 2014.
<<http://users.df.uba.ar/acha/Lab4/lockin1.pdf>>
- [13] "Building a Lock-in Amplifier" Princeton Lab. Web. 2 Oct. 2014.
<<https://www.princeton.edu/~romalis/PHYS312/Lock-in%20amplifier.pdf>>
- [14] Cameron, Jay K. "ADC Preamplifier Works the Gain/dynamic-range Trade-off to Achieve 14-bit Linearity." Texas Instruments, 11 July 2002. Web. 2 Oct. 2014.
<<http://staging.edn.com/Pdf/ViewPdf?contentItemId=4342444>>
- [15] J.C. Candy and G.C. Temes, Oversampling Methods for A/D and D/A Conversion, IEEE Transactions on Circuits and Systems, June 1987 (Beginning discussion on the effects of oversampling on in-band noise).
- [16] "SAM3-P256." Olimex. Web. 02 Oct. 2014.
<<https://www.olimex.com/Products/ARM/Atmel/SAM3-P256/>>
- [17] Craig Peacock. "USB in a NutShell, Making Sense of the USB Standard." Beyond Logic. Web. 04 Feb. 2015.
<<http://www.beyondlogic.org/usbnutshell/usb1.shtml>>.
- [18] "Microcontrollers (MCU)." 32-bit Piccolo Microcontroller. N.p., n.d. Web. 01 Oct. 2014.
<http://www.ti.com/lscds/ti/microcontrollers_16-bit_32-bit/c2000_performance/real-time_control/f2802x_f2803x_f2806x/overview.page>
- [19] "Atmel SAM3S Series." Cortex M3 32-bit Micro-controller. Atmel Inc., n.d. Web. 1 Oct. 2014.
<<http://www.atmel.com/products/microcontrollers/arm/sam3s.aspx>>
- [20] Atmel Inc. SAM3S4B, ARM Based Cortex M3 Device. Web. 20 Jan. 2015.
<http://www.atmel.com/Images/Atmel_6500_32-bit-Cortex-M3-Microcontroller_SAM3S_Datasheet.pdf>.
- [21] "AVAGO TECHNOLOGIES - HSMH-C190. - LED, SMD, RED, 17MCD, 639NM." HSMH-C190. Web. 02 Oct. 2014.

- <<http://nl.farnell.com/avago-technologies/hsmh-c190/led-smd-red-17mcd-639nm/dp/8554641>>
- [22] "VISHAY - VBP104SR - PHOTOPIN DIODE RG." VBP104SR. Web. 02 Oct. 2014.
<<http://nl.farnell.com/vishay/vbp104sr/photopin-diode-rg/dp/1779700>>
- [23] Jacobowicz, Lionel, et al. "Teaching about photodetection noise sources in the laboratory." Fifth International Topical Meeting on Education and Training in Optics. International Society for Optics and Photonics, 1997.
- [24] Osgood, Prof. Brad. "Lecture Notes EE 261 : The Fourier Transform and Its Applications." (n.d.): n. pag. Electrical Engineering Department. Stanford University. Web. 15 Jan. 2015.
<<http://see.stanford.edu/materials/lsoftae261/book-fall-07.pdf>>
- [25] Davis, Prof. Sumner. "Physics 111: Low Light Signal Measurements (LLS)." University of California, Berkeley. Web. 15 Jan. 2015.
<<http://www.dnatube.com/video/27021/Lec-23--Physics-111-Low-Light-Signal-Measurements-LLS>>.
- [26] Smith, Steven. Digital Signal Processing: A Practical Guide for Engineers and Scientists: Ch. 15, Moving Average Filter. Newnes, 2013.
- [27] Ogata, Katsuhiko. Modern Control Engineering. Englewood Cliffs, NJ: Prentice-Hall, 1970. Print.
- [28] R, Yates. "Fixed-Point Arithmetic: An Introduction." Digital Signal Labs. 2 Jan. 2013. Web. 11 Feb. 2015.
<<http://www.digitalsignallabs.com/fp.pdf>>.
- [29] Graeme, Jerald G. Photodiode amplifiers: op amp solutions. McGraw Hill, 1996.
- [30] Texas Instruments Incorporated. OPT101: Monolithic Photodiode and Single-Supply Transimpedance Amplifier (Rev. A): Web. 19 Jan. 2015.
<<http://www.ti.com/lit/ds/symlink/opt101.pdf>>.
- [31] WURTH ELEKTRONIK. EiSos@we-online.com WL-SMCW SMD Chip LED Top View Mono- Color Waterclear Web. 20 Jan. 2015.
<<http://katalog.we-online.de/led/datasheet/150060RS75000.pdf>>.
- [32] NXP Semiconductors, NPN Transistor, PDTC143X Series Rev. 11 9 December 2011, and Product Data. Web. 20 Jan. 2015.
<http://www.nxp.com/documents/data_sheet/PDTC143X_SER.pdf>.
- [33] ON Semiconductor. NSI45030AT1G Constant Current Regulator and LED Driver. Web. 20 Jan. 2015.
<http://www.onsemi.com/pub_link/Collateral/NSI45030A-D.PDF>.

- [34] ON Semiconductor. Low Noise Dual/Quad Operational Amplifiers. Web. 20 Jan. 2015.
<http://www.onsemi.com/pub_link/Collateral/MC33078-D.PDF>.
- [35] Texas Instruments Incorporated. Techniques For Implementing A Positive And Negative Output Voltage For Industrial And Medical Equipment
<<http://www.ti.com/lit/ml/szzn001/szzn001.pdf>>
Web. 20 Jan. 2015.
- [36] Andreas Hahn. "Application of Rail-to-Rail Operational Amplifiers." Texas Instruments, Application Report (1999). Web. 21 Jan. 2015.
<<http://www.ti.com/lit/an/sloa039a/sloa039a.pdf>>
- [37] [Snvs420B, Texas Instruments Incorporated, and]. LM7705 Low Noise Negative Bias Generator (Rev. B). Web. 21 Jan. 2015
<<http://www.ti.com/lit/ds/symlink/lm7705.pdf>>
- [38] Purdue University ME365: MEASUREMENT SYSTEMS. CHAPTER 3 DIGITAL CODING OF SIGNALS. Web. 21 Jan. 2015.
<<https://engineering.purdue.edu/ME365/Textbook/chapter3.pdf>>
- [39] Labs, Silicon. AN118 Improving ADC Resolution by Oversampling and Averaging Web. 21 Jan. 2015.
<<https://www.silabs.com/Support%20Documents/TechnicalDocs/an118.pdf>>
- [40] Atmel Inc. AVR121: Enhancing ADC Resolution by Oversampling. Web. 21 Jan. 2015.
<<http://www.atmel.com/images/doc8003.pdf>>.
- [41] Blair D P and Sydenham P H 1975, "Phase sensitive detection as a means to recover signals buried in noise," J. Plivs. E: Sci. Instrini. 8 621-7
- [42] K. G. Libbrecht, E. D. Black, and C. M. Hirata, "A basic lock-in amplifier experiment for the undergraduate laboratory," Am. J. Phys. 71, 1208, 2003.
- [43] P. Schaefer, R. D. Williams, G. K. Davis, and R. A. Ross, "Accuracy of position detection using a position-sensitive detector," IEEE Trans. Instrum. Meas., vol. 47, pp. 914919, Aug. 1998
- [44] Texas Instruments Inc. OPA381, OPA2381: Precision, Low Power, 18MHz Transimpedance Amplifier (Rev. B) Web. 28 Jan. 2015.
<<http://www.ti.com/lit/ds/symlink/opa381.pdf>>
- [45] Moore, Gavin. FTDI US232R-100, FTDI USB to Serial Converter. Web. 1 Feb. 2015.
<<http://www.farnell.com/datasheets/1640370.pdf>>
- [46] Microsoft Windows API Supportfor Serial Communications. Web. 01 Feb. 2015.

<<https://msdn.microsoft.com/en-us/library/ff802693.aspx>>.

- [47] Systems, Concurrent Software, and 2. The Critical Section Problem Problem Description. Web. 1 Feb. 2015.

<<http://crystal.uta.edu/~ylei/cse6324/data/critical-section.pdf>>

- [48] M. Wasif, A.J. van Genderen, G. Vdovin, "A compact, high precision position sensing embedded system for fast steering mirror" ICT OPEN 2015, March. 2015. Accepted.